Mechano-induced angiocrine signals from hepatic endothelial cells promote liver growth and regeneration

Inaugural-Dissertation

zur Erlangung des Doktorgrades
der Mathematisch-Naturwissenschaftlichen Fakultät
der Heinrich-Heine-Universität Düsseldorf

vorgelegt von

Linda Große-Segerath, geborene Lorenz
aus Essen

Düsseldorf, Juli 2020

aus dem Institut für Stoffwechselphysiologie
der Heinrich-Heine-Universität Düsseldorf

Gedruckt mit der Genehmigung der
Mathematisch-Naturwissenschaftlichen Fakultät der
Heinrich-Heine-Universität Düsseldorf

Berichterstatter:

1. Prof. Dr. Eckhard Lammert

2. Prof. Dr. Verena Keitel-Anselmino

Tag der mündlichen Prüfung: 03.12.2020

Table of Contents

I. Annotations to this thesis

Parts of this thesis have been published in (Lorenz et al., 2018), these were in particular parts of the fourth section “Experimental procedures” and figures of the fifth section “Results”.

Author contributions adapted from the manuscript (Lorenz et al., 2018): “**L.L.** and J.A. performed the majority of the experiments; J.A. performed most experiments on mouse embryos—many of which were repeated and/or finalized by **L.L.**, C.H. and S.U.—and contributed to correlation analyses; **L.L.** performed the experiments on human cells and the analyses of *ex vivo* perfused livers; T.B. performed the first embryonic experiments, planned and designed the first *ex vivo* liver perfusion experiments along with N.E. and performed partial hepatectomy experiments; C.H. contributed to manipulation of mouse embryos and whole embryo culture. S.F. and H.N. were supervised by K.A., and provided VEGFR3 knockout embryos, genotyping and knockout efficiencies. D.H. planned, designed and supervised the ex vivo liver perfusion experiments performed by N.E. R.H. and J.S. performed and analysed the contrast-enhanced ultrasound measurements. K.M., K.B. and M.R. recruited, screened and phenotyped human individuals within the German Diabetes Study of which M.R. is the principal investigator; J.-H.H. and K.B. performed the magnetic resonance imaging and 1H magnetic resonance spectroscopy analyses along with M.R.; and O.K. performed the correlation analyses and adjustments. D.E. isolated hepatic ECs from mouse embryos and was involved in immunohistochemical analyses of mouse embryos, discussions, data management and statistical evaluations. E.L. supervised and guided J.A., T.B.,C.H., S.U. and **L.L.** during their experiments and wrote the manuscript with the help from J.A. and **L.L.** All authors read and contributed to the manuscript.”

Parts of this thesis were adapted from my master thesis “Effects of mechanotransduction via beta1-integrin and VEGFR3 on paracrine endothelial signaling” that was prepared between 2015-2016 at the institute of metabolic physiology at Heinrich Heine University Düsseldorf.

II. List of abbreviations

A

ACN	Acetonitrile
Ang2	Angiopoietin-2
ANOVA	Analysis of variance

B

B2M	Beta-2-microglobulin
BMCs	Bone marrow cells
Bmp2	Bone morphogenetic protein
BSA	Bovine serum albumin

C

C19orf10	Open reading frame 10 on chromosome 19
Ca^{2+}	Calcium
CCl_4	Carbon tetrachloride
cDNA	Complementary DNA
CXCL12	C-X-C chemokine ligand 12

D

DAPI	4',6-Diamidino-2-Phenylindole
DDA	Data dependent acquisition mode
DDZ	German Diabetes Center
DTT	Dithiothreitol

E

E	Embryonic day
ECM	Extracellular matrix
ECs	Endothelial cells
EdU	5-ethynyl-2'-deoxyuridine
EGF	Epidermal growth factor
EGFR	Epidermal growth factor receptor
ELISAs	Enzyme-linked immunosorbent assays
ER	Endoplasmic reticulum
EthD-1	Ethidium homodimer-1

F

FA	Formic acid
FCS	Fetal calf serum

FcγR	Fc gamma receptor
FDRs	False discovery rates
FGFR1	Fibroblast growth factor receptor 1
FXR	Farnesoid X receptor

G

GAPDH	Glyceraldehyde 3-phosphate dehydrogenase
GLP-1	Glucagon-like peptide-1
Gpbar-1	G-protein coupled bile acid receptor TGR5

H

h	Hour
HEK293	Human embryonic kidney 293
HEPES	(4-(2-hydroxyethyl)-1-piperazineethanesulfonic acid
HGF	Hepatocyte growth factor
HLE	Hepatoma cell line
HNF4-α	Hepatocyte nuclear factor 4 alpha
HPRT	Hypoxanthine-guanine phosphoribosyltransferase
HRP	Horseradish peroxidase
HSCs	Hepatic stellate cells

I

ICAM-1	Intercellular adhesion molecule 1
ICH	Intracerebral hemorrhage
IgG	Immunoglobulin G
IL-6	Interleukin 6
iRT	Indexed retention time peptides

K

KCs	Kupffer cells
kDa	Kilodalton
KH	Krebs-Henseleit
KO	Knockout

L

LCL	Lower confidence limit
LC-MS/MS	Liquid chromatography tandem-mass spectrometry
LDL	Low-density lipoprotein
LSECs	Liver sinusoidal endothelial cells
LSM	Laser scan microscopy
LW/BW	Liver to bodyweight ratio
LYVE-1	Lymphatic vessel hyaluronan receptor-1

M

Mg^{2+}	Magnesium
MI	Myocardial infarction
min	Minute
MMPs	Matrix metalloproteinases
MVA	Motor vehicle accident
MYDGF	Myeloid-derived growth factor

N

NaCl	Sodium chloride
NAFLD	Non-alcoholic fatty liver disease
NDS	Normal donkey serum
NO	Nitric oxide

O

o/n	Over night

P

PBS	Phosphate-buffered saline
PCR	Polymerase chain reaction
PECAM-1	Platelet endothelial cell adhesion molecule
PFA	Paraformaldehyde
pH3	Phospho-Histone H3
PHx	Partial hepatectomy
PlGF	Placental growth factor
PLAs	Proximity ligation assays
PSMs	Peptide spectrum matches
p-Tyr	Tyrosine phosphorylation

R

RNA	Ribonucleic acid
rpm	Revolutions per minute
RSPO	R-spondin
RT	Room temperature

S

s.e.m.	Standard error of the mean
STEMI	ST-segment elevation MI
STM	Septum transversum mesenchyme

T

T2DM	Type 2 diabetes mellitus

TFA	Trifluoroacetic acid
TGF-β1	Transforming growth factor-β1
TNF-α	Tumor necrosis factor alpha

U

UCL	Upper confidence limit
uPA	Urokinase plasminogen activator

V

VE-Cadherin	Vascular endothelial cell cadherin
VEGFR	Vascular endothelial growth factor receptor
VEGFR2	Vascular endothelial growth factor receptor 2
VEGFR3	Vascular endothelial growth factor receptor 3
VNN1	Vascular non-inflammatory molecule-1

W

Wls	Cargo receptor Evi

2D	Two-dimensional
3D	Three-dimensional
36B4	Acidic ribosomal phosphoprotein P0

1. Summary

The liver is essential for many metabolic processes including glucose homeostasis and detoxification, but especially the high regenerative capacity makes the liver a unique organ in the human body. After acute liver injury such as two-thirds partial hepatectomy (PHx), the same amount of blood has to pass through the remaining part of the liver with its fewer blood vessels. Since the liver is a highly vascularized organ, it provides an excellent basis to sense mechanical forces that occur due to hemodynamic changes caused by blood perfusion and vasodilation. The vascular system within the liver consists of sinusoids lined with endothelial cells (ECs). ECs are known to be involved in the production and secretion of angiocrine signals, which are essential for organ growth, regeneration and disease.

Here, by using the liver as a model organ, we were the first to investigate whether hemodynamic changes sensed via sinusoidal mechanotransduction are able to promote the release of angiocrine signals and induce liver growth and regeneration. We performed *ex vivo* perfusion of mouse livers and *in vitro* mechanical stretching of human hepatic ECs to investigate whether hemodynamic changes result in the activation of mechanosensory complexes, including β1 integrin and VEGFR3. We found that an enhanced blood perfusion and mechanical stretching of hepatic ECs activate β1 integrin and VEGFR3 signaling, and induce the secretion of angiocrine signals such as HGF, IL-6, TNF-α and MMP9. Further, we performed co-culture experiments with human hepatic ECs and human hepatocytes to investigate whether the supernatant from mechanically stretched human hepatic ECs is able to induce human hepatocyte proliferation *in vitro*. Our results demonstrate that the supernatant from mechanically stretched human hepatic ECs is able to induce proliferation and prevent apoptosis of human hepatocytes. In addition, we report that the activation of endothelial β1 integrin is sufficient for the release of angiocrine signals that are able to promote proliferation of human hepatocytes. Next, we analyzed the supernatant from human hepatic ECs by using mass spectrometry-based proteomics to identify novel angiocrine signals. We could identify myeloid-derived growth factor (MYDGF) as a novel angiocrine signal. Finally, we used 2D human hepatocyte cultures and 3D organoid cultures to reveal the role of MYDGF on human hepatocyte proliferation. Our results showed that MYDGF is able to induce human hepatocyte proliferation *in vitro*.

In summary, we could show that blood perfusion and vasodilation sensed via sinusoidal mechanotransduction and the subsequent release of angiocrine signals result in liver growth and regeneration. With our findings, we provide a new, physiological relevant, mechanism that links mechano-induced angiocrine signals to liver regeneration.

2. Zusammenfassung

Die Leber ist für viele Stoffwechselprozesse, einschließlich der Glukosehomöostase und der Entgiftung unerlässlich. Insbesondere die enorme Regenerationsfähigkeit macht die Leber zu einem einzigartigen Organ im menschlichen Körper. Nach einer akuten Leberverletzung, wie der zwei Drittel partiellen Hepatektomie (PHx), muss die gleiche Menge an Blut durch den noch verbliebenen Teil der Leber und somit durch eine geringeren Anzahl an Blutgefäßen fließen. Da die Leber ein stark vaskularisiertes Organ ist, bietet sie eine ausgezeichnete Grundlage, um mechanische Kräfte zu erfassen, die aufgrund hämodynamischer Veränderungen durch Blutperfusion und Vasodilatation auftreten. Das Gefäßsystem innerhalb der Leber besteht aus Sinusoiden, die von Endothelzellen (ECs) ausgekleidet sind. Es ist bekannt, dass die ECs an der Produktion und Sekretion angiokriner Signale beteiligt sind, die für das Wachstum, die Regeneration und die Erkrankung von Organen unerlässlich sind.

Wir haben anhand der Leber als Modellorgan erstmals untersucht, ob hämodynamische Veränderungen, die über die sinusoidale Mechanotransduktion erfasst werden, in der Lage sind, die Freisetzung angiokriner Signale zu fördern und das Leberwachstum sowie die Leberregeneration zu induzieren. Wir führten *ex vivo* Perfusionen von Mauslebern und *in vitro* mechanische Streck-Experimente mit humanen hepatischen ECs durch. Mit Hilfe dessen untersuchten wir, ob hämodynamische Veränderungen zur Aktivierung mechanosensorischer Komplexe, wie zum Beispiel β1 Integrin und VEGFR3, führen. Wir fanden heraus, dass eine erhöhte Blutperfusion und mechanisches Strecken von hepatischen ECs β1 Integrin und VEGFR3 aktiviert und die Sekretion angiokriner Signale wie HGF, IL-6, TNF-α und MMP9 induziert. Darüber hinaus führten wir Co-Kultur-Experimente mit humanen hepatischen ECs und humanen Hepatozyten durch, um zu untersuchen, ob der Überstand von mechanisch gestreckten humanen hepatischen ECs in der Lage ist, die Proliferation von humanen Hepatozyten *in vitro* zu induzieren. Unsere Ergebnisse zeigen, dass der Überstand von mechanisch gestreckten humanen hepatischen ECs in der Lage ist, die Proliferation menschlicher Hepatozyten zu induzieren und deren Apoptose zu verhindern. Darüber hinaus konnten wir zeigen, dass die Aktivierung von endothelialem β1 Integrin ausreichend ist, um angiokrine Signale freizusetzen, die die Proliferation menschlicher Hepatozyten fördern. Als nächstes analysierten wir den Überstand von humanen hepatischen ECs mittels Massenspektrometrie, um unbekannte angiokrine Signale zu identifizieren. Wir konnten den myeloid-derived growth factor (MYDGF) als ein neuartiges angiokrines Signal identifizieren. Schließlich verwendeten wir 2D-Kulturen menschlicher Hepatozyten und 3D-

Organoidkulturen, um die Rolle von MYDGF bei der Proliferation menschlicher Hepatozyten aufzudecken. Unsere Ergebnisse zeigen, dass MYDGF in der Lage ist, die Proliferation menschlicher Hepatozyten *in vitro* zu induzieren.

Zusammenfassend konnten wir zeigen, dass Blutperfusion und Vasodilatation, die zu sinusoidaler Mechanotransduktion und der anschließenden Freisetzung angiokriner Signale führen, das Leberwachstum sowie die Leberregeneration induzieren. Mit unseren Ergebnissen liefern wir einen neuen, physiologisch relevanten Mechanismus, der mechanisch-induzierte angiokrine Signale mit der Leberregeneration verbindet.

3. Introduction

3.1 The liver

The liver is one of the most vital organs in the human body and is responsible for detoxification and glucose homeostasis. The liver accounts for approximately two percent of the total body weight and is located in the right upper abdomen. Anatomically, the liver is divided into four lobes. In humans these are called the larger right, left, caudate and quadrate lobe and in mice the larger left, right, caudate and median lobe (Treuting et al., 2011). Based on the Couinaud classification, which is broadly used in the clinic, the human liver is divided into eight segments, with each of them having its own vascular supply and biliary drainage (Couinaud, 1954).

Unlike other organs in the human body, the liver has a dual blood supply (Figure 1). The hepatic artery supplies oxygenated blood from the heart and the portal vein supplies venous, nutrient-rich blood, drained from parts of the gastrointestinal tract, the spleen and the pancreas (Ishibashi et al., 2009, Abdel-Misih and Bloomston, 2010). Within sinusoids, which are the smallest blood vessels of the liver, arterial and portal venous blood mixes, and the hepatic vein drains deoxygenated blood back to the heart (Ishibashi et al., 2009, Abdel-Misih and Bloomston, 2010).

On the microscopic level, the liver lobule is the smallest structural unit and the acinus is the smallest functional unit of the liver (Figure 1) (Kiernan, 1833, Rappaport et al., 1954). Lobules are hexagonal structures consisting of hepatocytes that are arranged as plates with intervening sinusoids. A hepatic venule, which branches from the hepatic vein, is located at the center and portal triads are located at the periphery of the liver lobule. One portal triad is located at each corner of the hexagon and consists of a branch of the hepatic artery, a branch of the portal vein, called hepatic arteriole and portal venule respectively, bile ducts and lymphatics (Ishibashi et al., 2009). The liver acinus is the functional unit of the liver and is defined mainly in terms of the blood supply. Acini are ellipse-shaped and extend from the portal triad to the hepatic venule (Häussinger, 2014). Hepatocytes along the axis from the portal triad to the hepatic venule are divided into three different zones that is referred to as metabolic zonation (Kietzmann, 2017).

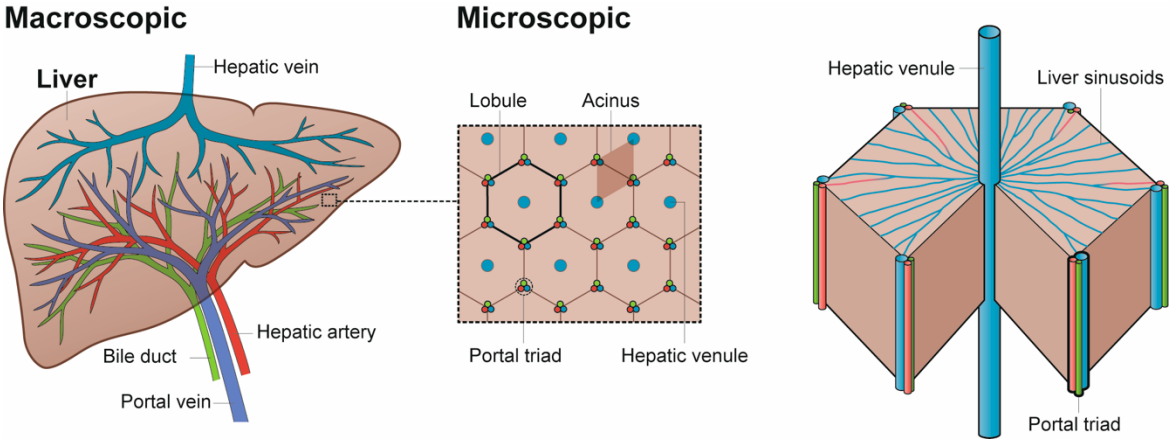

Figure 1: Schematic illustration of liver anatomy and physiology. The liver has a dual blood supply. The hepatic artery supplies oxygen-rich blood from the heart, and the portal vein supplies nutrient-rich blood from parts of the gastrointestinal tract, the spleen and the pancreas. The liver lobule and the liver acinus are microscopically the smallest units of the liver. The lobule has a hexagonal structure, while the acinus is ellipse-shaped. The blood flows from the portal triad, which consists of hepatic arteriole, portal venule, bile ducts and lymphatics (not shown), to the hepatic venule. Figure was drafted by Linda Große-Segerath, and illustrated by Yousun Koh.

The liver plays an important role in many metabolic processes, such as the synthesis of serum proteins, nutrient metabolism, the production and secretion of bile and detoxification (Häussinger, 2014, Trefts et al., 2017, Alamri, 2018). For example, albumin, which is essential for oncotic pressure, and acute phase proteins, which are needed in response to inflammation, are synthesized by the liver (Häussinger, 2014, Trefts et al., 2017). On the other hand, the liver is involved in protein catabolism by breaking down amino acids. Ammonia is a toxic by-product of the amino acid metabolism. In a process called urea cycle, ammonia is converted into urea that is subsequently excreted by the kidney in form of urine (Häussinger, 2014). Apart from its capacity to metabolize proteins, the liver is also responsible for glucose homeostasis. In order to provide the body with physiological amounts of glucose, glucose is synthesized into glycogen that is stored in the liver and can be degraded on-demand by glycogenolysis. Additionally, glucose can also be synthesized from non-carbohydrate precursors by gluconeogenesis (Alamri, 2018). Notably, the lipid metabolism is closely related to the carbohydrate metabolism. It includes a process called *de novo* lipogenesis, in which fatty acids can be synthesized from non-lipid sources. Besides, free fatty acids can be absorbed from the blood and used for energy metabolism or stored as triglycerides (Trefts et al., 2017). Next to its endocrine function, the liver is also an exocrine gland. This includes the production and secretion of bile, which is transported in the opposite direction to the blood flow, and stored in the gallbladder. Bile consists of water (approximately 95%), bile acids, which are exclusively synthesized by the liver,

phospholipids, electrolytes and bilirubin. Bile is necessary for the breakdown and the absorption of lipids during digestion (Boyer, 2013). Other central tasks of the liver are the detoxification of harmful substances like endo- and xenobiotics, as well as important functions in immunity (Häussinger, 2014, Trefts et al., 2017, Alamri, 2018).

To sum up, unlike other organs in the human body, the liver has a dual blood supply and is perfused from the portal vein and the hepatic artery. The liver is one of the most metabolically active organs and involved in synthesis of serum proteins, glucose homeostasis, production and secretion of bile and detoxification.

3.1.1 Cell types of the liver

In order to gain deeper insights into liver function, growth and regeneration, it is necessary to understand the different cell types of the liver (Figure 2). The liver consists of parenchymal and non-parenchymal cells. The parenchyma is mainly made up of hepatocytes, and with around 78% it represents the majority of liver volume (Blouin et al., 1977). Non-parenchymal cells account for around 6% and include sinusoidal endothelial cells, stellate cells, Kupffer cells, pit cells and cholangiocytes (also known as biliary epithelial cells). The remaining 16% of liver volume is formed by extracellular space, which includes the sinusoidal lumen, the space of Disse and bile canaliculi (Blouin et al., 1977, Ishibashi et al., 2009).

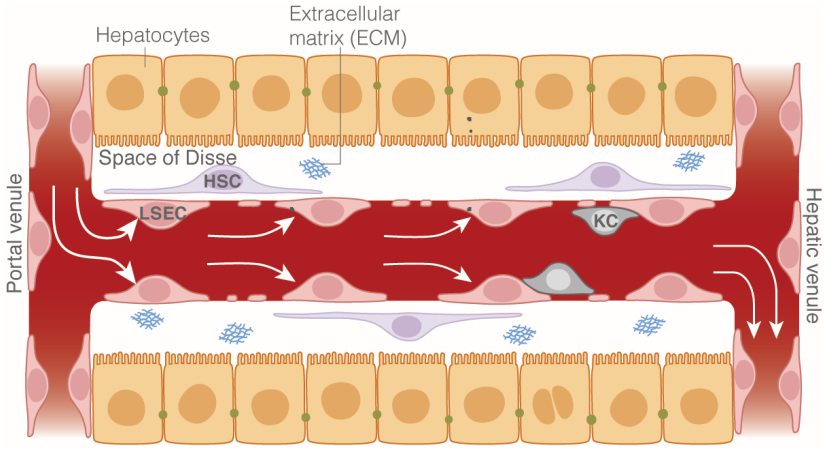

Figure 2: Schematic illustration of a liver sinusoid and the different cell types of the liver. The blood flows along sinusoids from the portal venule to the hepatic venule. Liver sinusoidal endothelial cells (LSECs) line the sinusoidal lumen. Kupffer cells (KCs) are adherent to LSECs and are, like LSECs, in direct contact with the blood. Both, LSECs and KCs, are separated by the space of Disse from hepatocytes. Hepatic stellate cells (HSCs) are located in the space of Disse. Modified from (Lorenz et al., 2018), illustrated by Yousun Koh.

Hepatocytes are the main cellular unit of the liver. Structurally, hepatocytes are organized as plates with dilated intercellular spaces between adjacent hepatocytes forming tubular channels known as bile canaliculi. The bile canaliculi transport the bile that is secreted by hepatocytes to cholangiocytes, which line the biliary tree (Tabibian et al., 2013). Cholangiocytes modify the bile, for example, by secretion of bicarbonate, chloride and water as well as absorption of bile acids, glucose and amino acids, before it is secreted into the digestive tract (Tabibian et al., 2013). Additionally, hepatocytes are responsible for detoxification of xenobiotics, production of plasma proteins such as albumin and fibrinogen and secretion of hormones such as hepcidin, which regulates iron homeostasis in the body. One hallmark of hepatocytes is their mononucleated or binucleated polyploidization, which occurs mainly during developmental stages and in adults with increasing age or as a result of different stimuli, such as cellular stress (Duncan et al., 2010, Celton-Morizur and Desdouets, 2010).

Hepatocytes are separated by the space of Disse from liver sinusoidal endothelial cells (LSECs) and hepatic stellate cells (HSCs). As the name implies, LSECs form a thin endothelial cell layer of the hepatic sinusoid. LSECs are typically characterized by fenestrae, which are 100-200 nm in diameter and clustered in sieve plates (Braet and Wisse, 2002). In general, fenestrae occupy 6-8% of the LSECs surface. Together with the lack of a basement membrane, they give LSECs the ability to function as a selective sieve that only allows molecules with diameters smaller than the diameter of fenestrae to pass (Sorensen et al., 2015, DeLeve, 2013). In addition to fenestrae, LSECs form unique kinds of mixed-type intercellular junctions (Adherens junctions co-occur with junctional adhesion molecules but not with common tight junction proteins such as claudin-5 or occludin) that control vascular permeability and cell trafficking and contribute to endothelial barrier function (Geraud et al., 2012). These morphological hallmarks of LSECs allow the passive transport of molecules from the sinusoidal lumen, through the space of Disse, to parenchymal and non-parenchymal cells of the liver (Braet and Wisse, 2002, Sorensen et al., 2015). In addition to their role as a permeable barrier, LSECs have an enormous endocytotic capacity (Sorensen et al., 2012). Via receptors for endocytosis, including mannose receptors and scavenger receptors, soluble macromolecular waste and colloids can be removed from the blood. For example, the scavenger receptor Stabilin-2, which is highly expressed on LSECs, is involved in the removal of oxidized and acetylated low-density lipoprotein (LDL) from the blood (Sorensen et al., 2012, Li et al., 2011). Both the expression of Stabilin-2 and the uptake of acetylated LDL are used as markers to assess the purity of LSECs (DeLeve and Maretti-Mira, 2017, Poisson et al., 2017). Furthermore, LSECs have similar functions to immune cells. These include Fc gamma receptor (FcγR)-

mediated endocytosis (mainly due to FcγRIIb2) of immune complexes, and the ability to recruit and adhere leukocytes during inflammation (Knolle and Wohlleber, 2016, Mousavi et al., 2007, Shetty et al., 2018). Interestingly, LSECs express hematopoietic markers such as CD45 and CD33 suggesting that LSECs originate from the bone marrow (Harb et al., 2009, Xie et al., 2010). This is further substantiated by studies showing that LSECs express the scavenger receptors Stabilin-1 and -2, which are also found on bone marrow sinusoidal ECs (Qian et al., 2009). Besides, LSECs also have some similarities to lymphatic ECs. Both either lack or have a minimal basement membrane (Sorensen et al., 2015) and express lymphatic vessel hyaluronan receptor-1 (LYVE-1) (Mouta Carreira et al., 2001) and vascular endothelial growth factor receptor 3 (VEGFR3) (Ding et al., 2010).

Kupffer cells are liver-resident macrophages located in the hepatic sinusoid, adherent to LSECs and in direct contact with blood components. Due to their location, Kupffer cells play a central role in the immune response. They have an enormous phagocytotic activity and present antigens to capture and clear pathogens from the blood (Dixon et al., 2013, Jenne and Kubes, 2013). Next to Kupffer cells also pit cells (liver-associated natural killer cells) are involved in the immune response against tumor cells or virus-infected cells by spontaneous cytotoxic activity (Luo et al., 2000).

HSCs are located between hepatocytes and LSECs in the space of Disse. Quiescent HSCs store retinoids in lipid droplets and maintain extracellular matrix (ECM) homeostasis (Häussinger, 2014). HSCs were identified as mesenchymal stem cells with the space of Disse being their stem cell niche. During liver development or upon injury, HSCs become activated to support hematopoiesis and regeneration (Haussinger and Kordes, 2019). However, chronic liver injury leads to an activation of HSCs into myofibroblast-like cells. These cells are implicated in the deposition of ECM proteins and promote the development of liver fibrosis (Friedman, 2008).

Although the general functions of the cell types of the liver are well-established, evidence of recent studies suggests that subpopulations within the same cell type are responsible for different functions. Single-cell RNA sequencing was used to better characterize the differences between subpopulations of the same cell type (Aizarani et al., 2019). By using this method, a human liver cell atlas was generated in which inter- and intra-population differences of liver cells were observed. Both hepatocytes and LSECs showed high transcriptome-wide heterogeneity, and new subtypes of hepatocytes, ECs and Kupffer cells were identified (Aizarani et al., 2019).

In conclusion, the different cell types of the liver are essential to maintain liver function. Due to heterogeneity of the cells, the same cell type can take over different tasks, while different cells can share similar function. This makes the liver an even more complex system.

3.1.2 Liver regeneration

One of the most fascinating abilities of the liver is its enormous regenerative capacity, which is used in clinical approaches to treat patients with end-stage liver disease. Besides transplanting the whole liver from a deceased donor, there are other application methods, which take advantage of the regenerative capacity of the liver (Miller and Diago Uso, 2013). For example, by split liver transplantation, the liver from a deceased donor is divided into two parts, and thus can be transplanted into two patients (Hackl et al., 2018). Furthermore, as the availability of livers from deceased donors is limited, living-donor transplantation was developed. Given the liver's unique capacity to regenerate after invasive procedures, part of it can be transplanted from a living donor into a patient without severely harming the donor (Marcos, 2000).

There are several different models available to study liver regeneration. For example, chemical-induced injury models such as the treatment with carbon tetrachloride (CCl_4), which can induce acute or chronic liver injury, or surgical resection models. Until now, the most popular surgical resection model to induce acute liver injury is partial hepatectomy (PHx), which was first studied in rodents in 1931. In this approach, two-thirds of the liver is surgically removed (Higgins, 1931). Within the regenerative process, the remaining liver is able to restore its original size in approximately 5-7 days in mice and 8-15 days in humans (Michalopoulos, 2007). Notably, in contrast to other tissues in which regenerative processes are often driven by stem cells or progenitor cells (Rafii and Lyden, 2003), the restoration of the lost liver mass is mediated by mature hepatocytes and non-parenchymal cells of the remaining liver (Michalopoulos, 2007). Thus, surgical removement triggers the increase in cell size (hypertrophy) and in cell number (proliferation) and leads to a restoration of the initial liver mass (Michalopoulos, 2007).

After PHx, hepatocytes, which are normally quiescent (in the G0 phase of the cell cycle), reenter the cell cycle due to different stimuli. The early responses include expression changes in a large number of genes, including *c-jun*, *c-fos*, and *c-myc* (Mohn et al., 1991, Morello et al., 1990). Moreover, activity of urokinase plasminogen activator (uPA), known to be involved in ECM remodeling by initiation of proteolytic cascades, increases already

five minutes after PHx (Mars et al., 1995, Mangnall et al., 2004). uPA catalyzes plasmin production, which leads to the degradation of fibrinogen, the substrate of plasmin and a component of the ECM (Kim et al., 1997). In addition, matrix metalloproteinases (MMPs) that also contribute to ECM remodeling show elevated levels of their inactive and active form half an hour and three hours after PHx, respectively (Kim et al., 2000). Remodeling of the ECM contributes to the mobilization of hepatocyte growth factor (HGF) that is deposited in the ECM. For example, uPA is able to convert inactive HGF into its active form (Mars et al., 1995). However, HGF is also synthesized by stellate cells and LSECs around three hours following PHx (Michalopoulos, 2007). HGF and its receptor Met (also known as c-Met), as well as epidermal growth factor (EGF) and its receptor (EGFR), are essential factors for liver regeneration (Michalopoulos, 2007). Injection of HGF into mice causes hepatocyte proliferation (Patijn et al., 1998), whereas homozygous deletion of HGF results in a reduced liver size and embryonic lethality (Schmidt et al., 1995). *In vitro* experiments show that recombinant HGF or EGF initiate DNA synthesis of primary human or rat hepatocytes, respectively (Gomez-Lechon et al., 1995, Richman et al., 1976). Although necessary for liver regeneration, HGF and EGF alone are not sufficient to drive liver regeneration. In addition to growth factors and their receptors, cytokines such as interleukin-6 (IL-6) and tumor necrosis factor (TNF) (Cressman et al., 1996, Yamada et al., 1997, Taub, 2004, Fausto et al., 2012), as well as bile acids are involved in regulating the regenerative process (Huang et al., 2006, Pean et al., 2013). For example, IL-6-deficient mice show an impaired liver regeneration after PHx (Cressman et al., 1996), and IL-6 trans-signaling was reported to control liver regeneration (Fazel Modares et al., 2019). Furthermore, blocking TNF-α signaling in rats, before performing a PHx, results in reduced cell proliferation of hepatocytes and non-parenchymal cells (Akerman et al., 1992). Bile acids are synthesized in the liver and can promote both cell proliferation and apoptosis, depending on the bile acid and the cell type (Häussinger et al., 2012, Keitel et al., 2008). Bile acids binding to the nuclear farnesoid X receptor (FXR), which is one of the main drivers of bile acid homeostasis, promote liver regeneration after liver resection or injury by transient elevated bile acid levels (Huang et al., 2006). However, sustained elevated levels and an overload of bile acids are toxic for the liver. The G-protein coupled bile acid receptor TGR5 (also known as Gpbar-1) protects the liver from bile acid overload and prevents bile acid toxicity after PHx (Pean et al., 2013). In general, multiple different growth factors, cytokines and bile acids promote the cell cycle progression of hepatocytes leading to hepatocyte proliferation. During the early or inductive phase of liver regeneration, hepatocytes proliferate (Fausto et al., 2012, Gilgenkrantz and Collin de l'Hortet, 2018, Michalopoulos, 2007). Thereafter, also cholangiocytes, followed by stellate cells and LSECs start to proliferate (Michalopoulos, 2007). The latter are essential to form sinusoidal

linings via angiogenesis and restore the sinusoidal network within the liver. This phase is called angiogenic phase of liver regeneration (DeLeve, 2013). Once the liver mass is restored, the regenerative process is terminated. Consequently, termination of liver regeneration needs a control system that mediates liver-to-body weight ratio and prevents liver overgrowth (Michalopoulos, 2007).

Upon acute liver injury induced by PHx, the liver is able to regenerate and the liver-to-body weight ratio is controlled and restored. In contrast, chronic liver injury caused by inflammation, viruses or toxins, disturbs the regenerative process and liver injury can progress in liver cirrhosis and hepatocellular carcinoma (Michalopoulos, 2017). This indicates that an essential stimulus differs between acute and chronic liver injury. A major difference between acute and chronic liver injury is the vascular perfusion within the liver. Since after PHx the same amount of blood has to pass through the remaining part of the liver, the liver's vasculature is exposed to enormous mechanical forces (Michalopoulos, 2007). By contrast, the vascular system undergoes less severe changes upon chronic liver injury. Gaining a thorough understanding about hemodynamic changes occurring upon liver injury is key for comprehending the mechanism of liver regeneration. Until now, the underlying mechanism of liver regeneration still challenges researchers and leaves many questions unanswered.

3.1.3 Mechanotransduction in the liver

Mechanotransduction is the transduction of external physical forces into downstream signals and is mediated by the cytoskeleton, mechanoreceptors like integrins, ion channels like Piezo, and the ECM. In general, cells are constantly exposed to different kinds of forces, which can vary between different cell or tissue types (Ingber, 2003). For instance, during embryogenesis, mechanical forces induce the growth of the lymphatic vasculature, due to an increased amount of interstitial fluid (Planas-Paz et al., 2012). Similarly, during embryonic liver development, the growth of the developing organ correlates with an enhanced vascular perfusion through the organ (Lorenz et al., 2018). In disease, mechanical forces such as a low or disturbed pattern of blood flow promote the formation of atherosclerotic plaques in arteries, and progress atherosclerosis (Kwak et al., 2014). Furthermore, hemodynamic alterations in the liver are associated with liver disease (Kowalski and Abelmann, 1953, Murray et al., 1958, Iwakiri and Groszmann, 2006, Kim et al., 2010). Thus, mechanical forces and mechanotransduction are key factors in the development, physiology and also in disease (Ingber, 2003).

The liver is a highly vascularized organ and therefore an excellent basis to sense mechanical forces and changes in these forces, which underlie, for example, vascular perfusion. LSECs, as the inner layer of sinusoids, are constantly exposed to multiple mechanical stimuli, such as blood flow and blood pressure. Whereas blood flow causes mainly shear stress, blood pressure causes circumferential stretch (Urner et al., 2018). The transduction of shear stress or stretch into downstream signals is accomplished by mechanotransducers. A well-known mechanosensory complex mediating EC response to shear stress consists of platelet endothelial cell adhesion molecule (PECAM-1), vascular endothelial cell cadherin (VE-cadherin) and vascular endothelial cell growth factor receptor 2 (VEGFR2) (Tzima et al., 2005). Furthermore, the ion channel Piezo1 is activated by shear stress and essential for the transduction of forces at the plasma membrane of ECs (Coste et al., 2010). Integrins, which link the ECM with the cytoskeleton, play a central role in mechanotransduction, either as direct mechanotransducers or as transmitters of force (Ingber, 1991, Katsumi et al., 2004, Planas-Paz et al., 2012).

Integrins comprise a family of 24 αβ heterodimers, which can be formed out of 18 α subunits and 8 β subunits (Hynes, 2002). β1 integrin represents the largest subgroup of integrins and is essential for embryonic development and the vascular system. The global knockout (KO) of *Itgb1* (β1 integrin gene) leads to embryonic lethality (Fassler and Meyer, 1995, Stephens et al., 1995). EC-specific genetic deletion of *Itgb1* using *Tie2-Cre* or *Flk1-Cre* transgenic mice also result in embryonic lethality at different time points of embryonic development (Tanjore et al., 2008, Lei et al., 2008, Carlson et al., 2008, Planas-Paz et al., 2012). Activation of integrins is associated with conformational changes of the subunits from a bent to an extended conformation, and can be mediated among others by mechanical forces (Sun et al., 2019). In their activated state, the extracellular domain of integrins can bind to the ECM. For example, α5β1 binds to the ECM component fibronectin, which stimulates the interaction of β1 integrin and VEGFR3, and induces tyrosine phosphorylation of VEGFR3 (Wang et al., 2001, Zhang et al., 2005). VEGFR3 is one of the three members of the vascular endothelial growth factor receptor (VEGFR) family. VEGFRs function as tyrosine-kinases, with an intracellular enzymatic tyrosine kinase domain and an extracellular ligand binding domain. Known ligands are VEGF-A, -B, -C, -D and placental growth factor (PlGF), with VEGF-C and VEGF-D binding to VEGFR3 (Tammela et al., 2005). However, in lymphatic ECs not only ligand binding, but also mechanical activation of β1 integrin can induce VEGFR3 phosphorylation (Planas-Paz et al., 2012).

Although mechanoresponsive signaling pathways have gained attention in ECs, little is known about these pathways in LSECs. Since the liver is a highly vascularized organ and

LSECs are constantly exposed to different mechanical stimuli, it is expected that mechanotransduction plays an important role in the liver and has been underestimated so far.

3.2 Angiocrine signals

Angiocrine signals are paracrine factors produced by ECs, and are involved in organ growth, regeneration and disease (Rafii et al., 2016, Kostallari and Shah, 2016). In general, EC-derived signals were discovered more than four decades ago (Gajdusek et al., 1980, Quesenberry and Gimbrone, 1980). They were shown to affect several organs, like the liver, pancreas, heart, lung, bone marrow and brain (Rafii et al., 2016, Augustin and Koh, 2017). Since ECs are involved in angiocrine signaling in distinct organs, the secretion of factors varies between organ-specific ECs. Angiocrine signals include growth factors, cytokines, chemokines, trophogens, ECM components and other EC-derived signals that have the potential to promote organ homeostasis and regeneration (Rafii et al., 2016).

3.2.1 Angiocrine signals in liver development, growth and homeostasis

EC-derived factors have the potential to promote organogenesis (Lammert et al., 2001, Matsumoto et al., 2001). In general, the three germ layers, the endoderm, mesoderm and ectoderm form internal organs during organogenesis. This process is based on orchestrated signaling between the germ layers to achieve proper development. ECs are involved in early organogenesis of the liver and the pancreas, which both develop by budding from the endoderm in a stepwise manner (Lammert et al., 2001, Matsumoto et al., 2001). Particularly, after hepatic specification from the gut endoderm, early ECs intervene between hepatic endoderm cells and the septum transversum mesenchyme (STM) to promote the proliferation and migration of hepatic endoderm cells into the STM (Matsumoto et al., 2001). This morphogenic process progresses the formation of the liver bud. Thus, the emergence of the hepatic bud requires endothelial-endoderm interaction, while the absence of ECs leads to defects in its formation (Matsumoto et al., 2001). However, it remains unclear which specific angiocrine signals are secreted by ECs during the early steps of organogenesis.

Embryonic liver growth in mice drastically increases between embryonic day (E) 12.5 and E 13.5. Directly before the burst of liver growth, liver perfusion starts at the liver periphery towards the center underscoring a correlation between vascular perfusion and liver growth (Lorenz et al., 2018). In particular, manipulating the blood flow through the embryonic liver vasculature correlates with the activation of the mechanoreceptors β1 integrin and VEGFR3. Both are essential for the production of angiocrine HGF and thus for the growing liver (Lorenz et al., 2018). Therefore, blood flow can act as a mechanical stimulus to activate mechanoresponsive proteins on ECs and trigger embryonic mouse liver growth (Lorenz et al., 2018).

Angiocrine signals are also essential in postnatal liver development to control liver growth and homeostasis (Rocha et al., 2015, Koch et al., 2017, Leibing et al., 2018, Kostallari and Shah, 2016). In particular, metabolic zonation, which is established shortly after birth (Torre et al., 2010), requires angiocrine signals for a proper maturation and maintenance in the adult liver (Rocha et al., 2015, Leibing et al., 2018). Wnt/β-catenin signaling, which is regulated by a cell surface complex (RSPO-LGR4/5-ZNRF3/RNF43) including R-spondin (RSPO), is required for this process (Planas-Paz et al., 2016). Both, the Wnt antagonist RSPO3 and Wnt ligands are EC-derived factors, and are essential to determine and preserve metabolic zonation, respectively (Rocha et al., 2015, Leibing et al., 2018). The latter were studied by using hepatic EC-specific genetic deletion of the cargo receptor Evi (short Wls), which is critical for exocytosis of Wnt ligands (Leibing et al., 2018). EC-specific genetic deletion of Wls results in a reduced liver-to-body weight ratio as well as in an impaired metabolic zonation. In contrast, the heterogeneity of ECs is not altered and the rescue of Wls shows a restored metabolic zonation (Leibing et al., 2018). This suggests that Wnt ligands secreted by hepatic ECs control liver growth and metabolic zonation (Leibing et al., 2018).

Angiocrine signals are not limited to developmental and growth-promoting processes, but are also involved in homeostasis. This has been shown for EC-derived Wnt ligands and the bone morphogenetic protein (Bmp2) (Wang et al., 2015, Koch et al., 2017). The latter affects iron homeostasis in the liver. EC-specific genetic deletion of *Bmp2* causes massive iron overload, which is mediated by the expression of hepatocyte hepcidin (a key regulator for iron homeostasis) (Koch et al., 2017). Further, EC-derived signals are also essential to maintain quiescence of hepatic stellate cells. Since HSCs are the main driver of liver fibrosis by producing collagen, they need to receive angiocrine signals from ECs in order to balance the production of collagen (Deleve et al., 2008, Xie et al., 2012). In general, the

interaction of all cell types within the liver and their contact to each other is essential to maintain liver homeostasis.

3.2.2 Angiocrine signals in liver regeneration and disease

In the adult system, angiocrine signals are not only involved in organ homeostasis but also in regeneration and disease (Kostallari and Shah, 2016, Rafii et al., 2016). Furthermore, angiocrine metabolic communication was recently shown to actively control skeletal muscle regeneration by the release of lactate (Zhang et al., 2020a). The model of PHx can be used to study the role of angiocrine signals in liver regeneration, since the residual liver vasculature and LSECs are still intact in the remaining part of the liver. In the recent years, several research groups reported on different angiocrine signals that are involved in hepatocyte proliferation after PHx (Ding et al., 2010, Zhang et al., 2020b, Hu et al., 2014, Rafii et al., 2016). For example, activation of VEGFR2 induces upregulation of the transcription factor Id1 in LSECs, which contributes to the release of angiocrine factors such as Wnt2 and HGF that are able to promote hepatocyte proliferation (Ding et al., 2010). By using mice with a LSEC-specific deletion of *Hgf* from E 9.5 onwards, HGF signaling was recently reported to control total liver and body weight as well as hepatocyte proliferation during regeneration (Zhang et al., 2020b). Furthermore, the downregulation of Angiopoietin-2 (Ang2) in LSECs shortly after PHx leads to a reduced production of transforming growth factor-β1 (TGF-β1) (Hu et al., 2014). Since TGF-β1 is a potent inhibitor of hepatocyte proliferation (Fausto et al., 1991), the downregulation of LSEC-derived Ang2 is essential for hepatocyte proliferation (Hu et al., 2014). By contrast, during the angiogenic phase of liver regeneration the recovery of Ang2 expression is necessary to control proliferation of LSECs in an autocrine manner (Hu et al., 2014).

Angiocrine signals promote liver regeneration after acute injury (Rafii et al., 2016). However, the angiocrine response of LSECs can shift after chronic injury and promote e.g. liver fibrosis. In particular, this was shown for the C-X-C chemokine ligand 12 (CXCL12) receptors CXCR7 and CXCR4 (Ding et al., 2014). CXCR7 is upregulated in LSECs after acute liver injury, and, together with CXCR4, induces an Id1-mediated upregulation of angiocrine factors (Ding et al., 2010, Ding et al., 2014). On the contrary, after chronic injury the activation of CXCR4, which is then dependent on fibroblast growth factor receptor 1 (FGFR1), is enhanced in LSECs. Enhanced signaling by CXCR4 shifts the regenerative response to the release of angiocrine signals that are able to provoke liver fibrosis.

Orchestrated signaling is therefore necessary to control liver regeneration and prevent liver fibrosis (Ding et al., 2014). In particular, Notch was reported as a critical player in liver regeneration and repair (Morell and Strazzabosco, 2014), since the activation of Notch can alter the release of angiocrine signals from LSECs. This can lead, for example, to an impaired liver regeneration after PHx or the development of fibrosis, which was shown in a mouse model in which chronic liver damage was induced by CCL_4 (Duan et al., 2018, Tanriverdi et al., 2016). Kruppel-like factor 2 (KLF2)-induced expression and secretion of Activin A from hepatic ECs was also identified as growth-inhibiting angiocrine signal in the regenerating liver after treatment with CCL_4 (Manavski et al., 2017).

To sum up, angiocrine signals are involved in liver development, growth, homeostasis, and regeneration (Rafii et al., 2016), pointing to an important role of hepatic ECs beyond that of a passive conduit. Since angiocrine signals play a key role in balancing the shift from liver regeneration to liver fibrosis (Ding et al., 2014), angiocrine signals could be used to prevent or treat liver disease.

3.3 Myeloid-derived growth factor (MYDGF)

The myeloid-derived growth factor (MYDGF) obtained its name in 2015 when it was discovered to have an impact on heart regeneration following myocardial infarction (MI) when present as a secreted protein (Korf-Klingebiel et al., 2015). In general, it is an evolutionary highly conserved protein and expressed in several different tissues, like the heart or the liver (Korf-Klingebiel et al., 2015). MYDGF is encoded by an open reading frame 10 on chromosome 19 (*C19orf10*) with a theoretical molecular mass of around 16 kilodalton (kDa). It consists of 142 amino acids, with a signal peptide at the N-terminus (Korf-Klingebiel et al., 2015, Bortnov et al., 2018). Interestingly, the three-dimensional structure was recently revealed by X-ray as well as protein nuclear magnetic resonance (NMR) spectroscopy and shows a unique folding structure that does not belong to any known growth factor or cytokine family (Ebenhoch et al., 2019, Bortnov et al., 2019). Only the base domain of vascular non-inflammatory molecule-1 (VNN1) was reported to share a sequence identity of 15% with human MYDGF (Bortnov et al., 2019). VNN1 is an ectoenzyme involved in the metabolism of coenzyme A and is highly expressed in many organs including the liver (Aurrand-Lions et al., 1996, Maras et al., 1999). However, a possible receptor or binding partners for MYDGF could not be identified until now.

Although MYDGF obtained its name in 2015, research on its function already began eleven years earlier when the homologous mouse protein of MYDGF was identified as SF20/IL25. The protein was identified as a novel bone marrow stromal-derived factor with impact on lymphoid cell proliferation (Tulin et al., 2001). However, the paper was retracted when the authors were unable to reproduce the cell proliferative effect of SF20/IL25 (Tulin et al., 2003). Subsequently, SF20/IL25 was identified as a secreted factor from adipocytes (Wang et al., 2004), and three years later it was identified as a fibroblast-like synoviocyte-derived factor that is secreted into the synovial fluid (Weiler et al., 2007). However, none of these studies identified a function for SF20/IL25, and as a result the protein was no longer called SF20/IL25. Instead, the name of the encoding gene *C19orf10* was used. Except for the literature mentioned here, in which C19orf10 was called SF20/IL25, the designation SF20/IL25 from other sources does not refer to C19orf10 (Weiler et al., 2007). *C19orf10* is overexpressed in hepatocellular carcinomas, and the undifferentiated, alpha-fetoprotein negative hepatoma cell line (HLE) proliferates in a dose-dependent manner when treated with FLAG-tagged C19orf10 (Sunagozaka et al., 2011).

C19orf10 was named MYDGF when it was first identified as a secreted protein from MACS-purified CXCR4^{high} bone marrow cells (BMCs) from patients with acute MI (Korf-Klingebiel et al., 2015). CXCR4^{high} BMCs represent a subpopulation of BMCs that are known to be involved in cardiac repair (Petit et al., 2007, Seeger et al., 2009). Thus, MYDGF is involved in protection and repair of the heart after MI. KO of *Mydgf* in mice did not show a visible phenotype, but KO mice that underwent MI had larger infarct scars and stronger systolic dysfunction (Korf-Klingebiel et al., 2015). The blood plasma levels of MYDGF vary between healthy individuals and people with coronary artery disease (Polten et al., 2019). In healthy individuals blood plasma levels of MYDGF are around 3 ng/ml. The blood plasma levels of people who had ST-segment elevation MI (STEMI) are three-fold higher and around 9 ng/ml (Polten et al., 2019). Interestingly, blood plasma levels of MYDGF are decreased in people who suffer from type 2 diabetes mellitus (T2DM) compared to apparently healthy non-diabetic individuals (Wang et al., 2020). In this context, it was shown that MYDGF has an effect on the incretin system and promotes Glucagon-like peptide-1 (GLP-1) secretion and production (Wang et al., 2020). Typically, blood plasma levels of MYDGF decrease slightly with increasing age (Polten et al., 2019). Next to its function as a secreted protein, MYDGF was also shown to reside in the endoplasmic reticulum (ER). The C-terminal sequence is necessary for its retention in the ER (Bortnov et al., 2018). However, MYDGF can be secreted if the C-terminal sequence is cleaved. Strikingly, full length and C-terminal truncated MYDGF appears in the supernatant of *MYDGF* overexpressed human embryonic kidney 293 (HEK293) cells (Bortnov et al., 2018).

In summary, MYDGF was identified as a novel BMC-derived signal that promotes heart regeneration after MI (Korf-Klingebiel et al., 2015). Since the expression of MYDGF was reported for several tissues, the potential role of secreted MYDGF needs to be further investigated in other organs including the liver.

3.4 Aims of the study

Given the liver's remarkable regenerative capacity after acute injury, it is one of the most fascinating organs in the human body. However, the underlying mechanism of regeneration remained unresolved for decades and is still not fully understood.

Hemodynamic changes after acute liver injury are proposed to contribute to liver regeneration. For example, after two-thirds PHx the same amount of blood has to pass through the remaining part of the liver (Michalopoulos, 2007). We hypothesize that hepatic ECs respond to hemodynamic changes that occur due to liver injury and play an essential role in the regenerative process. ECs are exposed to multiple mechanical stimuli, such as blood flow and blood pressure, and may be a key factor in liver regeneration. Therefore, they have received more and more attention and are no longer only considered as passive conduits (Ingber, 2003, Augustin and Koh, 2017). However, little is known about mechano-sensing pathways in hepatic ECs. Therefore, we aimed to discover whether mechanosensory complexes on hepatic ECs are able to sense mechanical stimulation and in turn translate these stimulations into downstream signals. Since β1 integrin and VEGFR3 are known for being involved in mechanoresponsive signaling pathways (Wang et al., 2001, Zhang et al., 2005, Planas-Paz et al., 2012), we studied whether hemodynamic changes can activate β1 integrin and VEGFR3 on hepatic ECs.

Angiocrine signals were reported to promote organ growth, homeostasis and regeneration in several organs (Rafii et al., 2016, Kostallari and Shah, 2016, Augustin and Koh, 2017), and also contribute to liver regeneration (Ding et al., 2010, Ding et al., 2014, Hu et al., 2014, Manavski et al., 2017, Zhang et al., 2020b). Although these signals are involved in liver regeneration, the mechanisms that cause the release of angiocrine signals are largely unknown. Here, we aimed to discover whether a mechanical stimulus is able to induce the release of angiocrine signals from hepatic ECs. Since angiocrine signals such as HGF, IL-6 and TNF-α were reported to contribute to liver regeneration after PHx (Michalopoulos, 2007, Cressman et al., 1996, Yamada et al., 1997), we wanted to further investigate

whether we can identify novel mechano-induced angiocrine signals, supporting liver regeneration.

Hepatocytes have an enormous potential to proliferate *in vivo after* invasive procedures such as PHx (Michalopoulos, 2007, Michalopoulos and DeFrances, 1997). In contrast, *in vitro* cultured hepatocytes cannot be expanded and lose their ability to proliferate (Runge et al., 2000a). This indicates that crucial stimuli are missing to induce human hepatocyte proliferation *in vitro*. Because of this issue, we aimed to discover whether hemodynamic changes and the release of mechano-induced angiocrine signals are able to induce hepatocyte proliferation *in vitro*.

To sum up, by using the liver as a model organ we aimed to investigate whether hemodynamic changes are able to activate mechanosensory complexes on hepatic ECs (that involves β1 integrin and VEGFR3). Furthermore, we studied whether hemodynamic changes are able to promote the release of angiocrine signals and in turn induce organ growth and regeneration. With this study, we link mechano-induced angiocrine signals to liver regeneration and significantly contribute to further reveal the mystery of liver regeneration.

4. Experimental procedures

4.1 Mouse models

Male C57BL/6J (Janvier) mice at the age of 12-14 weeks were used for *ex vivo* liver perfusion. All experiments were performed according to the German animal protection law (Animal Ethics Committee of the Landesamt für Natur, Umwelt und Verbraucherschutz, North Rhine–Westphalia).

4.2 *Ex vivo* liver perfusion

This method is modified after a previously described method used for rats (Sies, 1978). For open, non-recirculating perfusion, 12–14-week-old male C57BL/6J mice (Janvier) were killed either by cervical dislocation or by blood replacement with 37°C preheated bicarbonate-buffered Krebs-Henseleit saline solution containing pyruvate (0.3 mM) and l-lactate (2.1 mM), after narcotization with a mixture of xylazine (Bayer) and ketamine (Pfizer). The portal vein was cannulated with a 20G intravenous catheter (Hospira VENISYSTEMS, Abbocath-T) connected to a perfusion system. For the efflux, the inferior vena cava was also cannulated with a 20G intravenous catheter (Hospira VENISYSTEMS, Abbocath-T), which drained the perfusate into a measuring cylinder to monitor flow rates. The Krebs-Henseleit saline solution, containing phosphatase inhibitors (PhosSTOP™, Sigma-Aldrich, 4906845001) for protein analyses, was pumped by a peristaltic pump (at different flow rates) through an oxygenator (oxygenation with carbogen gas, 95% O_2 and 5% CO_2), a heater, a bubble trap (to prevent liver emboli) and, finally, through the cannulated liver. After 15 min of perfusion, the liver was deep-frozen in liquid nitrogen for protein analyses and after 1 h of perfusion, the liver was perfused with 4% paraformaldehyde (PFA) for fixation followed by immunohistochemical analyses.

4.3 Primary human cell culture experiments

All experiments with human primary cells were performed under aseptic conditions within a cell culture hood.

4.3.1 Human hepatic endothelial cells

Human hepatic ECs from different donors – sold as 'liver sinusoidal microvascular endothelial cells' – were purchased from PELOBiotech (PB-CH-153-5511); the human hepatic ECs were isolated from collagenase type 1-digested peripheral liver tissue via sequential cell sorting with anti-CD146, anti-CD31 and anti-VEGFR2 antibodies. More than 95% of the isolated cells were reported by the manufacturer to have cytoplasmic immunofluorescent staining for von Willebrand factor, PECAM-1 and Di-I-Ac-LDL uptake. Human hepatic ECs were grown in microvascular endothelial cell growth medium supplemented with microvascular endothelial cell growth kit enhanced (PELOBiotech, PB-MH-100-4099) containing growth factors and fetal calf serum (FCS) in a humidified atmosphere at 5% CO_2 and 37°C.

Table 1. Donor information of human hepatic ECs.

Hepatic ECs Lot #	Sex	Age (years)	Race	Body mass index (kg/m^2)	Cause of death
566.01.01.01.0T	Female	27	Caucasian	24.9	Anoxia
QC02B15F11	Male	49	Caucasian	29.3	Anoxia
QC12B15F11	Male	52	Caucasian	30.6	Anoxia
QC29B15F09	Female	59	Caucasian	18	Anoxia secondary to cardiovascular disease

4.3.2 Human hepatocytes

Human hepatocytes from different donors were purchased from Thermo Fisher Scientific (HMCPIS) or KaLy-Cell. Frozen hepatocytes were suspended in cryo-preserved hepatocyte recovery medium (Thermo Fisher Scientific, CM7000) and subsequently cultured in William's E medium (Gibco by Thermo Fisher Scientific, A1217601) plus primary hepatocyte thawing/plating supplements (Gibco by Thermo Fisher Scientific, CM3000), followed by cultivation (without expansion) in William's E medium plus primary hepatocyte maintenance supplements (Maintenance medium, Gibco by Thermo Fisher Scientific, CM4000). Human hepatocytes were grown in a humidified atmosphere at 5% CO_2 and 37°C.

Table 2. Donor information of human hepatocytes.

Hepatocytes Lot #	Sex	Age (years)	Race	Body mass index (kg/m^2)	Cause of death
HU4248	Female	12	Caucasian	20.2	Intracerebral hemorrhage (ICH)-stroke
HU8296	Male	23	Caucasian	24.6	Head Trauma
S1426T	Female	34	Caucasian	27.6	Cholangiocarcinoma
HU8284	Female	46	Caucasian	30.2	Self-inflicted gunshot wound
HU8287	Female	49	Caucasian	19.6	MVA (motor vehicle accident) trauma to head

4.3.3 Mechanical stimulation of human hepatic ECs

Human hepatic ECs were plated on stretch chambers (STREX, STB-CH-04), which were pre-coated with Speed Coating Solution (PELOBiotech, PB-LU-000-0002-00) over night (o/n) at room temperature (RT). Human hepatic ECs on stretch chambers were mechanically stretched for 90 min in microvascular endothelial cell growth medium without supplements (PELOBiotech, PB-MH-100-4099 - basal medium). Experiments were performed either with an automated cell-stretching system (STREX, STB-140-04) or with a manual cell-stretching system (STREX, STB-100-04). Human hepatic ECs were stretched 20% static for 30 min plus 20% cyclic (30 cycles/min) for 60 min with the automated cell-stretching system or 20% static for 90 min with the manual cell-stretching system.

4.3.4 Activation of β1 integrin in human hepatic ECs

Cover glasses (VWR, 631-1578) were placed into the wells of 24-well plates (SARSTEDT, 83.3922) and incubated with Speed Coating Solution (PELOBiotech, PB-LU-000-0002-00) o/n at RT. 12-well plates (SARSTEDT, 83.3921) were incubated with Speed Coating Solution for 10 min at RT. Human hepatic ECs were plated on 24- or 12-well plates and stimulated for 90 min with or without 1 µg/ml β1 integrin-activating antibody (R&D, MAB17782) or with 1 µg/ml IgG_1 Isotype control (R&D, MAB002).

4.3.5 Co-culture of human hepatic ECs and human hepatocytes

For co-culture experiments with human hepatic ECs and human hepatocytes, conditioned medium of mechanically unstretched versus stretched hepatic ECs or of β1 integrin-stimulated hepatic ECs was transferred to human hepatocytes plated on Permanox Chamber Slides (Thermo Fisher Scientific, C7182). Permanox Chamber Slides were pre-coated with Speed Coating Solution (PELOBiotech, PB-LU-000-0002-00) plus 50 µg/ml rat tail collagen I (Thermo Fisher Scientific, A1048301) o/n at RT. Hepatocytes were incubated for 6 h (a time found to be optimal for co-culturing) with conditioned medium, plus 1 mg/ml EdU (5-ethynyl-2'-deoxyuridine, Thermo Fisher Scientific, C10214) to allow immunofluorescent analyses of cell proliferation.

4.3.6 MYDGF treatment of human hepatocytes

Human hepatocytes were plated on Permanox Chamber Slides (Thermo Fisher Scientific, C7182), pre-coated with Speed Coating Solution (PELOBiotech, PB-LU-000-0002-00) plus 50 µg/ml rat tail collagen I (Thermo Fisher Scientific, A1048301) o/n at RT. Hepatocytes were incubated for 6 h in William's E medium plus primary hepatocyte maintenance supplements (Maintenance medium, Gibco by Thermo Fisher Scientific, CM4000) with or without final concentrations of 1 µg/ml or 5 µg/ml MYDGF (Novoprotein, CG64). 1 mg/ml EdU (Thermo Fisher Scientific, C10214) was added to allow immunofluorescent analyses of cell proliferation.

4.3.7 Cultivation and treatment of human hepatocyte organoids

Human hepatocytes were suspended in 24-well low attachment plates (Merck, CLS3473-24EA). Three different human hepatocyte donors were tested in hepatocyte organoid cultures, however only one donor (Male, 23 years, Caucasian, BMI: 24.6 kg/m^2, COD: head trauma) was able to form organoids. Human hepatocyte three-dimensional (3D) organoid medium (3D medium) consists of Advanced DMEM/F-12 (Gibco by Thermo Fisher Scientific, 12634010) plus 1x Penicillin-Streptomycin-Glutamine (Gibco by Thermo Fisher Scientific, 10378016), 10 mM HEPES (Gibco by Thermo Fisher Scientific, 15630-106), 1x B-27 Supplement (Gibco by Thermo Fisher Scientific, 17504044), 500 ng/mL R-Spondin-1 (PeproTech, 120-38), 3 µM CHIR 99021 (Tocris, 4423), 1.25 mM N-Acetyl-L-

cysteine (Sigma-Aldrich, A9165-5G), 10 mM Nicotinamide (Sigma-Aldrich, N0636-100G), 10 nM Gastrin I (Tocris, 3006), 50 ng/mL EGF (R&D Systems, 236-EG-200), 20 ng/ml TGF-α (PeproTech, 100-16A), 50 ng/mL FGF-7 (PeproTech, 100-19), 50 ng/mL FGF-10 (Miltenyi Biotec., 130-093-850), 25 ng/mL HGF (Miltenyi Biotec., 130-093-872), 2 µM A 83-01 (Tocris, 2939) and 10% Matrigel®Matrix (Corning, 356231). For the first three days of cultivation additionally 25 ng/ml Noggin (PeproTech, 120-10C), 50 ng/ml Wnt-3a (R&D Systems, 5036-WN-010) and 10 µM Y-27632 (STEMCELL Technologies, 72302) were added to 3D medium. After the first three days of cultivation in a humidified atmosphere at 5% CO_2 and 37°C, organoids were transferred into a new 24-well low attachment plate with freshly prepared 3D medium, and treated with or without 10 ng/ml MYDGF (Novoprotein, CG64) plus 1 mg/ml EdU (Thermo Fisher Scientific, C10214). After additional three days of cultivation in a humidified atmosphere at 5% CO_2 and 37°C, organoids were transferred into a black 96-well µ-clear bottom plate (Greiner Bio-One, 655090) to allow immunofluorescent staining and imaging. After the first three days of cultivation, bright-field images of representative organoids were taken with a stereomicroscope (Nikon, SMZ1500).

4.4 Staining methods

4.4.1 Immunohistochemical staining

Ex vivo perfused mouse livers were fixed with 4% PFA o/n at 4°C and subsequently equilibrated in 15% and 30% sucrose (Carl Roth) for cryo-preservation. Afterwards, the left or right liver lobe were placed with the visceral side down into Peel-A-Way® embedding molds (Polysciences, 18986-1), filled with Tissue-Tek® O.C.T™ compound embedding medium (Sakura, 4583). Liver lobes were frozen down and stored at -80°C. A cryostat microtome HM560 (Thermo Fisher Scientific) and MX35 premier plus microtome blades (Thermo Fisher Scientific, 3052835) were used to obtain consecutive 12-µm cryo-sections that were placed onto Super-Frost slides (Thermo Fisher Scientific, J1800AMNZ). Afterwards, slides were washed once with PBS (Ca^{2+}, Mg^{2+}) for 5 min and twice with PBS (Ca^{2+}, Mg^{2+}) containing 0.1% Triton X-100 (AppliChem) for 5 min. Before incubation of primary antibodies for 1 h at RT, the slides were blocked with PBS (Ca^{2+}, Mg^{2+}) containing 5% normal donkey serum (NDS, Jackson ImmunoResearch, 017-000-121), 3% bovine serum albumin (BSA, AppliChem, A1391) and 0.2% Triton X-100 (AppliChem) for 1 h at RT. The following primary antibodies were diluted in blocking solution and incubated for

1 h at RT: goat anti-ICAM-1 (R&D, AF796, 1/50) and rat anti-β1 integrin (BD Biosciences, 553715, 1/200). Afterwards, slides were washed once with PBS (Ca^{2+}, Mg^{2+}) for 5 min and twice with PBS (Ca^{2+}, Mg^{2+}) containing 0.1% Triton X-100 (AppliChem) for 5 min. Secondary antibodies donkey anti-goat Alexa Fluor 555 (Thermo Fisher Scientific, A-21432, 1/500), donkey anti-rat Alexa Fluor 488 (Thermo Fisher Scientific, A21208, 1/500), and for co-staining DAPI (Sigma-Aldrich, D9542, 1/1000) were diluted in blocking solution and incubated for 45 min at RT. Slides were mounted with Fluoroshield™ (Sigma-Aldrich, F6182) and stored at 4°C until imaging. Five images per liver were acquired at 63x magnification using laser scanning microscopy (LSM 710, Zeiss). Image analysis were done with Fiji (ImageJ). To determine the diameter of liver sinusoids, the inner vessel lumen was encircled using the freehand selection tool in Fiji. A macro in Fiji was used to determine the activated endothelial β1 integrin area. Therefore, first the ICAM-1-positive EC area was measured, and then a mask was created that measured the activated β1 integrin area within the ICAM-1-positive EC area.

4.4.2 Immunofluorescent staining

Human hepatic ECs that were plated on stretch chambers (STREX, STB-CH-04) or on cover glasses (VWR, 631-1578), which were previously placed into the wells of 24-well plates (SARSTEDT, 83.3922), were used for immunofluorescent staining. Hepatic ECs were fixed in 4% PFA (Thermo Fisher Scientific, J19943) for 15 min at RT or o/n at 4°C under agitation. Cells were blocked in PBS (Ca^{2+}, Mg^{2+}) containing 1% BSA (AppliChem, A1391), 0.1% Saponin (Sigma-Aldrich) and 2.5 % NDS (Jackson ImmunoResearch, 017-000-121) for 1 h at RT under agitation. The primary antibody mouse anti-activated β1 integrin (Merck, MAB2079Z) was diluted 1/100 in blocking solution and incubated for 1 h at RT under agitation. Afterwards, Phalloidin AlexaFluor™488 (Thermo Fisher Scientific, A12379) diluted 1/500 in blocking solution and DAPI (Sigma-Aldrich, D9542) diluted 1/1000 in blocking solution, were added for 45 min at RT under agitation. Human hepatic ECs on stretch chambers that were used for representative images of the cell length, were only incubated with Phalloidin AlexaFluor™488 (Thermo Fisher Scientific, A12379, 1/200) and DAPI (Sigma-Aldrich, D9542, 1/1000), without previous incubation of a primary antibody. After each step, except after blocking, hepatic ECs were washed thrice in PBS (Ca^{2+}, Mg^{2+}) for 5 min under agitation. A thin layer of hepatic ECs was excised from the stretch chambers. This thin layer of stretch chambers or cover glasses were mounted on Super-Frost slides (Thermo Fisher Scientific, J1800AMNZ) with Fluoroshield™ (Sigma-

Aldrich, F6182). Images were acquired using laser scanning microscopy (LSM 710, Zeiss) and image analysis were done with Fiji (ImageJ). Five images per stretch chamber were taken at 10x magnification or five images per well were taken at 20x magnification. For both, activated β1 integrin and DAPI an individual threshold was set and applied equally to each image to measure either activated β1 integrin-positive area or DAPI-positive area.

4.4.3 Proximity ligation assay

Proximity ligation assay (PLA) was used to detect areas of tyrosine phosphorylation close to VEGFR3 or VEGFR2, or to detect co-localization of VEGFR3 and β1 integrin. The PLA was performed on stretching chambers according to the protocol recommended by the company (Olink Bioscience). Hepatic ECs were previously fixed in 4% PFA (Thermo Fisher Scientific, J19943) for 15-30 min at RT. PBS (Ca^{2+}, Mg^{2+}) was used for washing steps, and PBS (Ca^{2+}, Mg^{2+}) containing 3% BSA (AppliChem, A1391), 5% NDS (Jackson ImmunoResearch, 017-000-121) and 0.2% Triton X-100 (AppliChem) was used for blocking and antibody dilution. For detection of tyrosine phosphorylation, a mouse anti-phosphotyrosine antibody (MerckMillipore, 05-1050, 1/100) was used in combination with either goat anti-VEGFR3 antibody (R&D Systems, AF349, 1/100) or goat anti-VEGFR2 antibody (R&D Systems, AF357, 1/200). To determine colocalization of VEGFR3 and β1 integrin, mouse anti-β1 integrin (MerckMillipore, MAB1987, 1/500) and goat anti-VEGFR3 (R&D Systems, AF349, 1/100) antibodies were used. For PLA labelling, anti-goat Plus Probe (Sigma-Aldrich, DUO92003, 1/10), anti-mouse Minus Probe (Sigma-Aldrich, DUO92004, 1/10), and in situ detection reagent orange (Sigma-Aldrich, DUO92007) were used. Five z-stack images per stretch chamber at 63x magnification were acquired using laser scanning microscopy (LSM 710, Zeiss). Image analysis were done with Fiji (ImageJ). PLA dots and cell nuclei were counted manually in a blinded manner.

4.4.4 EdU assay and pH3 staining

Human hepatocytes, cultured on Permanox Chamber Slides (Thermo Fisher Scientific, C7182) and incubated with different media plus 1 mg/ml EdU, were used for EdU Click-iT® reaction (Invitrogen, C10214 and C10337) or phospho-Histone H3 (pH3) staining. Therefore, hepatocytes were fixed in 4% PFA (Thermo Fisher Scientific, J19943) o/n at 4°C under agitation. On the next day, hepatocytes were washed once for 5 min with PBS

(Ca^{2+}, Mg^{2+}) and blocked for 10 min with PBS (Ca^{2+}, Mg^{2+}) containing 1% BSA (AppliChem, A1391), 0.1% Saponin (Sigma-Aldrich) and 2.5% NDS (Jackson ImmunoResearch, 017-000-121). Click-iT® EdU reaction (Invitrogen, C10214 and C10337) was performed for 30 min at RT according to the manufacturer's instructions. Afterwards, slides were washed thrice for 5 min with PBS (Ca^{2+}, Mg^{2+}), and incubated with PBS (Ca^{2+}, Mg^{2+}) containing 0.3% Triton X-100 (AppliChem) and 5% NDS (Jackson ImmunoResearch, 017-000-121) for 1 h at RT. Antibody dilution solution containing 0.3% Triton X-100 (AppliChem) and 1% BSA (AppliChem, A1391) in PBS (Ca^{2+}, Mg^{2+}) was used to dilute primary and secondary antibodies. These were as follows: rabbit anti-HNF4-α (CellSignaling, C11F12, 3113, 1/500) and anti-rabbit Alexa Fluor 555 (Invitrogen, A31572, 1/500). DAPI (Sigma-Aldrich, D9542, 1/1000) was used for co-staining. The primary antibody was incubated for 1 h at RT, and the secondary antibody plus DAPI were incubated for 1.5 h at RT. Before mounting with Fluoroshield™ (Sigma-Aldrich, F6182), slides were washed thrice with PBS (Ca^{2+}, Mg^{2+}) for 5 min. For pH3 staining all previous steps were performed in the same way, except for the EdU reaction. Primary and secondary antibodies were as follows: rabbit anti-phospho-Histone H3 (Sigma-Aldrich, 06-570, 1/50) and donkey anti-rabbit AF488 (Invitrogen, A21206, 1/500). Slides were stored at 4°C until images were acquired using laser scanning microscopy (LSM 710, Zeiss). A whole well of the Permanox Chamber Slides (Thermo Fisher Scientific, C7182) was imaged to analyze EdU proliferation. Therefore, tile scan images consisting of 7x7 tiles were acquired at 10x magnification. To analyze pH3 staining, seven images per well were acquired at 20x magnification. Images were taken with a laser scanning microscope (LSM 710, Zeiss), and proliferation was analyzed with Fiji (ImageJ). EdU-positive and pH3-positive cells were counted manually in a blinded manner.

4.4.5 Cell death assay

Apoptosis in human hepatocytes, cultured on Permanox Chamber Slides (Thermo Fisher Scientific, C7182) were determined using the *in situ* cell death detection kit (TUNEL), TMR red (Roche, 12156792910). Therefore, hepatocytes were fixed in 4% PFA (Thermo Fisher Scientific, J19943) o/n at 4°C under agitation. On the next day, hepatocytes were washed once for 5 min with PBS (Ca^{2+}, Mg^{2+}), and incubated in 10 mM Tris/HCl (Trizma® hydrochloride, Sigma-Aldrich) containing 40 µg/ml Proteinase K (Applichem, A4392, 0010) for 10 min at 37°C. Afterwards, slides were washed thrice with PBS (Ca^{2+}, Mg^{2+}) for 5 min, and incubated with permeabilization solution containing 0.1% Triton X-100 (AppliChem) in

0.1% sodium citrate (Sigma-Aldrich) for 2 min on ice. TUNEL staining was performed according to the manufacturer's instructions (Roche, 12156792910). Afterwards, slides were washed once with PBS (Ca^{2+}, Mg^{2+}) containing 0.2% Triton X-100 (AppliChem). For co-staining, slides were blocked with PBS (Ca^{2+}, Mg^{2+}) containing 3% BSA (AppliChem, A1391), 5% NDS (Jackson ImmunoResearch, 017-000-121) and 0.02% Triton X-100 (AppliChem) for 1 h at RT, and incubated with DAPI (Sigma-Aldrich, D9542) diluted 1/1000 in blocking solution for 45 min at RT. Before mounting with Fluoroshield™ (Sigma-Aldrich, F6182), slides were washed thrice with PBS (Ca^{2+}, Mg^{2+}) for 10 min. Five images per well were acquired at 20x magnification using laser scanning microscopy (LSM 710, Zeiss). Image analysis was done with Fiji (ImageJ). TUNEL-positive area and DAPI-positive area were analyzed by using an individual threshold that was set and applied equally to each image to measure either apoptotic cells or cell nuclei.

4.4.6 Whole mount staining

Human hepatocyte organoids in a black 96-well µ-clear bottom plate (Greiner Bio-One, 655090) were used for whole mount staining. Organoids were fixed in 4% PFA (Thermo Fisher Scientific, J19943) o/n at 4°C under agitation. On the next day, organoids were washed thrice in PBS (Ca^{2+}, Mg^{2+}), containing 0.1% Triton X-100 (AppliChem) for 5 min under agitation, followed by blocking in PBS (Ca^{2+}, Mg^{2+}), containing 0.1% Triton X-100, 10% NDS (Jackson ImmunoResearch, 017-000-121) and 1% BSA (AppliChem, A1391). Afterwards, proliferation was determined using a combination of two EdU click-iT® imaging kits (Invitrogen, C10214 and C10337) by incubating organoids for 30 min at RT under agitation. Subsequently, organoids were washed thrice in PBS (Ca^{2+}, Mg^{2+}), containing 0.1% Triton X-100, for 5 min under agitation. Primary antibody rabbit anti-HNF4-α (CellSignaling, C11F12, 3113) was diluted 1/250 in PBS (Ca^{2+}, Mg^{2+}), containing 0.1% Triton X-100, 10% NDS and 1% BSA, and incubated o/n at 4°C under agitation. On the next day, organoids were washed thrice in PBS (Ca^{2+}, Mg^{2+}), containing 0.1% Triton X-100, for 5 min under agitation, before and after incubation with secondary antibodies. Secondary antibody donkey anti-rabbit Alexa Fluor 555 (Invitrogen, A31572, 1/500) and for co-staining DAPI (Sigma-Aldrich, D9542, 1/1000) were incubated for 2 h at 4°C under agitation. Organoids were stored in PBS (Ca^{2+}, Mg^{2+}) until imaging. Images were acquired using laser scanning microscopy (LSM 710, Zeiss) and image analysis were done with Fiji (ImageJ). EdU-positive cells were counted manually, and DAPI-positive area was measured with a freehand selection tool in Fiji, both in a blinded manner.

4.4.7 Cell viability assay

Representative human hepatocyte organoids were used for cell viability assay. Human organoids were transferred into a 96-well µ-clear bottom plate (Greiner Bio-One, 655090) and stained with 2 µM calcein AM, 4 µM ethidium homodimer-1 (EthD-1) (Live-Dead Viability/Cytotoxicity Kit, Thermo Fisher Scientific, L3224) and co-stained with 10 µg/ml Hoechst 33342 (Thermo Fisher Scientific, H3570) in 3D medium (for medium composition see chapter 4.3.7). Calcein AM, EthD-1 and Hoechst were incubated for 30 min at 37°C and 5% CO_2. Z-stack images were acquired using laser scanning microscopy (LSM 710, Zeiss). For the shown representative images maximum intensity projections were processed with Fiji (ImageJ).

4.5 Western blotting

Western blots were performed to analyze phosphorylated and total VEGFR3 protein levels in *ex vivo* perfused mouse livers, as well as MYDGF and GAPDH protein levels in either supernatants or lysates from mechanically unstretched and stretched human hepatic ECs. For protein analyses of phosphorylated and total VEGFR3, 20 mg of *ex vivo* perfused mouse livers were placed with 500 µl lysis buffer containing 50 mM HEPES (Carl Roth), 150 mM NaCl (Carl Roth), 10% Glycerol (Carl Roth), 1% Triton X-100 (AppliChem), PhosSTOP™ phosphatase inhibitor (Sigma-Aldrich, 4906845001) and cOmplete™ protease inhibitor cocktail (Roche, 11697498001) into a gentleMACS M Tube (Miltenyi Biotec, 130-093-236) for tissue homogenization on gentleMACS™ Dissociator (Miltenyi Biotec, 130-093-235) using the protein dissociation program. Human hepatic ECs on stretch chambers were incubated in lysis buffer containing 50 mM HEPES (Carl Roth), 150 mM NaCl (Carl Roth), 10% Glycerol (Carl Roth), 1% Triton X-100 (AppliChem), PhosSTOP™ phosphatase inhibitor (4906845001, Sigma-Aldrich) and cOmplete™ protease inhibitor cocktail (11697498001, Roche) for 15 min on ice. Afterwards, cells were scratched with a cell scratcher from the stretch chambers. All lysates were centrifuged for 10 min at 13,000 rpm and 4°C, and protein amounts were determined using Pierce™ BCA™ Protein Assay (Thermo Fisher Scientific, 23225). In order to detect secreted MYDGF in the supernatants from unstretched and stretched hepatic ECs, supernatants were collected and immediately concentrated with Amicon Ultra-0.5 centrifugal filter units (Merck, UFC501096). 1 ml microvascular endothelial cell growth medium without supplements, which was present in each chamber of unstretched or stretched hepatic ECs,

was used for concentration. For the first concentration step 500 µl supernatant was transferred into the centrifugal filter unit and centrifuged for 15 min at 13,000 rpm at 4°C. Afterwards, the remaining 500 µl of supernatant was transferred into the same centrifugal filter unit and centrifuged for 15 min at 13,000 rpm at 4°C. 20 µg of *ex vivo* perfused mouse liver lysates and 20 µg of human hepatic EC protein lysates were diluted in dH_2O. Diluted lysates or 20 µl of concentrated supernatants were prepared with 2x Laemmli sample buffer (Bio-Rad, 1610747), plus 2-mercaptoethanol (Carl Roth) and heated for 5 min at 95°C. Samples were loaded on Mini-Protean™ TGX Stain-Free™ Protein Gels (Bio-Rad, 4568086) and transferred with the Trans-Blot® Turbo™ Transfer System (Bio-Rad, 1704156). Membranes were blocked in PBS (Ca^{2+},Mg^{2+}) containing 5% BSA (AppliChem) and 0.5% Tween-20 (Sigma-Aldrich or Carl Roth) for 1 h at RT under agitation. Primary antibodies were diluted in blocking buffer and incubated o/n at 4°C under agitation. The following antibodies were used: rabbit anti-VEGFR3 (Signalway Antibody, 21410, 1/750), rabbit anti-phospho-VEGFR3 (Cell Applications, CY1115, 1/1250), rabbit anti-MYDGF (Proteintech, 11353-1-AP, 1/1000) and rabbit anti-GAPDH (Abcam, Ab9485, 1/5000). After three times washing with PBS (Ca^{2+}, Mg^{2+}) containing 0.5% Tween-20 (Sigma-Aldrich or Carl Roth) for 10 min at RT, membranes were incubated with goat anti-rabbit IgG, HRP-linked secondary antibody (CellSignaling, 7074S) for 45 min at RT. After additionally three times washing with PBS (Ca^{2+},Mg^{2+}) containing 0.5% Tween-20 (Sigma-Aldrich or Carl Roth) for 10 min at RT, proteins were detected with Clarity™ Western ECL Substrate (Bio-Rad, 170-5061) and ChemiDoc MP Imaging System (Bio-Rad). Western blots were densitometrically analyzed using Image Laboratory Software Version 5.2 (Bio-Rad).

4.6 Colorimetric ELISAs and fluorogenic assays

All enzyme-linked immunosorbent assays (ELISAs) and fluorogenic assays were performed according to the protocol provided by the company (R&D Systems). For protein analyses of HGF and phosphorylated and total Met, 20 mg of *ex vivo* perfused mouse livers were placed with 500 µl lysis buffer containing 50 mM HEPES (Carl Roth), 150 mM NaCl (Carl Roth), 10% Glycerol (Carl Roth), 1% Triton X-100 (AppliChem), PhosSTOP™ phosphatase inhibitor (Sigma-Aldrich, 4906845001) and cOmplete™ protease inhibitor cocktail (Roche, 11697498001) into a gentleMACS M Tube (Miltenyi Biotec, 130-093-236) for tissue homogenization on gentleMACS Dissociator (Miltenyi Biotec, 130-093-235) using the protein dissociation program. Lysates were centrifuged for 10 min at 13,000 rpm and 4°C, and protein amounts were determined using Pierce™ BCA™ Protein Assay (Thermo

Fisher Scientific, 23225). 50 µg of *ex vivo* perfused mouse liver lysates were used for ELISAs: Quantikine mouse/rat HGF (R&D, MHG00), DuoSet phospho-HGFR/c-Met (R&D, DYC2480) and DuoSet total-HGFR/c-Met (R&D, DYC358). For quantification, phospho-Met protein levels were normalized to total-Met protein levels. Unstretched and stretched supernatants of human hepatic ECs were centrifuged at 13,000 rpm for 10 min at 4°C and immediately used for ELISAs or fluorogenic assays. Human HGF, IL-6 and TNF-α DuoSet ELISAs (R&D Systems, DY294, DY206, DY210) and MMP9-fluorokine assay (R&D Systems, F9M00) were used to analyze cell culture supernatants. All samples were run in duplicates and measured with NanoQuant Infinite M200 Reader (TECAN) or with SpectraFluor Plus reader (TECAN).

4.7 Reverse transcriptase PCR and quantitative real-time PCR

For gene expression analysis, ribonucleic acid (RNA) was isolated from human hepatic ECs on stretch chambers, which were either unstretched or mechanically stretched, using the High Pure RNA Isolation Kit (Roche, 11828665001) according to the manufacturer's instructions. Afterwards, complementary deoxyribonucleic acid (cDNA) was synthesized with Super-Script™ II Reverse Transcriptase (Thermo Fisher Scientific, 18064014) according to the protocol provided by the company (Thermo Fisher Scientific (Invitrogen™ by Life Technologies)). cDNA was diluted 1:5 with H_2O and following master mixes were used for qPCR:

5 µl FastStart Essential DNA Green Master (Roche, 06402712001)
2 µl H_2O PCR grade (Roche, 06402712001)
2 µl Primer Mix (Forward and reverse primer, 3 µM)
1 µl cDNA (previously diluted 1:5)

The following primer sequences were used for primer mixes (100 µM forward primer and 100 µM reverse primer were diluted to 3 µM in H_2O PCR grade), and for amplification:

Table 3. Primer sequences.

Primer	Primer sequences
Human *Mydgf* (Eurogentec)	Forward: 5' – TCG TGC ATT CCT TCT CCC AT – 3'
	Reverse: 5' – ACC TCT GCC TTG AAC TGT GT – 3'
Human *36B4* (Eurogentec)	Forward: 5' – GAA GAC AGG GCG ACC TGG AA – 3'
	Reverse: 5' – CCA CAT TGT CTG CTC CCA CA – 3'
Human *B2M* (Eurofins)	Forward: 5' – TTT CAT CCA TCC GAC ATT GA – 3'
	Reverse: 5' – CCT CCA TGA TGC TGC TTA CA – 3'
Human *HPRT* (Eurogentec)	Forward: 5' – GCA GAC TTT GCT TTC CTT GG – 3'
	Reverse: 5' – AAC ACT TCG TGG GGT CCT TT – 3'

Samples were run in duplicates on LightCycler® Nano instrument (Roche) with LightCycler® Nano Software 1.1 (Roche) using the following thermal profile:

Pre-Incubation:	95°C for 10 min
3-Step Amplification:	45 cycles of 95°C for 20 s to 60°C for 20 s to 72°C for 20 s
Melting:	65°C to 95°C at 0.1°C/s

Relative gene expression of *Mydgf* was normalized to either *36B4*, *B2M* or *HPRT* and calculated by using the comparative C_T method (Schmittgen and Livak, 2008).

4.8 Sample preparation and liquid chromatography coupled to tandem mass spectrometry (LC-MS/MS)

Mass spectrometry-based proteomics was used to analyze supernatants from unstretched and stretched hepatic ECs. Therefore, supernatants were centrifuged at 85,000 x g for 30 min at 4°C and concentrated with Amicon Ultra-0.5 centrifugal filter units with a 3 kDa cutoff (Merck, UFC500324) according to the manufacturer's instructions (Merck). The following steps were performed with adjusted parameters as previously described in (Hartwig et al., 2019). 20 µl of concentrated supernatant were loaded onto SDS-PAGE (10% polyacrylamide, 0.5 cm separation distance). Afterwards, the gels were fixed in 30% methanol / 7% acetic acid (v/v) (both, AppliChem) and stained with Coomassie blue (AppliChem) for visualization. Protein bands were excised and subjected to in-gel protease digestion. Therefore, proteins were reduced with 65 mM dithiothreitol (DTT,

AppliChem) for 15 min at 50°C under agitation at 350 rpm and alkylated with 216 mM Iodacetamide (AppliChem) for 15 min at RT in the dark. Before reduction and after alkylation protein bands were washed four times in an alternated manner with 25 mM ammonium bicarbonate (AppliChem) and with 25 mM ammonium bicarbonate plus 50% acetonitrile (ACN, (v/v)), Thermo Fisher Scientific). Protein bands were shrinked in 100% ACN, proteins were digested using 400 ng LysC/Trypsin mix (Promega, V5073) in 25 mM ammonium bicarbonate and 2% ACN (v/v) o/n at 37°C, and peptides were eluted twice in 1% trifluoroacetic acid (TFA, (v/v), Thermo Fisher Scientific) and 0.1% TFA / 90% ACN (v/v), respectively. Peptides were lyophilized, reconstituted in 1% TFA (v/v) supplemented with indexed retention time peptides (iRT Kit, Biognosys, Ki-3002-1), and separated by liquid chromatography (LC, Ultimate 3000, Thermo Fisher Scientific) using an EASYspray ion source equipped to an Orbitrap Fusion™ Lumos™ Tribrid™ mass spectrometer (Thermo Fisher Scientific). Peptides were desalted and separated using an Acclaim PepMap 100 C18 LC trap column (Thermo Fisher Scientific, 164535) and an EASY-Spray C18 column (Thermo Fisher Scientific, P/N ES803), respectively. Column temperature was set to 40°C, and a 100 min linear gradient from buffer A (0.1% formic acid (FA), Thermo Fisher Scientific) to 4-34% buffer B (80% ACN, 0.1% FA), followed by a 20 min linear increase to 50% buffer B, and a 1 min linear increase to 90% buffer B at a flow rate of 300 nl/min was used. Mass spectrometry data were acquired using data dependent acquisition mode (DDA). Parameters were described in (Hartwig et al., 2019). MS spectra were analyzed with Proteome Discoverer (Thermo Fisher Scientific, Version 2.2.0.388) and the HTSequest search engine using FASTA files from *Homo sapiens* (SwissProt TaxID 9606 (version 2017-10-25)), *Bos taurus* (SwissProt TaxID 9913 (version 2017-10-25)), and a general contaminant FASTA file consisting of ~250 sequences from different origin. Additional HTSequest search settings were: enzyme trypsin (full), maximum missed cleavages: 2, peptide length: 6-144, fragment mass tolerance: 0.04 Da, modifications: carbamidomethyl (fixed), and methionine oxidation and N-terminal acetylation (dynamic). The peptide spectrum matches (PSMs) were validated with the Percolator node, and the strict and relaxed false discovery rates (FDRs) for PSMs were set to 0.01 and 0.05, respectively. For protein distribution across different samples, only unique peptides based on protein groups were used. Proteins that originate from contaminants, bovine, or with an undefined origin, either from bovine or from human were not considered for further analysis.

4.9 Statistics

Statistical significance was determined by using GraphPad Prism software (GraphPad Software, LLC.) Except for the paired data, all data are shown as means ± standard error of the mean (s.e.m.). Two-tailed student's *t*-test (paired or unpaired with Welch's correction) and one-way ANOVA followed by Tukey's post hoc-test with 95% confidence intervals with lower and upper confidence limits (LCL, UCL). Exact *P* values are stated in each figure and figure legend, with $P < 0.05$ considered statistically significant. Significant outliers ($P = 0.05$) were identified using GraphPad Prism Grubbs' outlier method and excluded from the statistical analysis.

4.10 Personal contributions

Linda Große-Segerath performed most of the experiments and was supervised by Prof. Dr. Eckhard Lammert; funded by the DFG, SFB 974.

Dr. Jennifer Axnick and Dr. Tobias Buschmann started the research project on the liver (funded by the DFG, SFB 974), and performed experiments on embryonic liver development and liver regeneration. Both planned and designed the first *ex vivo* mouse liver perfusion experiments together with Nicole Eichhorst. Nicole Eichhorst performed *ex vivo* liver perfusion experiments. Linda Große-Segerath analyzed *ex vivo* liver perfusion experiments shown in Figure 4 and 5 A, and planned, designed and analyzed experiments shown in Figure 5 B and 6 A, B.

Within collaboration, Dr. Sonja Hartwig and Dr. Stefan Lehr (German Diabetes Center (DDZ)) performed and analyzed the LC/MS-MS experiment.

Linda Große-Segerath co-supervised Paula Follert during her Master Thesis in 2019-2020. Paula Follert worked on isolation of hepatic ECs from mice, silencing of *MYDGF* in human hepatic ECs and 3D human hepatocyte organoid cultures, after organoid cultures were established by Linda Große-Segerath.

Linda Große-Segerath and Jessica Mrugala co-supervised Lea Weiß during her Bachelor Thesis in 2017. Lea Weiß worked on mechano-induced angiocrine signals in mouse pancreatic islets, a related topic to this thesis.

5. Results

Angiocrine signals derived from ECs such as growth factors and cytokines promote organ homeostasis and regeneration (Rafii et al., 2016, Kostallari and Shah, 2016). Hemodynamic changes provide excellent mechanical stimuli to drive the regenerative process following acute liver injury (e.g. two-thirds PHx) (Michalopoulos, 2007). In this work, we used the liver as a model organ to investigate whether hemodynamic changes are able to activate mechanosensory complexes on hepatic ECs, promote the release of angiocrine signals and thus induce organ growth and regeneration.

First, we used *ex vivo* perfused mouse livers and *in vitro* cultured human hepatic ECs to study whether hemodynamic changes result in the activation of mechanosensory complexes including β1 integrin and VEGFR3 and the release of angiocrine signals. Next, we investigated whether the supernatant from mechanically stretched human hepatic ECs, which contains mechano-induced angiocrine signals, can promote both proliferation and survival of human hepatocytes *in vitro*. Further, we hypothesized that several yet unidentified mechano-induced angiocrine signals are involved in liver growth and regeneration, and we identified MYDGF as a novel angiocrine signal with impact on human hepatocyte proliferation *in vitro*.

5.1 Hemodynamic changes in *ex vivo* perfused mouse livers correlate with the activation of mechano-induced downstream signaling

Hemodynamic changes in the liver as a result of two-thirds PHx, were proposed to trigger liver growth and regeneration (Michalopoulos, 2007). However, a mechanism how hemodynamic changes contribute to liver regeneration is missing. Here, we used *ex vivo* liver perfusion in mice to determine whether changes in vascular perfusion are involved in mechano-induced signaling pathways. Therefore, the portal vein was cannulated, connected to a perfusion system, and perfused with pre-warmed, oxygenated Krebs-Henseleit (KH) buffer (Figure 3). The perfusion rate through the liver could be variably adjusted and ranged from 2 ml/min to 8 ml/min. The *ex vivo* liver perfusion experiments were performed by Nicole Eichhorst.

Since hemodynamic changes in mice are difficult to monitor, the normal perfusion rate for *ex vivo* perfusion experiments needed to be calculated to mimic *in vivo* conditions. The liver

receives about 25% of the cardiac output, therefore the normal perfusion rate for *ex vivo* experiments was determined using one fourth of the cardiac output (Laflamme et al., 2012). Since the cardiac output in mice is approximately 11 ml/min to 16 ml/min, the normal perfusion rate was set to 4 ml/min. This perfusion rate was used as a control for the first *ex vivo* perfusion experiments in which liver cross-sections were generated. Indeed, a reported monitoring procedure to obtain hemodynamic parameters in mice showed that the perfusion of the portal vein was less than 4 ml/min and about 2 ml/min (Xie et al., 2014). Therefore, we used perfusion rates ranging from 2 ml/min to 8 ml/min to analyze lysates of *ex vivo* perfused mouse livers. An advantage of the *ex vivo* perfusion system is that perfusing the liver with KH buffer ensures the absence of blood components and therefore allows to investigate whether an increased vascular perfusion and mechanical stretching alone are sufficient enough to promote activation of mechanosensory complexes and the secretion of angiocrine signals.

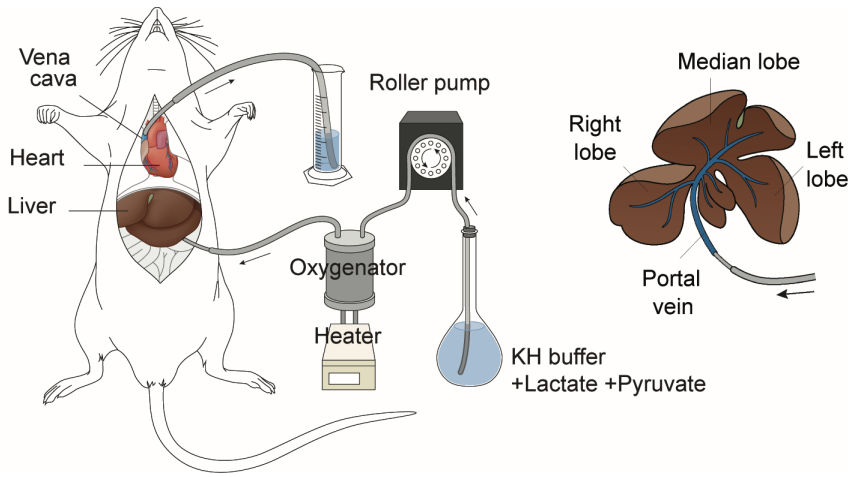

Figure 3. Schematic illustration of an *ex vivo* perfused mouse liver. To allow perfusion of the adult mouse liver, the portal vein and the inferior vena cava were cannulated. Whereas the latter is responsible to ensure the efflux of the Krebs-Henseleit (KH) buffer, the portal vein is connected to a perfusion system, and perfused with pre-warmed, oxygenated KH buffer containing lactate and pyruvate. Modified from (Lorenz et al., 2018). Illustrated by Yousun Koh.

Before studying whether hemodynamic changes are able to activate mechanosensory complex and angiocrine downstream signaling, we wanted to confirm that the liver vasculature responds to *ex vivo* liver perfusion (Figure 4). Therefore, we used cross-sections of livers, which were perfused at flow rates of 4 ml/min and 8 ml/min. We validated that an increase in the perfusion rate from 4 ml/min to 8 ml/min leads to the vasodilation of the vasculature in the liver cross-sections (Figure 4 A-C). Thus, we decided to move forward with the *ex vivo* liver perfusion method to mimic hemodynamic changes to identify possible downstream signaling.

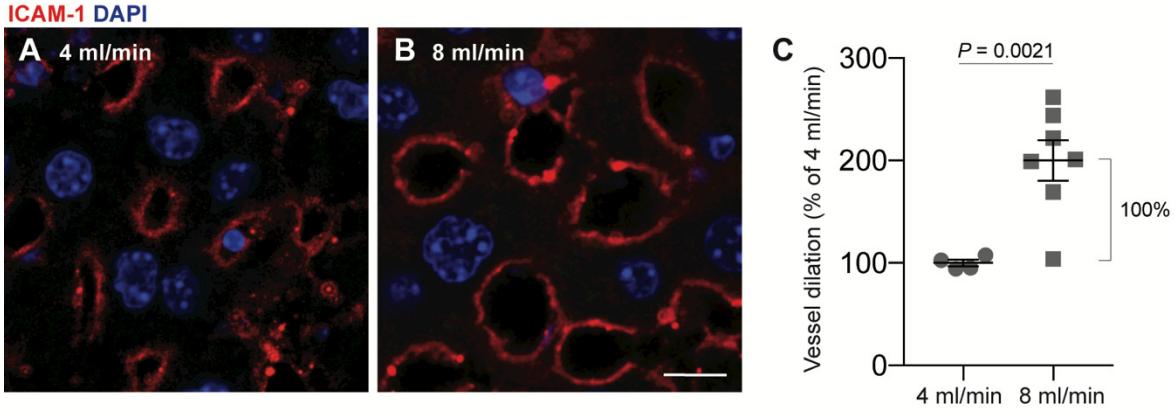

Figure 4: Increasing the perfusion rate of *ex vivo* perfused mouse livers induces vessel dilation. (A, B) Representative LSM images of cross-sections through *ex vivo* perfused mouse livers, at perfusion rates of 4 ml/min (A) and 8 ml/min (B) stained for blood vessels (ICAM-1, red) and cell nuclei (DAPI, blue). Scale bar, 10 µm. (C) Quantification of vessel dilation, shown as percentage of 4 ml/min (*P* = 0.0021 (51.67; 148.60)). Data are shown as means ± s.e.m. with n = 4 livers at a perfusion rate of 4 ml/min versus n = 7 livers at a perfusion rate of 8 ml/min. Statistical significance was determined using an unpaired two-tailed student's *t*-test with 95% confidence interval (lower confidence limit; upper confidence limit).

Mechanosensory complexes on ECs are essential for translating hemodynamic changes such as an increased blood perfusion into downstream signals. Integrins are common mechanoreceptors that are involved in mechanotransduction. Since β1 integrin was shown to interact with VEGFR3 and to induce its activation (Ingber, 1991, Katsumi et al., 2004, Wang et al., 2001, Zhang et al., 2005, Planas-Paz et al., 2012), we studied whether enhanced vascular perfusion leads to activation of β1 integrin and VEGFR3. Further, we aimed to elucidate whether vasodilation can lead to the release of angiocrine signals, which are critical for organ growth and regeneration (Rafii et al., 2016, Augustin and Koh, 2017, Kostallari and Shah, 2016).

We generated cross-sections of *ex vivo* perfused mouse livers and analyzed whether β1 integrin can be activated by an increased vascular perfusion (Figure 5 A). We used an antibody against an epitope of murine β1 integrin, which is only accessible after activation of this integrin (Lenter et al., 1993). Since β1 integrin is expressed in the whole liver, we used the image analysis program Fiji (ImageJ) to create an artificial mask to measure only the activated β1 integrin-positive area on ECs (ICAM-1-positive area). Our results show that an increase in the perfusion rate of *ex vivo* perfused mouse livers from 4 ml/min to 8 ml/min activates β1 integrin on hepatic ECs (Figure 5 A). Next, we tested whether an increased vascular perfusion can activate VEGFR3 (Figure 5 B). Therefore, we lysed mouse livers perfused at perfusion rates of 2 ml/min, 4 ml/min, 6 ml/min or 8 ml/min for

15 min and performed Western Blot analyses. The tyrosine phosphorylation of VEGFR3 increased proportionally to the perfusion rate between 2 ml/min and 6 ml/min, but did not increase further at a perfusion rate of 8 ml/min (Figure 5 B, Western Blots are shown in the supplementary information; Supplementary Figure 1). In conclusion, our results confirm the hypothesis that enhanced vascular perfusion can activate β1 integrin and VEGFR3 in the liver.

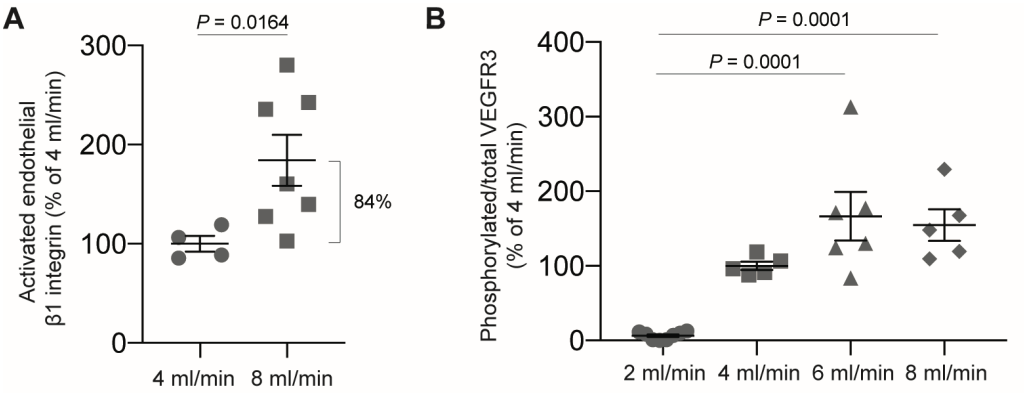

Figure 5: Increasing the perfusion rate of *ex vivo* perfused mouse livers correlates with the activation of β1 integrin and VEGFR3. (A) Quantification of activated endothelial β1 integrin in *ex vivo* perfused mouse livers, shown as percentage of 4 ml/min (n = 4 livers at a flow rate of 4 ml/min versus n = 7 livers at a flow rate of 8 ml/min, $P = 0.0164$ (20.74; 147.50)); (B) Tyrosine phosphorylation of VEGFR3 normalized to total VEGFR3, shown as percentage of 4 ml/min (n = 8 livers at a flow rate of 2 ml/min, n = 5 livers at a flow rate of both 4 ml/min and 8 ml/min, and n = 6 livers at a flow rate of 6 ml/min (2 ml/min versus 6 ml/min, $P = 0.0001$ (91.32; 228.90); 2 ml/min versus 8 ml/min, $P = 0.0001$ (75.64; 220.90)). Data are shown as means ± s.e.m. Statistical significance was determined using an unpaired two-tailed student's *t*-test (A), or one-way ANOVA followed by Tukey's test (B), both with 95% confidence interval (lower confidence limit; upper confidence limit).

Further, we wanted to know whether an enhanced vascular perfusion leads to secretion of HGF, which is a common angiocrine signal involved in liver regeneration (Michalopoulos, 2007, Zhang et al., 2020b). Therefore, we analyzed HGF levels in lysates of *ex vivo* perfused mouse livers by performing ELISAs (Figure 6 A). We found HGF levels to be tendentially increased in *ex vivo* perfused livers at a perfusion rate of 8 ml/min compared to 2 ml/min (Figure 6 A). To support our hypothesis that angiocrine signals like HGF can be secreted due to enhanced vascular perfusion, we analyzed Met (also known as c-Met), the receptor for HGF, by performing ELISAs (Figure 6 B). Similar to VEGFR3 phosphorylation, also Met phosphorylation increased at a perfusion rate of 8 ml/min compared to 2 ml/min. This increase in phosphorylated Met was proportional to the *ex vivo* liver perfusion within the perfusion rates between 2 ml/min and 6 ml/min (Figure 6 B). The

addition of phosphatase inhibitors to the KH buffer during the perfusion was necessary to observe the phosphorylation of both, VEGFR3 and Met in *ex vivo* perfused liver lysates.

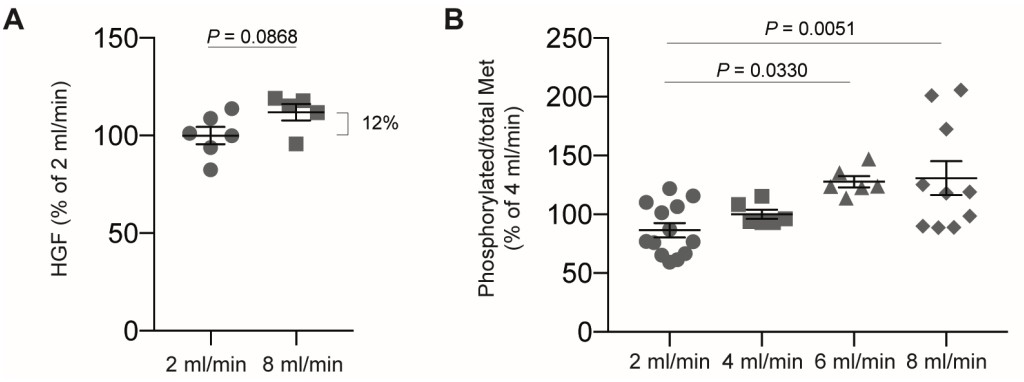

Figure 6: Increasing the perfusion rate of *ex vivo* perfused mouse livers correlates with the activation of HGF and Met. (A) HGF protein amount of *ex vivo* perfused mouse livers at a flow rate of 2 ml/min versus 8 ml/min, shown as percentage of 2 ml/min (n = 6 livers at a flow rate of 2 ml/min, n = 5 livers at a flow rate of 8 ml/min, *P* = 0.0868 (-2.11; 25.97)). (B) Phosphorylated Met normalized to total Met, shown as percentage of 4 ml/min (n = 13 livers at a flow rate of 2 ml/min, n = 6 livers at a flow rate of both 4 ml/min and 6 ml/min, and n = 10 livers at a flow rate of 8 ml/min (2 ml/min versus 6 ml/min, *P* = 0.0330 (2.58; 79.93); 2 ml/min versus 8 ml/min, *P* = 0.0051 (11.27; 77.19). Data are shown as means ± s.e.m. Statistical significance was determined using an unpaired two-tailed student's *t*-test (A), or one-way ANOVA followed by Tukey's test (B), both with 95% confidence interval (lower confidence limit; upper confidence limit).

Our results show that an increased perfusion of *ex vivo* perfused mouse livers widens the vascular lumen of liver sinusoids (Figure 4). This increased vascular perfusion activates a mechanosensory complex that involves β1 integrin and VEGFR3 (Figure 5). In addition, angiocrine downstream signaling is induced, such as the secretion of HGF and the phosphorylation of its receptor Met (Figure 6). With our findings we could demonstrate for the first time that hemodynamic changes are able to promote mechano-induced angiocrine downstream signaling.

5.2 Mechanical stimulation of human hepatic ECs correlate with the activation of mechano-induced downstream signaling

Based on our results gained with the *ex vivo* perfused mouse livers, we investigated whether these observations can be transferred to the human system. Therefore, we used primary human cells from different donors in an *in vitro* cell culture system. First, we

established a system capable of mimicking *in vivo* conditions of vasodilation and associated stretching of ECs. Therefore, we plated primary human hepatic ECs on elastic stretch chambers (Figure 7 A), and placed them onto stretch chamber devices (Figure 7 B-D). Hepatic ECs were either stretched permanently with a manual cell stretching device (Figure 7 B, C), or they were stretched with a combination of permanent and cyclic stretch in an automated cell stretching machine (Figure 7 D). With the latter, eight stretch chambers could be stretched simultaneously. Human hepatic ECs were stretched for 1.5 hours and stained for F-actin to determine whether they respond to mechanical stretching. We could show that human hepatic ECs respond to mechanical stretching with elongation of their length (Figure 7 E-G). Thus, we propose that mechanical stretching, which mimics *in vivo* vascular lumen widening, can be used to analyze the activation of mechanosensory complexes as well as the release of angiocrine signals from human hepatic ECs *in vitro.*

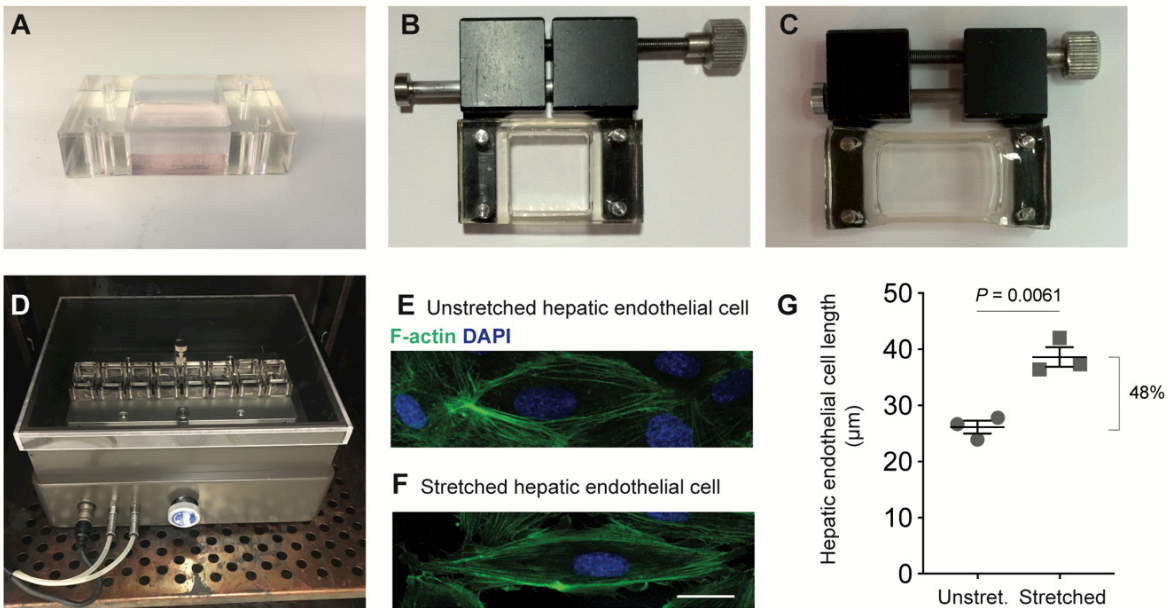

Figure 7: Mechanical stimulation of hepatic ECs results in cell elongation. (A) Image of an elastic stretch chamber. (B, C) Images of the manual cell stretching system. Chamber on the unstretched (B) and stretched (C) cell stretching unit. (D) Image of the automated cell stretching system. (E, F) LSM images of unstretched (E) and stretched (F) hepatic ECs stained for F-actin (green) and nuclei (DAPI, blue). Scale bar, 20 µm. (G) Quantification of the cell length of mechanical unstretched (Unstret.) and stretched hepatic ECs (P = 0.0061 (6.34; 18.65)). Human hepatic EC donor: female, 59 years. Data are shown as means ± s.e.m. with n = 3 stretch chambers each. Statistical significance was determined using an unpaired two-tailed student's *t*-test with 95% confidence interval (lower confidence limit; upper confidence limit).

5.2.1 Mechanical stimulation of human hepatic ECs induces β1 integrin activation, VEGFR3 phosphorylation and interaction between β1 integrin and VEGFR3

Under physiological conditions, hepatic ECs encounter low pressure from the blood vasculature (Poisson et al., 2017). Interestingly, also lymphatic ECs encounter low pressure, and both hepatic and lymphatic ECs express the same mechanosensory proteins (Ding et al., 2010). In lymphatic ECs mechano-induced activation of β1 integrin was reported to activate VEGFR3, whereby β1 integrin is upstream of VEGFR3 (Planas-Paz et al., 2012). Similarly, in our study in mice we could show that hemodynamic changes activate β1 integrin and VEGFR3 and promote the release of angiocrine signals. To validate the results of our mouse study in the human system, we investigated whether mechanical stretching can activate a mechanosensory complex that includes β1 integrin and VEGFR3 on human hepatic ECs. To this end we performed immunofluorescent staining and PLAs of unstretched and stretched human hepatic ECs (Figure 8-11).

First, we aimed to investigate whether mechanical stimulation can activate β1 integrin on human hepatic ECs (Figure 8). Therefore, we mechanically stretched human hepatic ECs for 1.5 hours and used unstretched hepatic ECs as controls (Unstret.). Our analysis revealed that mechanical stimulation induces activation of β1 integrin on human hepatic ECs (Figure 8 A-E).

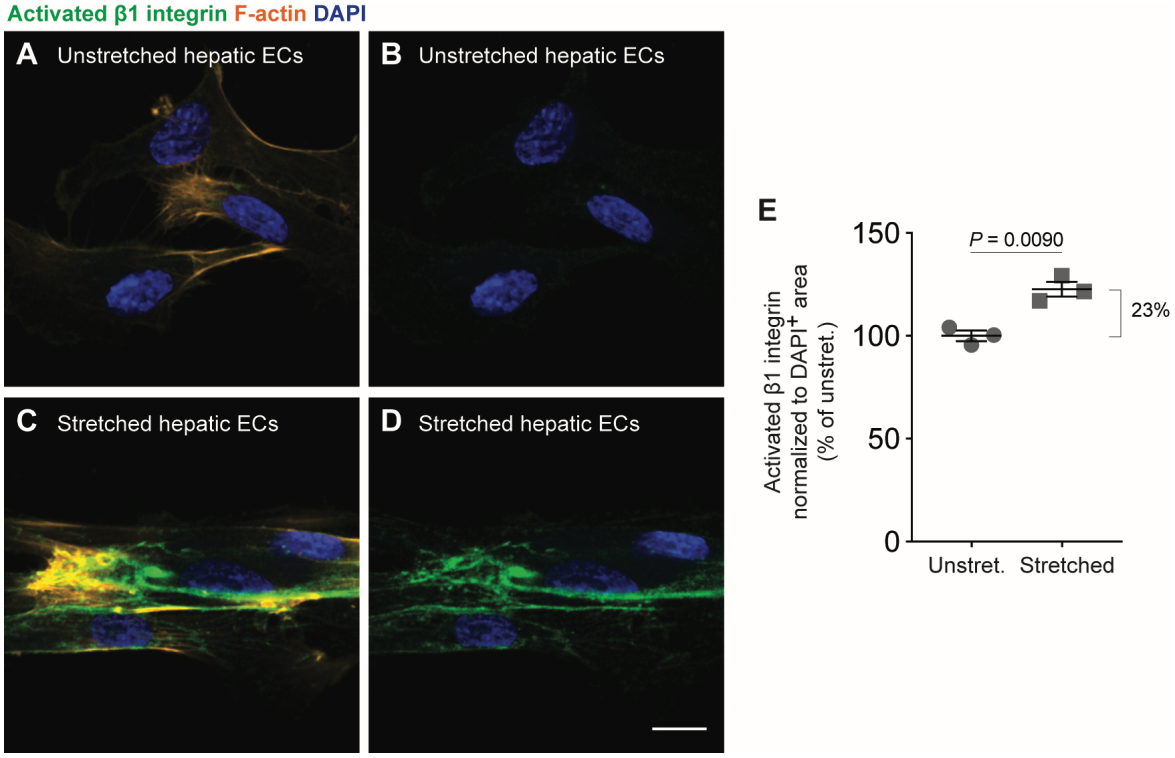

Figure 8: Mechanical stimulation of hepatic ECs induces β1 integrin activation. (A-D) Representative LSM images of unstretched (A, B) and stretched (C, D) hepatic ECs stained for activated β1 integrin (green), F-actin (orange) and cell nuclei (DAPI, blue). Scale bar, 20 µm. (E) Quantification of activated β1 integrin normalized to DAPI-positive area of unstretched and stretched hepatic ECs, shown as percentage of unstretched (Unstret.) hepatic ECs (P = 0.0090 (9.87; 35.31)). Human hepatic EC donor: male, 52 years. Data are shown as means ± s.e.m. with n = 3 stretch chambers each. Statistical significance was determined using an unpaired two-tailed student's *t*-test with 95% confidence interval (lower confidence limit; upper confidence limit).

As our results in the *ex vivo* liver perfusion model demonstrated that hemodynamic changes correlate with VEGFR3 activation (Figure 5), we wanted to know whether this also holds true in human hepatic ECs (Figure 9). Hence, we subjected human hepatic ECs to mechanical stretching and subsequently performed PLAs using antibodies against VEGFR3 and phospho-Tyrosine (p-Tyr). Consistent with the activation of β1 integrin, also the number of VEGFR3/p-Tyr PLA dots per cell is significantly increased in mechanically stretched hepatic ECs compared to unstretched controls (Figure 9 A-E).

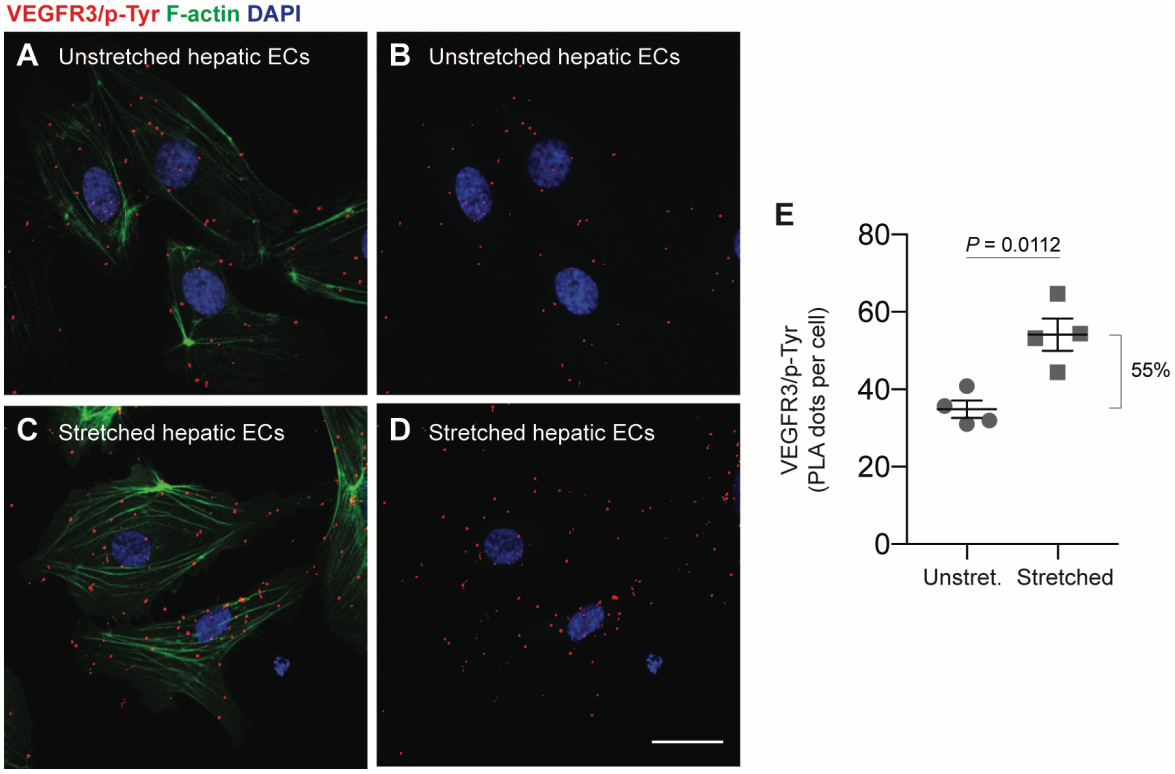

Figure 9: Mechanical stimulation of hepatic ECs induces VEGFR3 tyrosine phosphorylation. (A-D) Representative LSM images of unstretched (A, B) and stretched (C, D) hepatic ECs showing VEGFR3 tyrosine phosphorylation (VEGFR3/p-Tyr) as PLA dots (red), F-actin (green) and cell nuclei (DAPI, blue). Scale bar, 20 µm. (E) Quantification of VEGFR3/p-Tyr per cell of unstretched and stretched hepatic ECs (P = 0.0112 (6.84; 31.76)). Human hepatic EC donor: female, 59 years. Data are shown as means ± s.e.m. with n = 4 stretch chambers each. Statistical significance was determined using an unpaired two-tailed student's t-test with 95% confidence interval (lower confidence limit; upper confidence limit).

In addition to VEGFR3, also VEGFR2 has been implicated to have an important role in mechanotransduction (Shay-Salit et al., 2002, Tzima et al., 2005, Mammoto et al., 2009). It was previously reported that VEGFR3 can form heterodimers with VEGFR2 (Dixelius et al., 2003, Alam et al., 2004, Nilsson et al., 2010, Zarkada et al., 2015), and that both together with an adapter protein are able to build a mechanosensory complex (Coon, 2015). Since VEGFR2 is expressed on hepatic ECs, we wanted to know whether VEGFR2 also responds to mechanical stimulation (Figure 10). Unstretched and stretched hepatic ECs were analyzed by performing PLAs using antibodies against VEGFR2 and p-Tyr. In contrast to activation of VEGFR3 upon mechanical stimulation, phosphorylation of VEGFR2 was not increased, but rather decreased or almost unchanged in stretched compared to unstretched hepatic ECs (Figure 10 A-E). However, it should be noted that while we observed averagely up to 55 VEGFR3/p-Tyr PLA dots per stretched cell, the number of VEGFR2/p-Tyr PLA dots per cell was considerably lower.

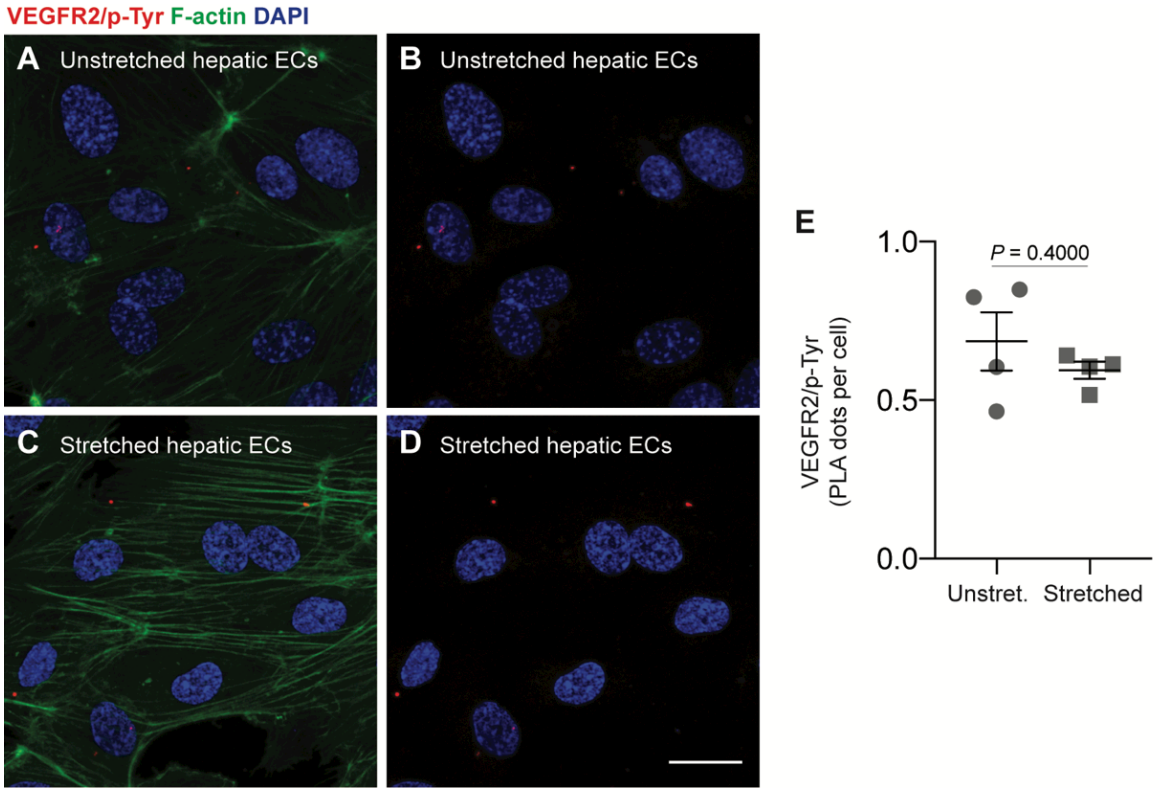

Figure 10: Mechanical stimulation of hepatic ECs results in slightly decreased VEGFR2 tyrosine phosphorylation. (A-D) Representative LSM images of unstretched (A, B) and stretched (C, D) hepatic ECs showing VEGFR2 tyrosine phosphorylation (VEGFR2/p-Tyr) as PLA dots (red), F-actin (green) and cell nuclei (DAPI, blue). Scale bar, 20 µm. (E) Quantification of VEGFR2/p-Tyr PLA dots per cell of unstretched and stretched hepatic ECs (P = 0.4000 (-0.37; 0.19)). Human hepatic EC donor: female, 59 years. Data are shown as means ± s.e.m. with n = 4 stretch chambers each. Statistical significance was determined using an unpaired two-tailed student's *t*-test with 95% confidence interval (lower confidence limit; upper confidence limit).

Finally, we investigated interaction between β1 integrin and VEGFR3 by analyzing their physical proximity (Figure 11). Therefore, we performed PLAs using antibodies against β1 integrin and VEGFR3. Colocalization of β1 integrin and VEGFR3 is significantly increased upon mechanical stimulation as determined by the number of VEGFR3/β1 integrin PLA dots per cell (Figure 11 A-E), indicating that β1 integrin and VEGFR3 are able to build a mechanosensory complex in response to mechanical stretching.

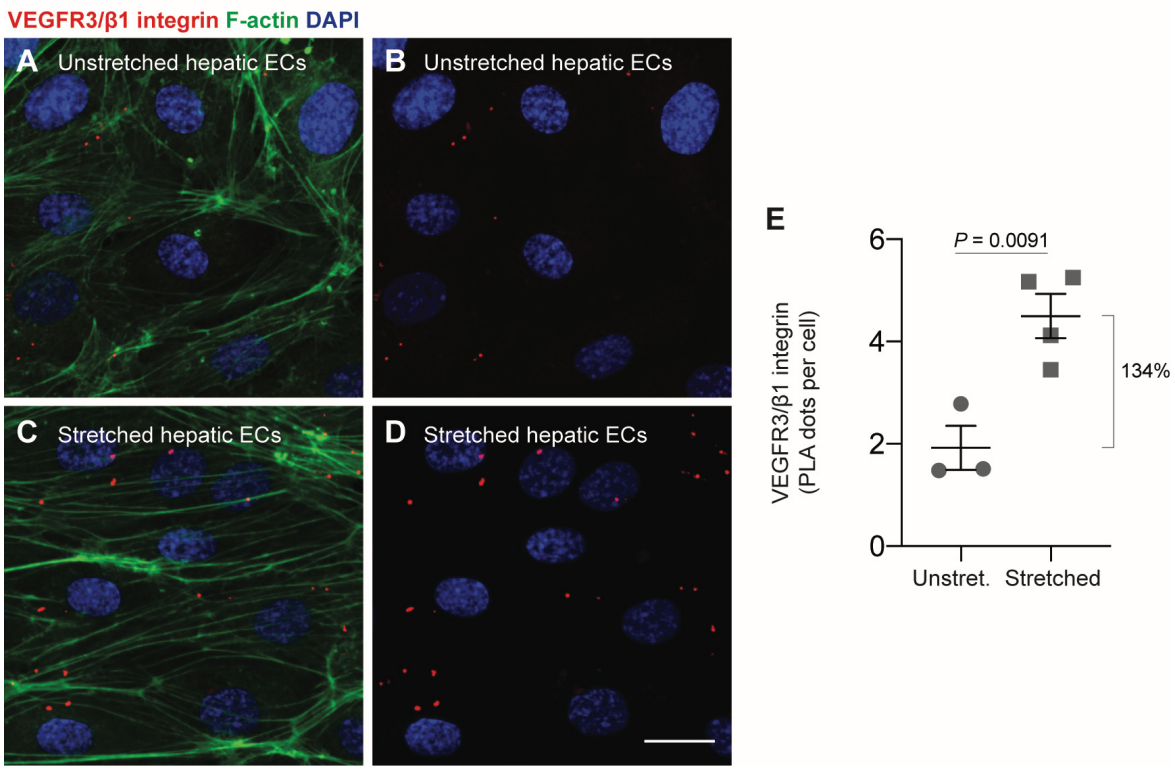

Figure 11: Mechanical stimulation of hepatic ECs induces interaction between β1 integrin and VEGFR3. (A-D) Representative LSM images of unstretched (A, B) and stretched (C, D) hepatic ECs showing interaction between VEGFR3/β1 integrin as PLA dots (red), F-actin (green) and cell nuclei (DAPI, blue). Scale bar, 20 µm. (E) Quantification of VEGFR3/β1 integrin PLA dots per cell of unstretched and stretched hepatic ECs (P = 0.0091 (0.99; 4.16)). Human hepatic EC donor: female, 59 years. Data are shown as means ± s.e.m. with n = 3 unstretched chambers versus n = 4 stretched chambers. Statistical significance was determined using an unpaired two-tailed student's t-test with 95% confidence interval (lower confidence limit; upper confidence limit).

In summary, our results show that mechanical stretching of human hepatic ECs, which mimics *in vivo* widening of the blood vessels lumen, activates mechanosensory proteins including β1 integrin and VEGFR3, and triggers their interaction.

5.2.2 Mechanical stimulation of human hepatic ECs induces secretion of angiocrine signals

Angiocrine signals have been reported for several organs and are paracrine factors produced by ECs to stimulate organ growth and regeneration (Cleaver and Melton, 2003, Nikolova and Lammert, 2003, Rafii et al., 2016, Kostallari and Shah, 2016, Augustin and Koh, 2017). Here, we aimed to investigate whether mechanical stimulation induces the secretion of angiocrine signals from human hepatic ECs. Therefore, we focused on the

analysis of common angiocrine signals such as growth factors and cytokines including HGF, IL-6 and TNF-α (Figure 12). One characteristic common to all of them is that they are necessary for normal liver regeneration (Bohm et al., 2010, Michalopoulos, 2007, Huh et al., 2004, Taub, 2004). We cultivated human hepatic ECs on stretch chambers and subsequently stretched them mechanically or left the controls unstretched. To identify angiocrine signals in the supernatant of unstretched and mechanically stretched human hepatic ECs we performed ELISAs or fluorogenic assays. Hepatic ECs were kept in starvation medium without supplementation of growth factors, cytokines or fetal calf serum to identify angiocrine signals secreted exclusively during mechanical stimulation. Human hepatic ECs release more HGF, IL-6 and TNF-α upon mechanical stretching compared to unstretched hepatic ECs (Figure 12 A-C). In addition, the activity of MMP9, which contributes to ECM remodeling and is involved in the release and activation of ECM-bound HGF (Kim et al., 2000, Olle et al., 2006, Zhou et al., 2015), is increased upon mechanical stretching of human hepatic ECs compared to unstretched hepatic ECs (Figure 12 D).

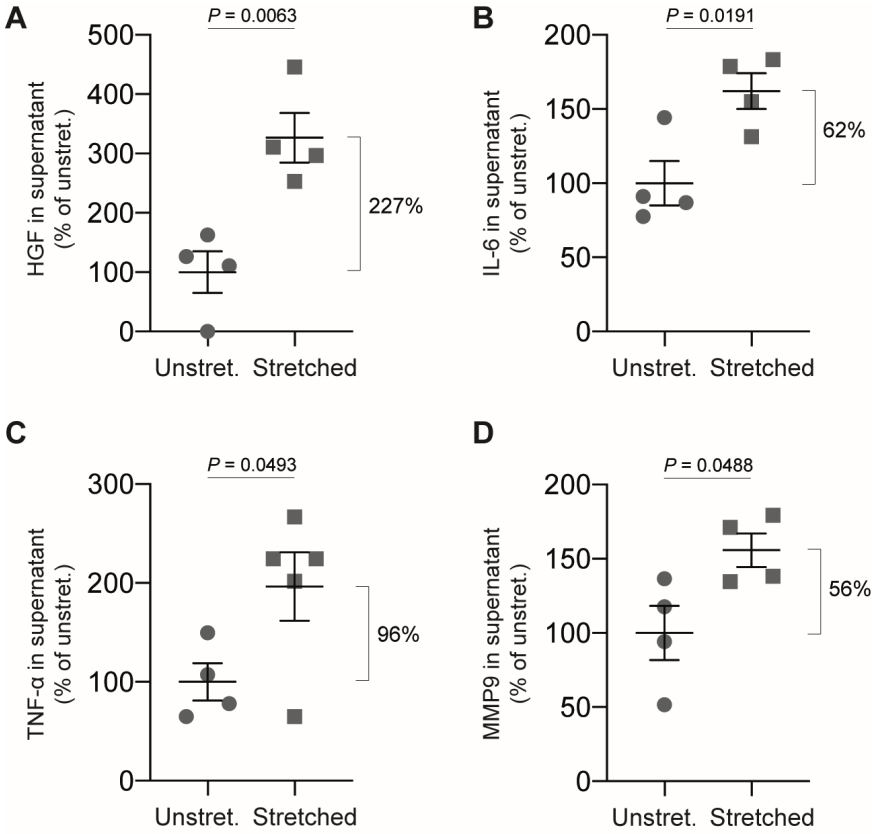

Figure 12: Mechanical stimulation of hepatic ECs induces secretion of HGF, IL-6, TNF-α and MMP9. (A-D) Quantification of HGF (A), IL-6 (B), TNF-α (C) and MMP9 (D) protein concentrations in supernatant of unstretched and stretched hepatic ECs. HGF (n = 4 stretch chambers each, *P* = 0.0063 (92.61; 360.60)); IL-6 (n = 4 stretch chambers each, *P* = 0.0191 (14.51; 109.70)) and TNF-α (n = 4 unstretched chambers versus n = 5 stretched chambers, *P* = 0.0493 (0.43; 192.40)), protein concentrations were determined by ELISAs, shown as percentage of unstretched hepatic ECs. MMP9 (n = 4 stretch chambers each, *P* = 0.0488 (0.44; 111.20)) protein concentrations were determined by a fluorescent assay, shown as percentage of unstretched hepatic ECs. Human hepatic EC donors: male, 52 years (A), male, 49 years (B), female, 59 years (C, D). Data are shown as means ± s.e.m. and statistical significance was determined using an unpaired two-tailed student's *t*-test with 95% confidence interval (lower confidence limit; upper confidence limit).

In summary, our results show that mechanical stimulation activates a mechanosensory complex on human hepatic ECs consisting of β1 integrin and VEGFR3 (Figure 8, 9, 11). Furthermore, mechanical stretching of human hepatic ECs, which mimics hemodynamic changes, for example following PHx, stimulates the release of angiocrine signals such as HGF, IL-6, TNF-α and MMP9 (Figure 12).

5.3 Endothelial mechanotransduction promotes proliferation and survival of human hepatocytes

The liver has a remarkable regenerative capacity and is able to restore its original size after acute injury (Michalopoulos, 2007). This process takes about 5-7 days in mice and about 8-15 days in humans (Michalopoulos, 2007). Notably, the restoration of the lost liver mass is mediated by mature hepatocytes and non-parenchymal cells of the remaining liver (Michalopoulos, 2007). Hepatocytes are the first cells to proliferate, followed by LSECs and HSCs (Michalopoulos, 2007). Although hepatocytes show an enormous proliferative capacity *in vivo*, their *in vitro* propagation and the induction of a proliferative response remains a challenge (Hu and Li, 2015, Garnier et al., 2018, Hu et al., 2018, Runge et al., 2000a). One explanation for such a difference between *in vivo* and *in vitro* is the lack of a crucial stimulus. Since angiocrine signals are thought to induce liver regeneration after PHx (Ding et al., 2010, Zhang et al., 2020b, Hu et al., 2014, Rafii et al., 2016), we anticipated that supernatant of mechanically stretched human hepatic ECs and thus the presence of mechano-induced angiocrine signals can drive hepatocyte proliferation *in vitro*.

5.3.1 Supernatant from mechanically stimulated human hepatic ECs induces proliferation and prevents apoptosis of human hepatocytes

So far, we demonstrated that mechanosensory complexes on hepatic ECs get activated upon mechanical stretching (Figure 8, 9, 11), and hepatic ECs can release mechano-induced angiocrine signals (Figure 12). As a next step, we tested whether conditioned medium of mechanically stretched human hepatic ECs is able to stimulate proliferation of human hepatocytes *in vitro*. Therefore, we established a co-culture system of human hepatic ECs and human hepatocytes (Figure 13). We transferred the supernatant from either unstretched or mechanically stretched human hepatic ECs onto *in vitro* cultured human hepatocytes and incubated them for six hours (a time found to be optimal for co-culturing) with the conditioned medium.

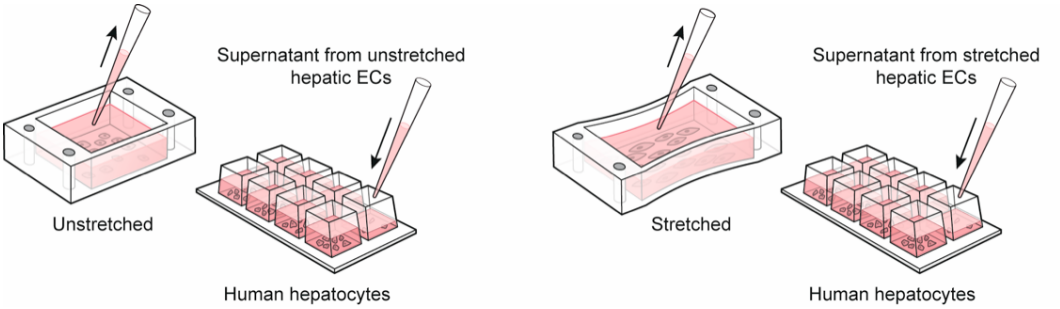

Figure 13: Schematic illustration of co-cultures of human hepatic ECs and human hepatocytes. Workflow of how supernatants were taken from unstretched or stretched hepatic ECs to treat human hepatocytes. Human hepatic ECs were either unstretched or mechanically stretched for 1.5 hours. Subsequently the supernatant was transferred onto *in vitro* cultured human hepatocytes, and incubated for six hours. Figure was drafted by Linda Große-Segerath, and illustrated by Yousun Koh.

Human hepatocytes were incubated with the conditioned medium of human hepatic ECs plus 5-ethynyl-2'-deoxyuridine (EdU) to allow immunofluorescent analyses of proliferating hepatocytes (Figure 14 A, B). In order to validate that proliferating cells are hepatocytes, we additionally checked whether hepatocytes express the hepatocyte marker HNF4-α (Figure 14 A, B). Our results show that supernatant from stretched hepatic ECs induces human hepatocyte proliferation (Figure 14 C-E). Notably, we observed differences in the proliferative capacity of hepatocytes in three different human donors (female, 12 years; male, 23 years; female, 46 years). Hepatocytes of the youngest donor showed better proliferative response upon treatment with supernatant from mechanically stretched hepatic ECs than hepatocytes from the older donors. To further confirm these results, we repeated this experiment with another proliferation marker, namely phospho-Histone H3 (pH3) (Figure 14 F). Consistent with the analysis of the EdU staining, the analysis of pH3 staining also shows that the proliferation of hepatocytes treated with the supernatant of stretched hepatic ECs increases compared to hepatocytes treated with the supernatant from unstretched hepatic ECs (Figure 14 F). Our data strongly suggests that the supernatant from mechanically stretched human hepatic ECs and the release of mechano-induced angiocrine signals are essential to induce human hepatocyte proliferation *in vitro*.

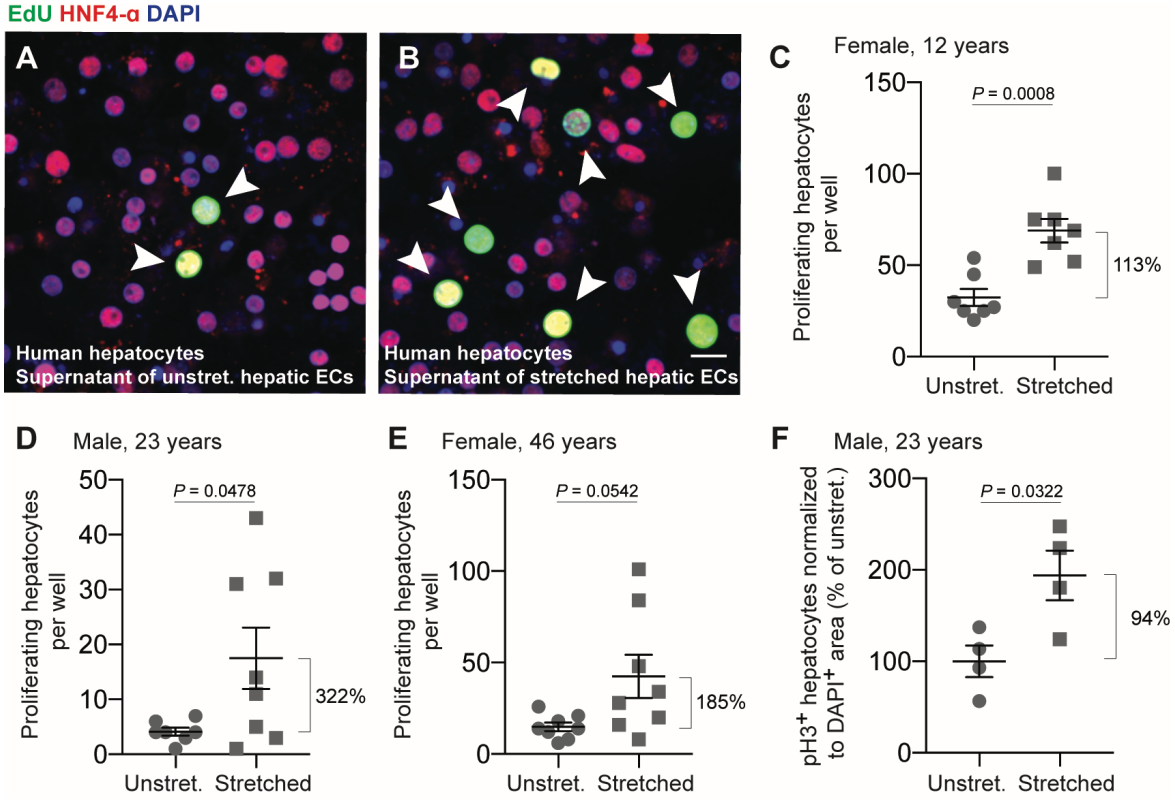

Figure 14: Supernatant from stretched hepatic ECs induces proliferation of human hepatocytes. (A, B) Representative LSM images of human hepatocytes treated with supernatant from unstretched (A) and stretched (B) hepatic ECs showing proliferating hepatocytes (EdU, green) indicated by white arrowheads, HNF4-α (red) and cell nuclei (DAPI, blue). Scale bar, 20 µm. (C-E) Quantifications of proliferating human hepatocytes in three different donors treated with supernatant from unstretched versus stretched hepatic ECs. Human hepatocyte donors: female, 12 years (C, n = 7 wells each, *P* = 0.0008 (18.93; 54.22)); male, 23 years (D, n = 7 and n = 8 wells human hepatocytes treated with supernatant from unstretched and stretched hepatic ECs, respectively, *P* = 0.0478 (0.17; 26.55)); female, 46 years (E, n = 8 wells each, *P* = 0.0542 (-0.64; 55.64)). Human hepatic EC donor: male, 52 years. (F) Quantification of proliferating human hepatocytes treated with the supernatant from unstretched versus stretched hepatic ECs as determined by the number of pH3-positive cells normalized to cell nuclei area (*P* = 0.0322 (11.79; 176.20)). Human hepatocyte donor: male, 23 years. Human hepatic EC donor: male, 52 years. Data are shown as means ± s.e.m. and statistical significance was determined using an unpaired two-tailed student's *t*-test with 95% confidence interval (lower confidence limit; upper confidence limit).

Further, we wanted to know whether supernatant from mechanically stretched human hepatic ECs is able to prevent apoptosis of human hepatocytes (Figure 15). Therefore, we performed TUNEL apoptosis assays in human hepatocytes treated with the supernatant from either unstretched or stretched hepatic ECs. We determined the apoptosis of human hepatocytes by the area of TUNEL-positive cells and normalized them to the DAPI-positive area. Our results show a significant decrease in apoptotic human hepatocytes treated with

the supernatant from stretched hepatic ECs compared to human hepatocytes treated with the supernatant from unstretched hepatic ECs (Figure 15 A-C).

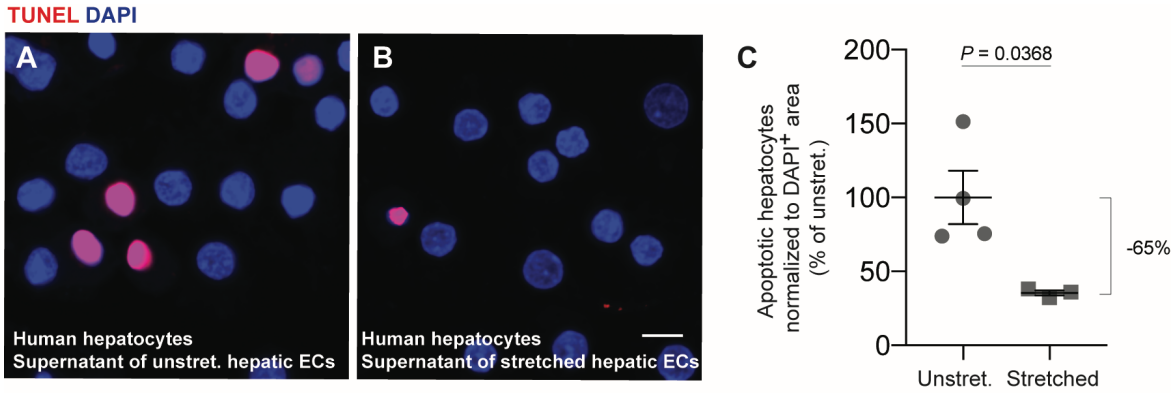

Figure 15: Supernatant from stretched hepatic ECs prevents apoptosis of human hepatocytes. (A, B) Representative LSM images of human hepatocytes treated with supernatant from unstretched (A) and stretched (B) hepatic ECs showing apoptotic hepatocytes (TUNEL, red) and cell nuclei (DAPI, blue). Scale bar, 10 µm. (C) Quantification of apoptotic human hepatocytes treated with supernatant from unstretched versus stretched hepatic ECs normalized to DAPI-positive area, shown as percentage of human hepatocytes treated with supernatant from unstretched (Unstret.) hepatic ECs (P = 0.0368 (7.40; 121.70)). Human hepatocyte donor: female, 12 years and human hepatic EC donor: female, 59 years. Data are shown as means ± s.e.m. with n = 4 and n = 3 wells human hepatocytes treated with supernatant from unstretched and stretched hepatic ECs, respectively. Statistical significance was determined using an unpaired two-tailed student's *t*-test with 95% confidence interval (lower confidence limit; upper confidence limit).

5.3.2 Endothelial β1 integrin activation induces proliferation of human hepatocytes

Our results showed that supernatant from mechanically stretched hepatic ECs induces human hepatocyte proliferation (Figure 14) and prevents human hepatocytes from apoptosis (Figure 15). Next, we wanted to address whether mechanosensory complexes on hepatic ECs are sufficient to drive the proliferative response. Therefore, we investigated the role of β1 integrin on hepatocyte proliferation *in vitro*. First, we analyzed whether we can stimulate the activation of β1 integrin on human hepatic ECs in the absence of a mechanical stimulus (Figure 16). We treated hepatic ECs for 1.5 hours with a β1 integrin-activating antibody (Wayner et al., 1993). As expected, we observed a significant increase of activated β1 integrin on hepatic ECs treated with the β1 integrin-activating antibody compared to untreated controls (Figure 16 A-C). To exclude possible side effects of the

β1 integrin-activating antibody, hepatic ECs were treated with an isotype control. Treatment with the isotype control did not lead to an activation of β1 integrin on human hepatic ECs (Figure 16 C).

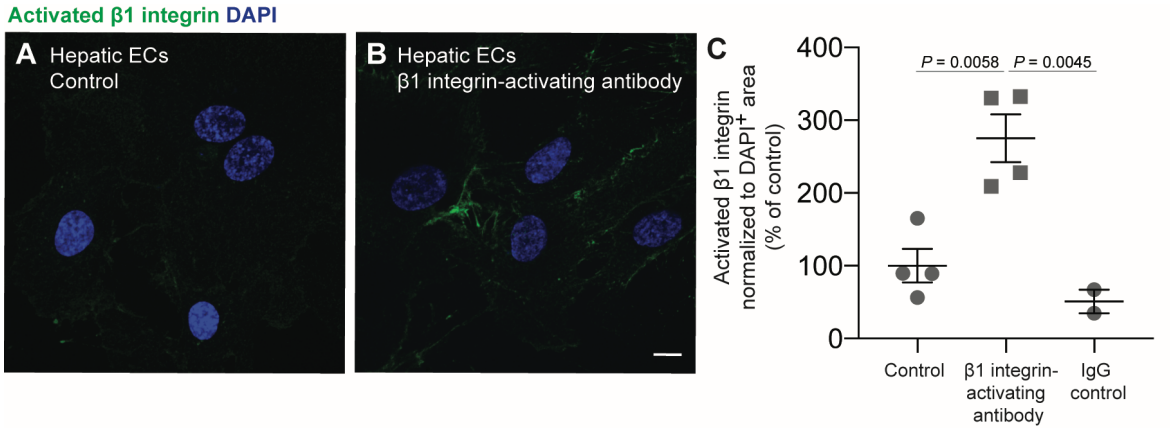

Figure 16: Activation of endothelial β1 integrin by using a β1 integrin-activating antibody. (A, B) Representative LSM images of hepatic ECs treated without (A) or with (B) β1 integrin-activating antibody. Staining shows activated β1 integrin (green) and cell nuclei (DAPI, blue). Scale bar, 10 µm. (C) Quantification of activated β1 integrin area normalized to DAPI-positive area, shown as percentage of control, in hepatic ECs treated without or with β1 integrin-activating antibody (P = 0.0058 (64.06; 286.00)) and of hepatic ECs treated with an immunoglobulin G (IgG) isotype control (P = 0.0045 (88.23; 360.10)). Human hepatic EC donor: male, 52 years. Data are shown as means ± s.e.m. with n = 4 wells of hepatic ECs treated without or with β1 integrin-activating antibody and with n = 2 wells of hepatic ECs treated with an IgG isotype control. Statistical significance was determined using one-way ANOVA followed by Tukey's test with 95% confidence interval (lower confidence limit; upper confidence limit).

Since we could activate β1 integrin on human hepatic ECs (Figure 16), our next step was to investigate the role of activated β1 integrin to promote proliferation of human hepatocytes. Therefore, we performed co-culture experiments and exposed human hepatocytes to the supernatant of either β1 integrin-activating antibody treated or untreated human hepatic ECs (Figure 17 A, B). Additionally, unconditioned medium containing β1 integrin-activating antibody and conditioned medium of hepatic ECs treated with an isotype control were also exposed to human hepatocytes (Figure 17 C, D). Our results show that exposure to conditioned medium of human hepatic ECs treated with β1 integrin-activating antibody induces proliferation of human hepatocytes. In contrast, exposure to the supernatant of untreated hepatic ECs, unconditioned medium containing β1 integrin-activating antibody, or hepatic ECs treated with an isotype control were not able to stimulate hepatocyte proliferation (Figure 17 E).

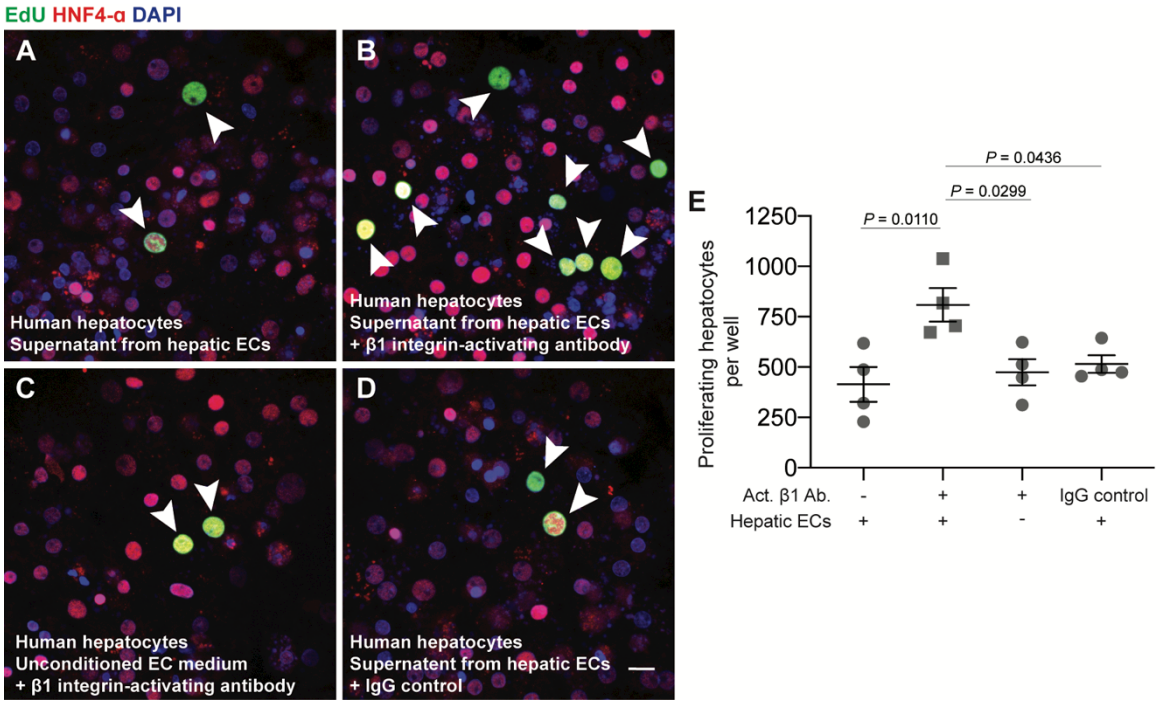

Figure 17: Supernatant from β1 integrin activated hepatic ECs induces proliferation of human hepatocytes. (A, B) Representative LSM images of human hepatocytes after incubation with supernatant from hepatic ECs treated without (A) or with (B) β1 integrin activating antibody. (C, D) Representative LSM images of human hepatocytes treated with unconditioned medium plus β1 integrin-activating antibody without previous incubation with hepatic ECs (C) and with conditioned medium of ECs treated with an IgG control (D). (A-D) Staining shows proliferating cells (EdU, green), HNF4-α (red) and cell nuclei (DAPI, blue). Scale bar, 20 µm. (E) Quantification of proliferating human hepatocytes after incubation with supernatant from hepatic ECs without or with β1 integrin-activating antibody (P = 0.0110 (91.40; 698.60)), with β1 integrin-activating antibody without previous incubation on hepatic ECs (P = 0.0299 (31.15; 638.40)) and with supernatant from hepatic ECs with IgG control (P = 0.0436 (8.99; 664.80)). Human hepatocyte donor: female, 12 years and human hepatic EC donor: male, 52 years. Data are shown as means ± s.e.m. with n = 4 wells of human hepatocytes. Statistical significance was determined using one-way ANOVA followed by Tukey's test with 95% confidence interval (lower confidence limit; upper confidence limit).

In summary, supernatant from mechanically stretched human hepatic ECs stimulates proliferation and prevents apoptosis of human hepatocytes (Figure 14, 15). According to our results, the activation of β1 integrin on hepatic ECs is involved in this process (Figure 17).

5.4 Identification of MYDGF as a novel angiocrine signal and its role in the liver

We demonstrated that conditioned medium of mechanically stretched human hepatic ECs stimulates the proliferation of human hepatocytes (Figure 14), and we identified angiocrine signals such as HGF, IL-6, TNF-α and MMP9 to be involved in this process (Figure 12). Although these signals are essential for liver regeneration (Bohm et al., 2010, Michalopoulos, 2007, Huh et al., 2004, Taub, 2004, Kim et al., 2000), they alone are not sufficient to drive the regenerative process. Thus, we hypothesize that several unidentified, mechano-induced, growth-promoting angiocrine signals are involved in hepatocyte proliferation and liver regeneration.

Consequently, we aimed to identify novel angiocrine signals using mass spectrometry-based proteomics (Figure 18). To this end, we plated primary human hepatic ECs on elastic stretch chambers, placed them onto stretch chamber devices and stretched them with a combination of permanent and cyclic stretch in the automated cell stretching machine. Since several growth factors, cytokines and also fetal calf serum are supplemented to the EC medium that might interfere with our mass spectrometry-based analysis, human hepatic ECs were cultivated in EC medium without any supplementation. We either used unstretched or mechanically stretched human hepatic ECs and analyzed the supernatant by liquid chromatography-tandem mass spectrometry (LC-MS/MS) (Figure 18 A). We identified 70 proteins in the supernatant from unstretched and mechanically stretched human hepatic ECs (Figure 18 B). 45 of these proteins were present in both the supernatant from unstretched and stretched hepatic ECs. Interestingly, 22 proteins were exclusively present in the supernatant from stretched human hepatic ECs, but not in the supernatant from unstretched human hepatic ECs, and three proteins were exclusively present in the supernatant from unstretched human hepatic ECs, but not in the supernatant from stretched human hepatic ECs.

Using LC-MS/MS we identified MYDGF, among other proteins (Protein list of LC-MS/MS data are shown in the supplementary information; Supplementary table 1), to be particularly present in the supernatant from mechanically stretched human hepatic ECs. Since MYDGF was recently identified as a secreted protein, which promotes heart regeneration after MI (Korf-Klingebiel et al., 2015), we investigated its role in the liver.

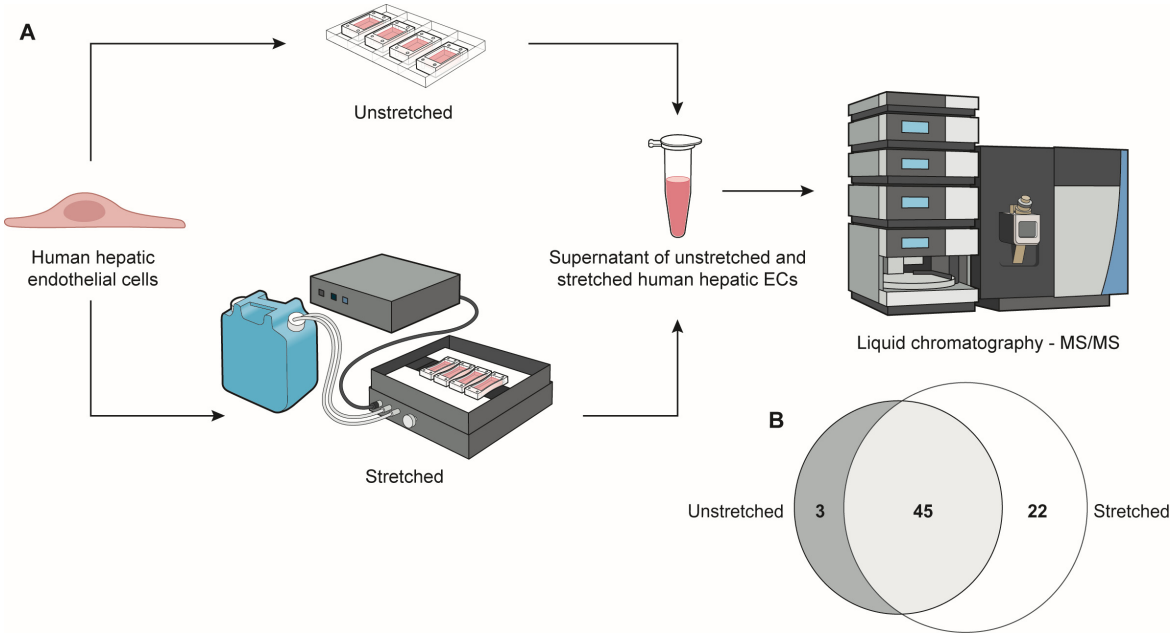

Figure 18: Identification of proteins from unstretched and mechanically stretched human hepatic ECs using mass spectrometry-based proteomics. (A) Schematic overview of the experimental procedure. Human hepatic ECs were either unstretched or mechanically stretched for 1.5 hours and the supernatants were analyzed via LC-MS/MS. (B) Identification of proteins that were present in both the supernatant from unstretched and stretched human hepatic ECs, and proteins that were exclusively present in the supernatant from either unstretched or stretched human hepatic ECs. Human hepatic EC donor: male, 52 years. Mass spectrometry was performed with n = 3 technical replicates of supernatant from unstretched versus stretched hepatic ECs in cooperation with Dr. Sonja Hartwig and Dr. Stefan Lehr (German Diabetes Center Düsseldorf). Figure was drafted by Linda Große-Segerath, and illustrated by Yousun Koh.

5.4.1 Mechanical stimulation of hepatic ECs induces expression and secretion of MYDGF

First, we intended to reproduce our observation that MYDGF is secreted from mechanically stretched human hepatic ECs. Therefore, we used human hepatic ECs that were either unstretched or mechanically stretched and analyzed them by using qPCR and Western Blot (Figure 19, Western Blots of each experiment are shown in the supplementary information; Supplementary Figure 2).

We used hepatic ECs from a 52-year-old male donor to compare the *Mydgf* mRNA expression between unstretched and mechanically stretched hepatic ECs. *Mydgf* mRNA expression was increased in mechanically stretched compared to unstretched human hepatic ECs, as determined by qPCR using acidic ribosomal phosphoprotein P0 (*36B4*),

beta-2-microglobulin (*B2M*) and hypoxanthine-guanine phosphoribosyltransferase (*HPRT*) as housekeeping genes (Figure 19 A-C). Further, we analyzed the supernatant from unstretched and mechanically stretched human hepatic ECs by Western Blot. Hepatic ECs were unstretched or mechanically stretched and the supernatant of each stretch chamber was collected and concentrated. We used hepatic ECs from two different donors and performed the experiment three times (once with hepatic ECs from a 27-year-old female and twice with hepatic ECs from a 52-year-old male). Consistent to the increase of *Mydgf* mRNA expression in mechanically stretched compared to unstretched human hepatic ECs, the secretion of MYDGF was also increased (Figure 19 D, E). Indeed, the secretion of MYDGF from hepatic ECs showed a high variability within the same stretching experiment (Western Blots of all three experiments of figure 19 D-F are shown in the supplementary information; Supplementary Figure 2). After analyzing MYDGF levels in the supernatants of unstretched and stretched human hepatic ECs, we used the corresponding lysates of unstretched and stretched human hepatic ECs to determine whether there is a difference in glyceraldehyde-3-phosphate dehydrogenase (GAPDH) levels. The protein levels of GAPDH, which is used as a housekeeping protein, did not significantly change in the lysates from unstretched compared to mechanically stretched human hepatic ECs (Figure 19 D, F).

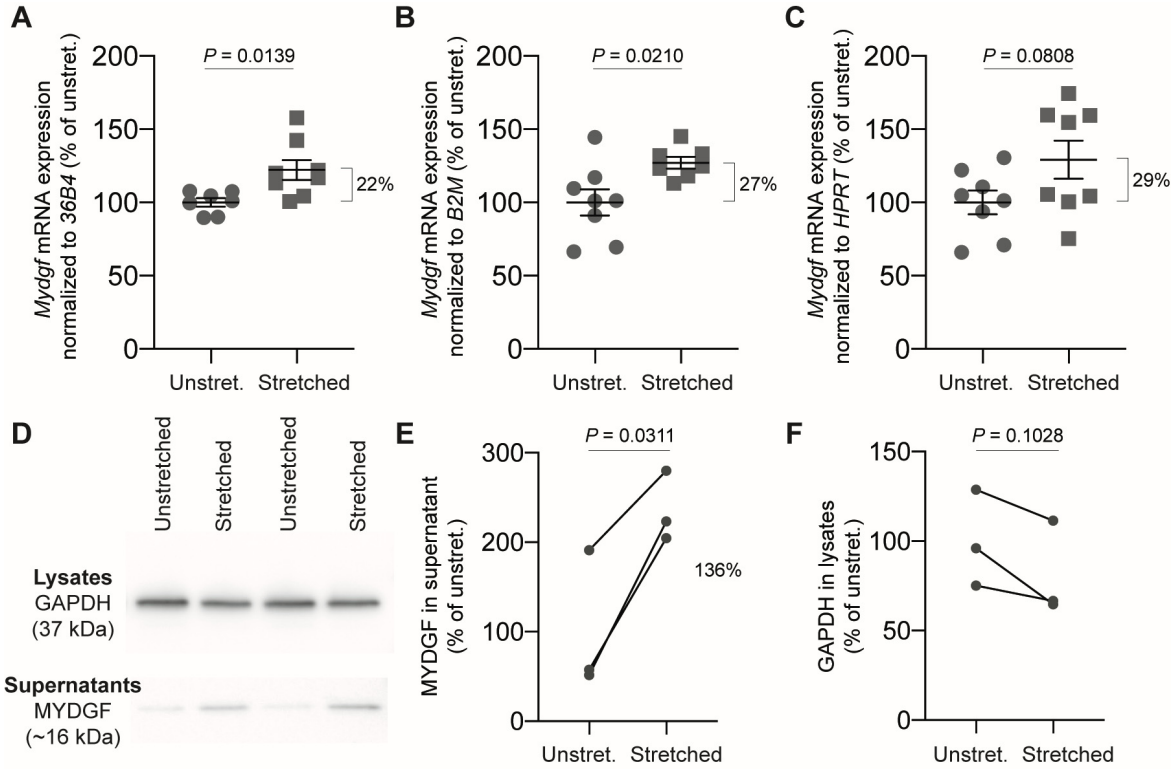

Figure 19: Mechanical stimulation of hepatic ECs increases *Mydgf* mRNA expression and MYDGF protein levels. (A-C) Quantifications of *MYDGF* expression levels in unstretched and mechanically stretched hepatic ECs normalized to three different housekeeping genes, shown as percentage of unstretched. (A) *36B4* (n = 7 unstretched chambers versus n = 8 stretched chambers, *P* = 0.0139 (5.65; 38.69)), (B) *B2M* (n = 8 unstretched chambers versus n = 7 stretched chambers, *P* = 0.0210 (5.04; 49.07)), (C) *HPRT* (n = 8 stretch chambers each, *P* = 0.0808 (-4.19; 62.51)). (D) Western Blot images of unstretched and stretched hepatic ECs, showing MYDGF protein levels (~16 kilodalton (kDa)) in the supernatant, and GAPDH protein levels (37 kDa) in lysates from either unstretched or stretched human hepatic ECs. (E) Quantification of MYDGF protein levels in the supernatant from unstretched and stretched hepatic ECs, shown as percentage of unstretched (n = 3 independent experiments with 6-10 stretch chambers each, *P* = 0.0311 (30.31; 241.30)). (F) Quantification of GAPDH protein levels in lysates from unstretched and stretched hepatic ECs, shown as percentage of unstretched (n = 3 independent experiments with 6-10 stretch chambers each, *P* = 0.1028 (-47.62; 9.48)). Human hepatic EC donors: male, 52 years (A-C) and two of three independent experiments in (E, F); female, 27 years one of three independent experiments in (E, F). Data in (A-C) are shown as means ± s.e.m. and statistical significance was determined using an unpaired (A-C) or paired (E, F) two-tailed student's *t*-test with 95% confidence interval (lower confidence limit; upper confidence limit).

To sum up, by using a mass spectrometry-based approach as well as qPCR and Western Blot we reported an increase in MYDGF secretion by human hepatic ECs after mechanical stimulation.

5.4.2 Treatment with MYDGF induces proliferation and prevents apoptosis of human hepatocytes

Further, we wanted to elucidate whether MYDGF alone is sufficient to drive human hepatocyte proliferation (Figure 20). Therefore, we treated *in vitro* cultured human hepatocytes of two different donors (male, 23 years; female, 49 years) with recombinant MYDGF for six hours in the presence of the proliferation marker EdU (Figure 20 A, B). To our knowledge, we were the first to treat human hepatocytes with recombinant MYDGF. Therefore, we tested two different concentrations of MYDGF. The hepatocytes from the 23-year-old donor were treated with 1 ng/ml MYDGF (Figure 20 C, D) and the hepatocytes from the 49-year-old donor with 5 ng/ml MYDGF (Figure 20 E). Using immunofluorescent analysis, we show a significant increase of human hepatocyte proliferation, as determined by the number of EdU-positive cells, in human hepatocytes treated with MYDGF compared to untreated hepatocytes (Figure 20 C-E). In addition, these results indicate that a higher concentration of MYDGF does not simultaneously increase the proliferative response of human hepatocytes. However, we used two different donors of human hepatocytes. Hence, further experiments are needed to find out whether hepatocytes from different donors need to be treated with different doses of MYDGF or whether lower doses than 5 ng/ml MYDGF stimulate hepatocyte proliferation to a greater extent.

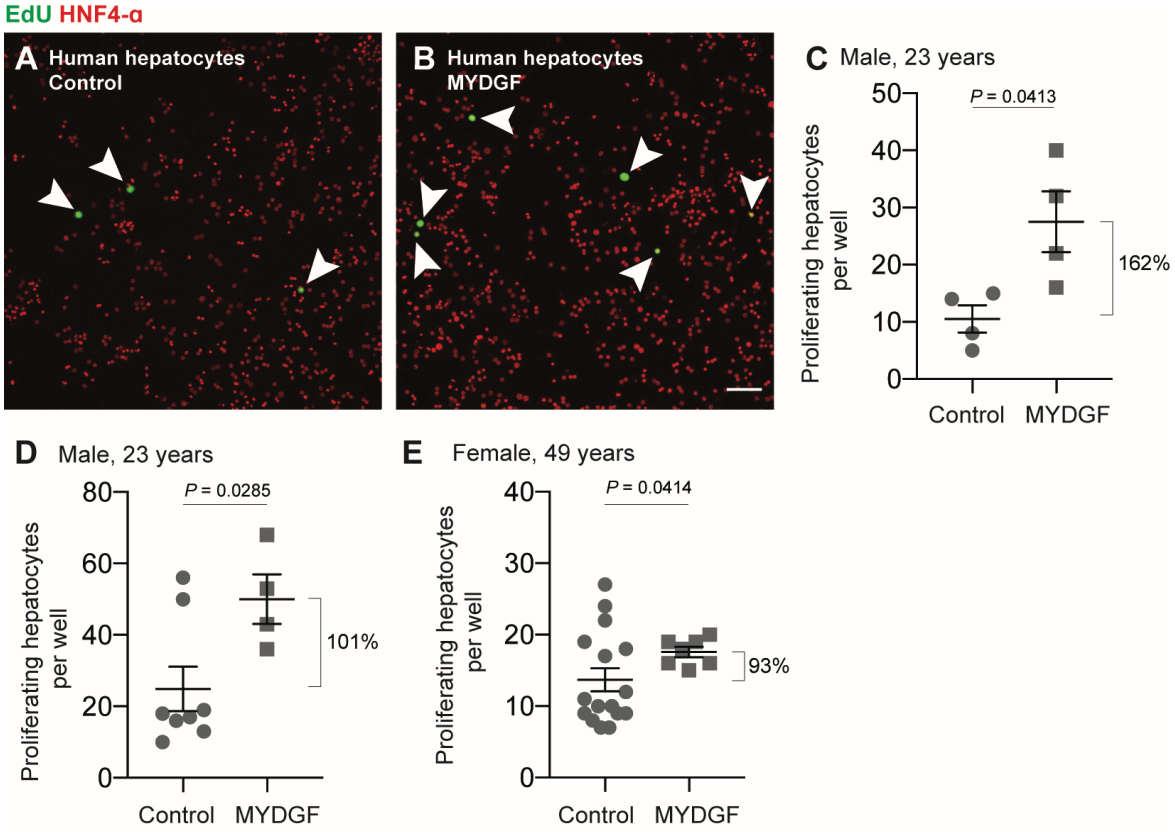

Figure 20: MYDGF induces human hepatocyte proliferation. (A, B) Representative LSM images of human hepatocytes treated without (A) or with (B) recombinant MYDGF, showing proliferating hepatocytes (EdU, green) indicated by white arrowheads and HNF4-α (red). Scale bar, 100 µm. (C-E) Quantifications of proliferating human hepatocytes in two different donors after incubation without or with MYDGF. Human hepatocyte donors: male, 23 years (C, n = 4 wells each, *P* = 0.0413 (1.07; 32.93), and D, n = 8 and n = 4 wells human hepatocytes treated without or with MYDGF, respectively, *P* = 0.0285 (3.43; 46.82)); Female, 49 years (E, n = 16 wells and n = 7 wells human hepatocytes treated without or with MYDGF, respectively, *P* = 0.0414 (0.17; 7.60)). Data are shown as means ± s.e.m. and statistical significance was determined using an unpaired two-tailed student's *t*-test with 95% confidence interval (lower confidence limit; upper confidence limit).

In order to determine whether treatment with MYDGF is sufficient to prevent apoptosis of *in vitro* cultured human hepatocytes, we performed TUNEL apoptosis assays in two different hepatocyte donors, a 23-year-old male and a 34-year-old female (Figure 21). Our results show less apoptotic human hepatocytes upon treatment with MYDGF, as determined by TUNEL-positive cell area normalized to DAPI-positive cell area (Figure 21 A-D).

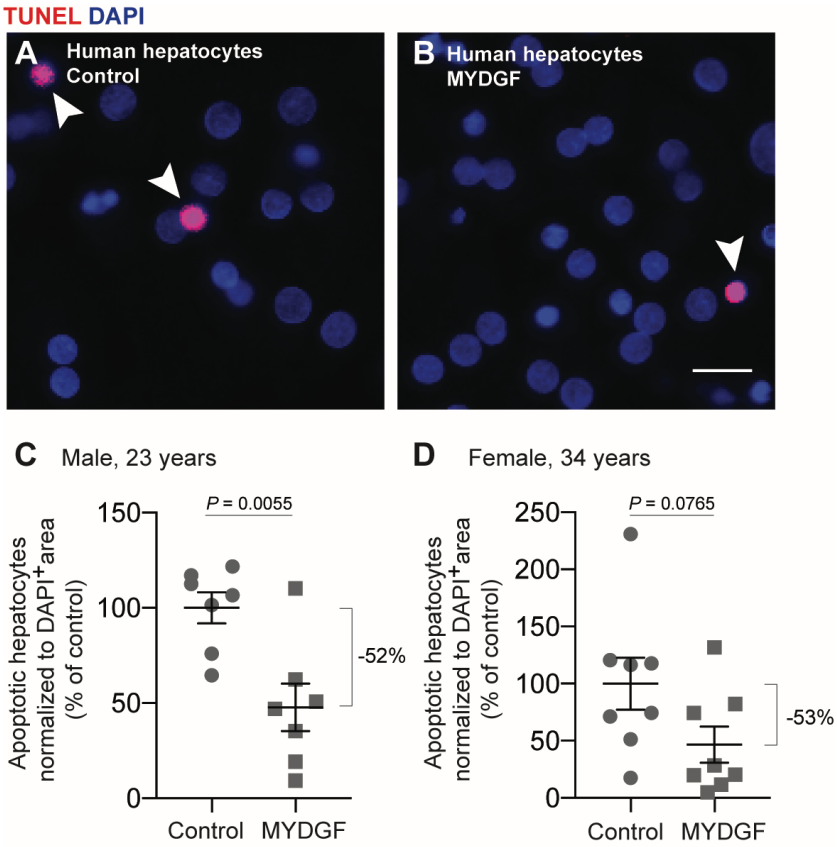

Figure 21: MYDGF prevents apoptosis of human hepatocytes. (A, B) Representative LSM images of human hepatocytes incubated without (A) or with (B) recombinant MYDGF, showing apoptotic hepatocytes (TUNEL, red) and cell nuclei (DAPI, blue). Scale bar, 20 µm. (C, D) Quantifications of apoptotic human hepatocytes in two different donors after incubation without or with MYDGF, normalized to DAPI-positive area; shown as percentage of control. Human hepatocyte donors: male, 23 years (C, n = 7 wells each, *P* = 0.0055 (19.11; 85.39)), and female, 34 years (D, n = 8 wells each, *P* = 0.0765 (-6.59; 113.30)). Data are shown as means ± s.e.m. and statistical significance was determined using an unpaired two-tailed student's *t*-test with 95% confidence interval (lower confidence limit; upper confidence limit).

In summary, our results show that treatment with MYDGF alone is sufficient to induce human hepatocyte proliferation and to prevent human hepatocytes from apoptosis.

5.4.3 Treatment with MYDGF induces growth and proliferation of human hepatocyte organoids

2D culture of human cells is a widely accepted tool for improving our understanding of several cellular processes. However, 2D cultures of human hepatocytes suffer from limitations such as rapid changes in differentiation markers of hepatocytes and their

insufficient polarization (Duval et al., 2017, Runge et al., 2000b, LeCluyse et al., 1994). Therefore, we decided to use a 3D cell culture system (Hu et al., 2018, Peng et al., 2018, Garnier et al., 2018) to mimic more physiologically the *in vivo* situation for human hepatocytes (Figure 22).

To grow human hepatocyte organoids we developed a protocol using a combination of two previously published protocols (Hu et al., 2018, Garnier et al., 2018) as well as a protocol to grow mouse liver organoids that was kindly provided by Dr. Lara Planas-Paz. Human hepatocyte organoids were not grown in Matrigel drops, but rather in Matrigel suspensions, and organoids were cultivated only for up to one week (Figure 22 A). We have grown human hepatocyte organoids (Figure 22 B) that were previously described as “grape-like” structures (Hu et al., 2018), and analyzed them in a cell viability assay or by performing whole-mount-staining. Our results show that the grown organoids are viable, except for a few dead cells that got stuck to the outer membrane (Figure 22 C). Furthermore, organoids consist of hepatocytes as shown by expression of the hepatocyte marker HNF4-α (Figure 22 D).

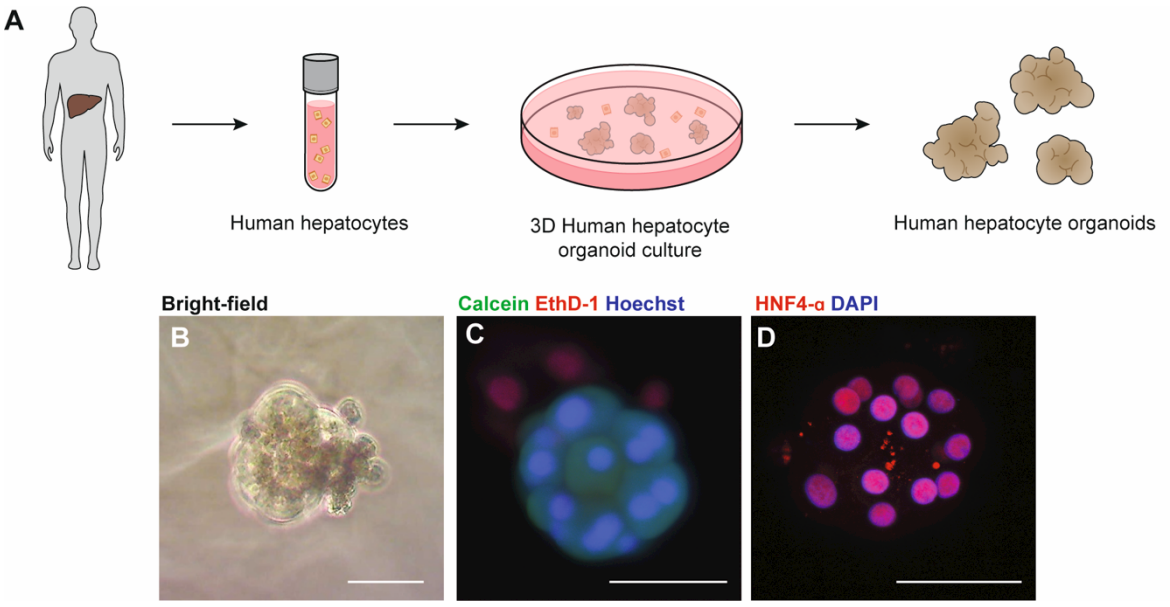

Figure 22: 3D organoids grown from human hepatocytes. (A) Schematic illustration of growing organoids from human adult hepatocytes. (B) Representative bright-field image of a human hepatic organoid after three days of cultivation. Scale bar, 100 µm. (C, D) Representative LSM images of human hepatocyte organoids, (C) showing viable cells (calcein, green), dead cells (EthD-1, red) and cell nuclei (Hoechst, blue) and (D) HNF4-α and DAPI (pink). Scale bars, 50 µm. (A) was drafted by Linda Große-Segerath, and illustrated by Yousun Koh.

In a next step, we investigated the role of MYDGF in human hepatocyte 3D organoid culture. We treated human hepatocyte organoids without or with recombinant MYDGF in the presence of the proliferation marker EdU for three days and performed whole-mount staining (Figure 23). The 3D medium for the cultivation of human hepatocyte organoids contains several growth factors including HGF and EGF, which are necessary for the formation of organoids from isolated hepatocytes. The final concentration of growth factors supplemented to 3D medium varies between 20 ng/ml and 500 ng/ml and is 25 ng/ml for HGF and 50 ng/ml for EGF. Since lower concentrations of HGF such as 10 ng/ml are reported to increase the proliferation of the 2D *in vitro* cultured hepatoma cell line HepG2 (Tsai et al., 2017), we assumed that higher concentrations of growth factors are generally necessary for 3D organoid cultures. Therefore, we increased the concentration of MYDGF in human hepatocyte 3D organoid culture compared to human hepatocyte 2D culture. Human hepatocyte organoids were treated with 10 ng/ml MYDGF (Figure 23 C, D). The organoid area was increased upon treatment with MYDGF, and there was also a slight increase in hepatocyte proliferation upon treatment with 10 ng/ml MYDGF compared to untreated control organoids (Figure 23 C, D). We further increased the concentration of MYDGF to 100 ng/ml to observe whether a higher concentration of MYDFG can increase the proliferative response of human hepatocyte organoids (Data not shown). Although we observed an increase in proliferation by about 50% in human hepatocyte organoids treated with 100 ng/ml MYDGF compared to untreated control organoids, the result was statistically not significant (Data not shown). In future experiments, lower MYDGF concentrations comparable to the MYDGF concentration of a 2D hepatocyte culture (e.g. 1 ng/ml MYDGF) could be tested. However, to conclude, our 2D and 3D *in vitro* culture experiments indicate a potential role for EC-derived MYDGF in the liver.

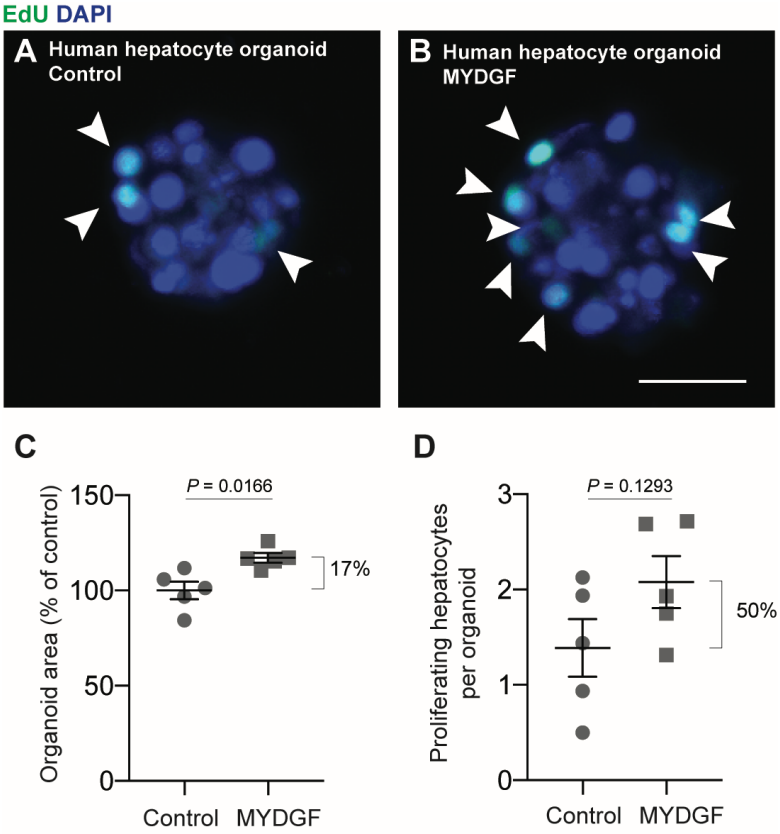

Figure 23: MYDGF induces growth and tendential proliferation of human hepatocyte organoids. (A, B) Representative LSM images of human hepatocyte organoids treated without (A) or with (B) MYDGF, showing proliferating hepatocytes (EdU, green) and cell nuclei (DAPI, blue). Scale bar: 50 µm. (C) Quantification of organoid area that were treated without or with MYDGF, shown as percentage of control (P = 0.0166 (4.36; 29.93)). (D) Quantification of proliferating human hepatocytes per organoid treated without or with MYDGF (P = 0.1293 (-0.25; 1.63)). Human hepatocyte donor: male, 23 years. Data are shown as means ± s.e.m. with n = 5 wells with 7-8 organoids each. Statistical significance was determined using an unpaired two-tailed student's *t*-test with 95% confidence interval (lower confidence limit; upper confidence limit).

6. Discussion

The aim of this study was to identify whether hemodynamic changes of the liver's vasculature, modeled by increased blood perfusion of a liver and mechanical stretching of hepatic ECs, are able to activate mechanosensory proteins and induce the release of angiocrine signals to promote liver regeneration. By using *ex vivo* liver perfusion in mice and an *in vitro* co-culture system of human hepatic ECs and human hepatocytes, we demonstrated that mechanosensory complexes, particularly β1 integrin and VEGFR3, become activated due to hemodynamic changes (Figure 5, 8, 9, 11). Mechanical stretching of human hepatic ECs triggers the release of angiocrine signals (Figure 12) and the supernatant from mechanically stretched human hepatic ECs induces proliferation and prevents apoptosis of human hepatocytes (Figure 14, 15). We performed mass spectrometry to identify additional mechano-induced angiocrine signals that contribute to liver regeneration and discovered MYDGF as a novel angiocrine signal. Addition of MYDGF to human hepatocytes stimulated their proliferation (Figure 20, 23). These results support a link between the activation of mechanosensory complexes and the release of mechano-induced angiocrine signals and offers an explanation for the underlying mechanism that regulates the induction as well as the termination of liver regeneration.

6.1 Hemodynamic changes as a stimulus for liver regeneration

It was proposed that after acute liver injury such as two-thirds PHx the blood amount passing through the remaining part of the liver is essentially unaltered (Michalopoulos, 2007, Michalopoulos, 2010). In consequence, the vascular bed would experience enormous changes as the portal vein continues the regular drainage of blood from the intestine, spleen and pancreas (Michalopoulos, 2007). There are mainly two ways that explain how the remaining one-third of the liver is perfused with an unaltered amount of blood after two-thirds of the liver is removed. On the one hand, it is possible that the blood flow velocity is increased, or on the other hand, the liver vasculature can compensate for the increased amount of blood by vasodilation. After performing PHx in mice, we could show an increase in the blood volume (relative to the analyzed liver area) in the remaining 1/3 of the liver (Lorenz et al., 2018). However, also the blood flow velocity was increased after PHx in half of the analyzed mice (Lorenz et al., 2018). In rats in which portal pressure is kept stable during and after performing PHx, liver regeneration is impaired by missing circumferential stretch, which in turn leads to a lack of activated HGF (Marubashi et al.,

2004). This indicates that vasodilation rather than an increased blood flow velocity is driving the regenerative process. Consistent with the hypothesis that hemodynamic changes induce vasodilation of the vasculature, we and others could show that after performing PHx in mice and rat (Lorenz et al., 2018, Morsiani et al., 1998), or after *ex vivo* liver perfusion in mice (Figure 4), the diameter of blood vessels is increased. Based on these results, we conclude that vasodilation of the intrahepatic blood vessels stretches ECs that line the blood vessels lumen. However, the shear stress-induced release of nitric oxide (NO) can also modulate the vascular tone (Pastor and Hadengue, 2000) and is reported to be required for liver regeneration (Schoen et al., 2001). Since the blood flow velocity, which exerts shear stress on hepatic ECs, was increased only in some mice, we suggest that this plays a minor role during liver regeneration. Rather, the dilation of vessels and circumferential stretch is the crucial stimulus to induce liver regeneration. In line with this, it was reported that shear stress can induce expression of growth-inhibiting angiocrine signals in the regenerating liver (Manavski et al., 2017). Since the vascular bed expands during regeneration, there could be a switch of mechanical stimulation from circumferential stretch to shear stress and the release of angiocrine signals may switch from growth-promoting to growth-inhibiting signals. In this thesis we mimicked the *in vivo* vasodilation of blood vessels with *in vitro* mechanical stretching of hepatic ECs to discover the underlying mechanism of how hemodynamic changes induce liver regeneration.

6.2 Role of mechano-induced angiocrine signals in the liver

In this work, we hypothesized that hemodynamic changes trigger the release of angiocrine signals from hepatic ECs, which induce proliferation of hepatocytes. To investigate this hypothesis, we used *ex vivo* liver perfusion in mice (Figure 3) and *in vitro* stretching of human hepatic ECs (Figure 7), with the aim to mimic the vasodilation of blood vessels in the regenerating liver. We identified a mechanoresponsive signaling pathway that involves the activation of β1 integrin and VEGFR3 in response to an enhanced vascular perfusion and mechanical stretching of hepatic ECs (Figure 5, 8, 9, 11). While mechanical activation of β1 integrin was already shown to increase VEGFR3 phosphorylation on lymphatic ECs (Planas-Paz et al., 2012), we have identified a similar interaction on hepatic ECs (Figure 11). Furthermore, we report that mechanical stretching of hepatic ECs triggers the release of angiocrine signals (Figure 12). Notably, already in the mouse embryo, both β1 integrin and VEGFR3 are required for liver growth and the production of angiocrine HGF (Lorenz et al., 2018). Although our results provide a

mechano-dependent β1 integrin-VEGFR3 signaling pathway on hepatic ECs, it remains unclear how the activation of β1 integrin and VEGFR3 is linked to the release of angiocrine signals. Beside integrins and VEGFRs, there are several other mechanoresponsive proteins such as PECAM-1 (Neubauer et al., 2000) and VE-cadherin (Geraud et al., 2012) expressed on hepatic ECs. Together with VEGFR2, the latter two build a mechanosensory complex that responds to blood flow and activates integrins on aortic ECs (Tzima et al., 2005). Phosphorylation of VEGFR2 on hepatic ECs activates the VEGFR2-Id1 pathway, which induces the expression of Wnt2 and HGF in a mechanically independent manner (Ding, 2010). Although the phosphorylation of VEGFR family member VEGFR2 induces the expression of angiocrine signals, it is still unclear how phosphorylation of VEGFR3 can induce angiocrine signals such as HGF in hepatic ECs. In future experiments, RNA sequencing of unstretched and mechanically stretched human hepatic ECs may gain more insights into how mechanical stimulation activates angiocrine downstream signaling via the β1 integrin-VEGFR3 signaling pathway on hepatic ECs. In addition, this approach may also lead to identification of other mechanosensory complexes that are activated by mechanical stimulation. Mechanoresponsive signaling pathways have generally gained more attention in ECs, nevertheless these pathways should also be better studied in hepatic ECs.

Our results show that mechanical stretching activates mechanoresponsive proteins on hepatic ECs and triggers the release of angiocrine signals (Figure 5, 6, 8, 9, 11, 12). Furthermore, we could show that the supernatant from mechanically stretched human hepatic ECs, which contains mechano-induced angiocrine signals such as HGF, IL-6, TNF-α and MMP9, promotes the proliferation of human hepatocytes (Figure 14). Since mechanical stretching of ECs activates β1 integrin, hepatocyte proliferation is also increased when ECs are treated with β1 integrin-activating antibody instead of using stretch as a mechanical stimulus (Figure 17). Prior studies have focused on the role of integrin signaling in hepatocytes rather than in hepatic ECs. The loss of β1 integrin in hepatocytes impairs liver regeneration, while the loss of αv β8 integrin promotes the regenerative process (Speicher et al., 2014, Greenhalgh et al., 2019). In line, integrins can play a role in both organ health and disease (Ingber, 2003). Recently, mechanotransduction via integrins was reported to be involved in angiocrine downstream signaling in congestive hepatopathy (Hilscher et al., 2019). In both, liver regeneration after PHx and congestive hepatopathy, sinusoids become dilated and ECs get stretched. Biaxial stretch of murine hepatic ECs activates Piezo channels, which then activate Notch signaling pathways and trigger the release of CXCL1 (Hilscher et al., 2019). RNA sequencing and ingenuity pathway analysis revealed that the subunits αv and β3 integrin are involved in the activation of Piezo channels. Angiocrine CXCL1 recruits neutrophils in the sinusoids and promotes

the formation of microthrombi and portal hypertension (Hilscher et al., 2019). Similar to the secretion of CXCL4, which provokes liver fibrosis after chronic liver injury (Ding et al., 2014), CXCL1 promotes liver disease (Hilscher et al., 2019). Furthermore, it is also known that Notch signaling pathways impair liver regeneration after acute liver injury and promote liver fibrosis after chronic liver injury (Duan et al., 2018, Tanriverdi et al., 2016). While Hilscher et al. reported an αv and β3 integrin-dependent signaling pathway that promotes liver disease, our results indicate that mechano-induced β1 integrin interact with VEGFR3 and induce the release of angiocrine signals to promote liver regeneration (Lorenz et al., 2018). Variable parameters such as different modes of cell starvation before stretching or strain amplitudes may cause the activation of different signaling pathways on hepatic ECs. In contrast to Hilscher et al. who starved murine hepatic ECs for six hours before stretching, we did not starve the human hepatic ECs before stretching (we only incubated them in starvation medium during stretching). Furthermore, we used half an hour uniaxial static stretch followed by one hour uniaxial cyclic stretch (30 cycles/min) to stretch human hepatic ECs, while Hilscher et al. used biaxial cyclic stretch for four hours (60 cycles/min) to stretch murine hepatic ECs. Although the protocols differ in the aforementioned points, both approaches indicate that mechanical alterations can induce mechano-induced downstream signaling pathways to promote the release of angiocrine signals that either provoke liver disease or promote liver regeneration.

Our results provide, for the first time, a role of mechano-induced angiocrine signals in the liver to promote liver regeneration. However, our system only allowed for uniaxial stretch of hepatic ECs to mimic vasodilation of the blood vessels. It would be interesting to study further conditions, including biaxial stretch of hepatic ECs, which may stimulate different physiological conditions. Further, it is reported that shear stress also occurs early in liver regeneration. Therefore, not only the release of angiocrine signals due to stretch, but also the release due to shear stress needs to be investigated. Hepatic ECs could be exposed to mechanical stretch and shear stress, and techniques such as RNA sequencing could then be used to identify novel angiocrine signals not yet associated with the liver by analyzing differentially expressed genes encoding these angiocrine signals.

To sum up, mechanosensory pathways in hepatic ECs that promote the release of angiocrine signals offer new opportunities to understand liver regeneration and treat liver disease, although the underlying mechanisms need to be further investigated.

6.3 MYDGF as a novel mechano-induced angiocrine signal

Our results provide strong evidence that supernatant from mechanically stretched human hepatic ECs, which contains mechano-induced angiocrine signals such as HGF, IL-6, TNF-α and MMP9, promote human hepatocyte proliferation (Figure 12, 14), and are essential for liver regeneration. However, we propose that other, unidentified angiocrine signals are also involved in the regenerative process. To identify novel angiocrine signals in the supernatant of stretched human hepatic ECs, we used a mass spectrometry-based approach (Figure 18). We identified MYDGF as a novel angiocrine signal with impact on human hepatocyte proliferation *in vitro* (Figure 20, 23). MYDGF was first identified as a secreted protein from bone marrow-derived monocytes and macrophages and is involved in protection and repair of the heart after MI (Korf-Klingebiel et al., 2015). While MYDGF is also required for angiogenesis after ischemic injury, it is not essential for embryonic development (Korf-Klingebiel et al., 2015). Beside its role in the heart, a possible role of MYDGF in tissue repair in other organs is also suspected (Korf-Klingebiel et al., 2015). Our results support a possible role of MYDGF in liver regeneration. MYDGF was found in the supernatant of stretched but not unstretched human hepatic ECs and addition of MYDGF to human hepatocytes *in vitro* induced proliferation and prevented apoptosis (Figure 20, 21).

Although hepatic ECs are involved in developmental, homeostatic and regenerative processes, neither their developmental origin nor their origin and renewal in the adult system are fully clarified. Interestingly, lineage tracing in mice identified that liver vessels derive from the endocardium, which forms the innermost layer of the developing heart (Zhang et al., 2016). In addition, it was shown that the endocardial-derived embryonic liver vasculature persists in the adult system, and forms multiple types of hepatic ECs (Zhang et al., 2016). Furthermore, there is also evidence that adult hepatic ECs originate from the bone marrow (Harb et al., 2009, Sorensen et al., 2015). Mature hepatic ECs divide rarely, but after injury, resident EC progenitor cells and bone marrow-derived progenitor cells repopulate the liver to restore the vascular network (Harb et al., 2009, Wang et al., 2012a). In line, the recruitment of bone marrow-derived hepatic ECs was reported to be essential for liver regeneration (Wang et al., 2012b). Interestingly, hepatic ECs in the injured liver express both hematopoietic and endothelial cell markers such as CD45 and CD33 (Harb et al., 2009), and bone marrow sinusoidal ECs were shown to express Stabilins (Qian et al., 2009), which are also reported as markers for hepatic ECs (DeLeve and Maretti-Mira, 2017). Based on our results, we could show that mechanically stretched hepatic ECs, which

might originate from the bone marrow, are able to secrete MYDGF. Consistently, also MYDGF that is involved in heart repair after MI was reported to be secreted from bone marrow-derived cells, specifically from bone marrow-derived monocytes and macrophages. Since hepatic ECs as well as monocytes and macrophages express the same hematopoietic markers such as CD45 and CD33, and both can originate from bone marrow (Lambert et al., 2017), it may also be that hepatic ECs can secrete MYDGF in the injured liver, similar to monocytes and macrophages in the injured heart.

In conclusion, our results provide evidence that hepatic ECs can secrete angiocrine signals that are essential for liver regeneration and, like MYDGF, have not yet been identified. The discovery of novel angiocrine factors and their role during liver regeneration can pave the way for the development of therapeutic implications to treat liver diseases. A possible way for future research, is the optimization of the right cocktail of angiocrine factors to increase hepatocyte proliferation and thus promote liver regeneration in the absence of blood flow as a stimulus.

6.4 Limited proliferative capacity of human hepatocytes *in vitro*

Primary human hepatocytes are considered as the golden standard for human hepatocyte-based *in vitro* systems (Guguen-Guillouzo and Guillouzo, 2010, Vinken and Hengstler, 2018, Fraczek et al., 2013). However, despite the enormous proliferative response of hepatocytes *in vivo* after injury, *in vitro* cultured hepatocytes are not expandable or generally able to proliferate (Hu and Li, 2015, Garnier et al., 2018, Hu et al., 2018, Runge et al., 2000a). Our results demonstrate that supernatant from mechanically stretched human hepatic ECs induces proliferation and prevent apoptosis of human hepatocytes *in vitro* (Figure 14, 15). These results indicate that growth-promoting angiocrine signals, which are absent during *in vitro* cultivation, are essential for the proliferative response of human hepatocytes. Beside their inability to proliferate, human hepatocytes were also reported to dedifferentiate and to have an insufficient polarization in culture (Duval et al., 2017, Runge et al., 2000b, LeCluyse et al., 1994, Godoy et al., 2013). Furthermore, *in vitro* cultured hepatocytes are not divided into different metabolic zones. Metabolic zonation was reported decades ago, when hepatocytes were shown to be uniform on histological level along the sinusoid, whereas their function was highly heterogenous (Jungermann and Kietzmann, 1996). Consistently, hepatocytes resident in different zones also differ in their proliferative response (Wang et al., 2015). Specifically,

hepatocytes located in close proximity to the portal vein proliferate twice the rate as other hepatocytes (Wang et al., 2015). Concerning our results, up to 1% of human hepatocytes, which were co-cultured with the supernatant from human hepatic ECs in a *2D in vitro* system, were able to proliferate. Thus, it needs to be further investigated which hepatocytes are able to respond to angiocrine signals with proliferation and which expression profile these hepatocytes have. By using 3D organoid cultures we could show that even up to 10% of human hepatocytes proliferate. In line, 3D organoid cultures were reported to mimic *in vivo* conditions more physiologically (Hu et al., 2018, Garnier et al., 2018). Therefore, 3D cultured hepatocytes are generally able to proliferate to a higher extent. Although 3D hepatocyte organoid cultures are an improvement of 2D hepatocyte cultures, one key stimulus, namely the vascularization, is missing in both systems. Indeed, new techniques such as the production of functional artificial blood vessels (Andrique et al., 2019) or the development of 3D liver-like tissues with capillary-like structures branching from perfusable channels (Mori et al., 2020) also consider vascularization. However, cultivation of human hepatocytes is still challenging and the right cocktail of angiocrine signals that is able to induce human hepatocyte proliferation, which is comparable to *in vivo* hepatocyte proliferation, is not yet identified.

Our results not only show that supernatant from mechanically stretched human hepatic ECs induces proliferation of human hepatocyte, but also that the novel angiocrine signal MYDGF is able to induce proliferation of human hepatocytes *in vitro* (Figure 20, 23). In our experimental setup, we used an EdU incorporation assay to determine hepatocyte proliferation, whereby EdU (a nucleoside analogue of thymidine) is incorporated during active DNA synthesis. Accordingly, the cells are in the S Phase of the cell cycle. Although the incorporation of EdU is widely accepted to determine cell proliferation, our next step will be to confirm our results with another proliferation assay. For example, hepatocytes could be stained with the proliferation markers pH3 or Ki-67. While pH3 identifies cells in the M phase of the cell cycle, Ki-67 identifies cells in all phases of the cell cycle except for cells in the G_0 phase (Romar et al., 2016). The use of a different proliferation marker will strengthen our hypothesis that MYDGF induces proliferation of human hepatocytes *in vitro*. Since *in vitro* cultivated human hepatocytes differ from human hepatocytes *in vivo*, the *in vitro* generated results of human hepatocyte proliferation need to be validated in a mouse model to prove the role of MYDGF in liver growth and regeneration. Therefore, we are in process to overexpress *Mydgf* over time by using adeno-associated viruses in mice to identify its physiological role in the liver.

In general, identification of angiocrine signals with the ability to promote human hepatocyte proliferation contribute to improve culture conditions for human hepatocytes *in vitro*. In addition, *in vitro* systems that better mimic the *in vivo* situation could help to further elucidate the underlying mechanism of liver regeneration.

6.5 Clinical relevance of the pathway involved in liver regeneration

Globally, more than 56 million people die each year, approximately 3.5% of them from liver disease (Collaborators, 2018, Asrani et al., 2019). The mortality rate of people who suffer from liver diseases increased between 1990 and 2017, and this trend will continue in the future (Collaborators, 2018). The most common causes of death from liver disease are due to liver cirrhosis and hepatocellular carcinoma (Asrani et al., 2019). Since the morphology and the function of the liver is disturbed in the diseased state, most liver diseases progress in a similar way. While liver fibrosis is initially a beneficial and wound healing process in which the liver repairs itself by depositing ECM proteins, this response can progress to liver cirrhosis over time. The most common causes of liver cirrhosis are hepatitis C, non-alcoholic fatty liver disease (NAFLD) and alcohol-related disease. Once the liver is cirrhotic, the blood flow through the stiffer liver declines while the pressure in the portal vein increases. Since liver regeneration is impaired in cirrhotic livers, our findings, also contribute to a better understanding of diseases such as cirrhosis and its potential treatment.

Decompensated cirrhosis can lead to complete dysfunction of the liver and also liver cancer. Therefore, patients with acute or chronic end-stage liver disease require liver transplants (Rai, 2013). Limitations of liver transplantation are the poor quality of livers rendering them non-transplantable and the shortage of donor availability. When a liver transplant is available, it is usually rinsed and cooled with preservation fluid and stored on ice until transplantation. This procedure is known as “static cold storage” (Jia et al., 2018). However, the interruption of the blood supply to the liver during transportation and the sudden re-perfusion upon transplantation can cause complications such as ischaemia reperfusion-related injuries (Nasralla et al., 2018). While static cold storage of liver transplants does not allow optimal preservation due to the missing perfusion, it has been reported that machine perfusion of the liver has the potential to expand the available pool of transplantable livers (Brockmann et al., 2009, Jia et al., 2018, Nasralla et al., 2018). During normothermic machine perfusion, the liver transplant is perfused with oxygenated

blood and nutrients and remains on body temperature to maintain the liver in a physiological state (Brockmann et al., 2009, Nasralla et al., 2018). Advantages of normothermic liver transplantation compared to static cold storage are fewer transplant injuries and rejections and longer mean preservation times (Nasralla et al., 2018). Recently, a perfusion machine has been developed that is capable of providing blood supply from both the hepatic artery and the portal vein while mimicking core functions of the body, which are necessary for the livers health (Eshmuminov et al., 2020). Flow and pressure sensors monitor the blood flow of the portal vein and the hepatic artery as it flows into the liver and out of the vena cava. Additionally, the machine is also able to mimic pulsatile flow in the hepatic artery (Eshmuminov et al., 2020). Furthermore, the glucose metabolism is monitored, metabolic waste products are removed and the liver is moved slightly to avoid pressure necrosis (Eshmuminov et al., 2020). This perfusion technology can preserve liver function for one week *ex vivo* and additionally improve the function of poor quality livers that otherwise could not be transplanted (Eshmuminov et al., 2020). In addition, another study reported that fatty livers can be conserved with normothermic perfusion, and the severity of steatosis decreased in parallel in a pig model (Jamieson et al., 2011). While we found that enhanced vascular perfusion promotes liver regeneration, it has also been shown for liver transplantation that machine perfusion is required to restore liver function and to increase the rate of good quality transplantable livers.

In addition, innovative approaches such as liver-on-chip and 3D-printed partial liver transplants are based on the regenerative capacity of the liver (Bizzaro et al., 2019, Goulart et al., 2019). Therefore, a better understanding of the underlying mechanism of liver regeneration is beneficial to improve these new bioengineered approaches.

In summary, a better understanding of the complex process involved in liver regeneration might help to understand disease in which the regenerative process is disturbed. New techniques based on vascular perfusion to maintain the livers function and innovative *in vitro* approaches based on the regenerative capacity of the liver may positively contribute to improve the shortage of liver transplants and may help patients on long waiting lists for liver transplantation.

6.6 Conclusion

Based on our results we propose a model to explain the induction of liver regeneration (Figure 24). After PHx, the same amount of blood has to pass through the remaining part of the liver (Michalopoulos, 2007). Thus, an enhanced vascular perfusion in the remaining vascular bed of the liver leads to a vasodilation of the vasculature, and stretches LSECs that line the blood vessels lumen. Since LSECs express mechanosensory proteins, they are able to sense hemodynamic changes. Upon mechanical stretching, mechanosensory complexes including β1 integrin and VEGFR3 get activated on LSECs, and subsequently LSECs release angiocrine signals. Beside common angiocrine signals such as HGF, IL-6, TNF-α and MMP9 that were reported to be essential for liver regeneration, we also suggest that novel angiocrine signals such as MYDGF are involved in the regenerative process. Thus, we propose that several mechano-induced angiocrine signals support hepatocyte proliferation and drive liver regeneration. Hepatocytes are the first cells that start to proliferate in the regenerating liver, followed by LSECs, HSCs and cholangiocytes (Michalopoulos, 2007). Once the liver mass is restored and the vascular bed has reached its final size, there is no longer a vasodilation within the liver's vasculature and the regenerative process is terminated. This indicates that the induction and also the termination of liver regeneration requires a control system like hemodynamic changes that mediates liver-to-body weight ratio and, in particular, prevents overgrowth of the liver after the regenerative process is terminated. Our model suggests a novel mechanism of how hemodynamic changes regulate the release of growth-promoting angiocrine signals that are crucial for liver regeneration. Simultaneously, our model also explains the termination of the regenerative process. Once the liver's vascular bed is restored, ECs are no longer mechanically stretched and consequently, there is no longer a release of growth-promoting angiocrine signals.

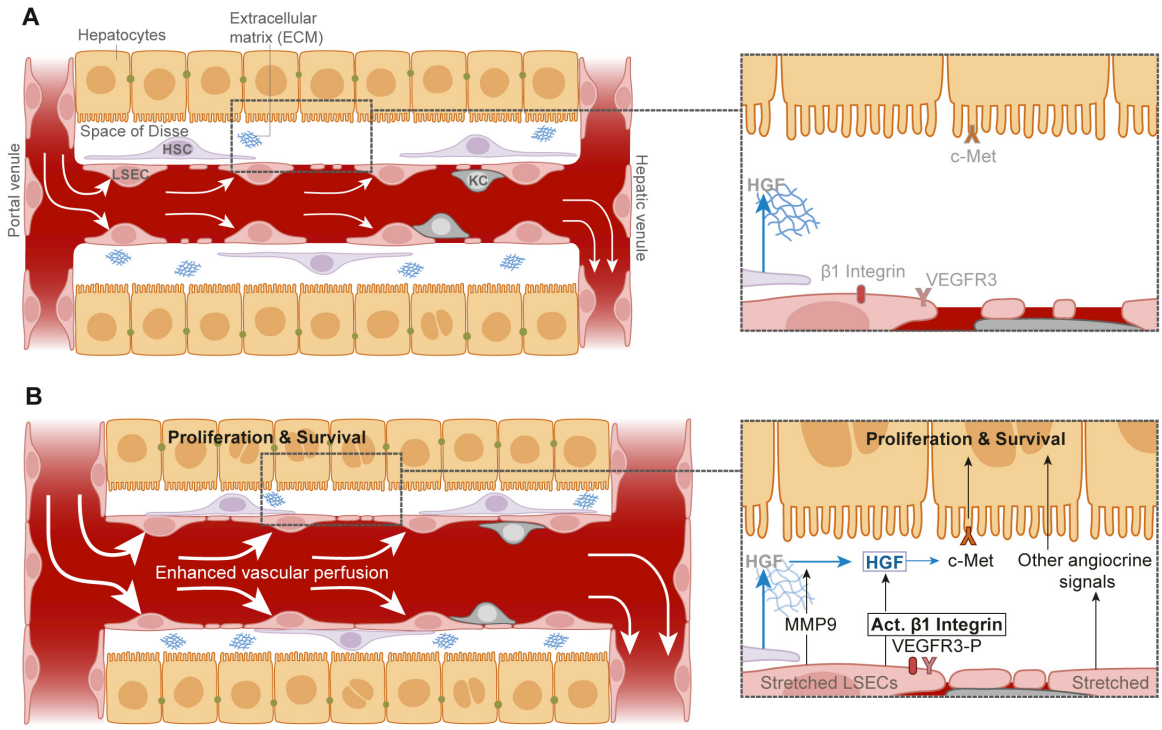

Figure 24: Schematic illustration of a liver sinusoid and how vasodilation and mechanical stretching of LSECs contribute to liver regeneration. (A, B) Liver sinusoid with LSECs, HSCs, KCs and hepatocytes under normal blood flow (A), and with enhanced vascular perfusion (B). The higher perfusion enlarged the vascular lumen of the sinusoid and stretches LSECs. Mechanosensory proteins on LSECs including β1 integrin and VEGFR3 get activated and LSECs release common angiocrine signals such as HGF, IL-6, TNF-α, MMP9 as well as novel angiocrine signals such as MYDGF. The release of angiocrine signals enhance proliferation and survival of hepatocytes and contribute to liver regeneration. Adapted from (Lorenz et al., 2018). Illustrated by Yoshun Koh.

6.7 Outlook

The underlying mechanism of liver regeneration challenges researchers for decades. With our model we propose a possible mechanism of liver regeneration and contribute to further decipher the mystery of this complex process. However, there are still many open questions to be answered and although our study contributes to reveal the process of liver regeneration, it also raises further questions.

Our next step will be to use RNA sequencing to identify genes coding for angiocrine signals secreted from hepatic ECs that promote liver regeneration. Both mechanically stretched and unstretched human hepatic ECs as well as human hepatic ECs exposed to shear stress will be analyzed. This would allow identification of differently up- or downregulated

genes in these conditions. Recently, the heterogeneity of human hepatic ECs and human hepatocytes were reported by using single-cell RNA sequencing (Aizarani et al., 2019). Since we observed that only a small population of hepatocytes responded to angiocrine signals, we propose to use single-cell RNA sequencing to study differences between the proliferating and non-proliferating human hepatocytes in our co-culture system. With these new insights, we will create optimal *in vitro* culture conditions for human hepatocytes to enable their cultivation and expansion *in vitro,* and continue to uncover the signaling pathways that are essential for liver regeneration.

Further, we identified MYDGF as a novel angiocrine signal that is able to promote human hepatocyte proliferation *in vitro*. However, *in vivo* studies to validate whether MYDGF is one of the key players in liver regeneration need to be performed. Studies, whereby adeno-associated viruses are injected into mice to overexpress *Mydgf* are already in progress. Additionally, we will test, whether mechano-induced secretion of MYDGF is β1 integrin dependent and investigate which other mechanotransducers are involved in this process. All together, these will help to reveal the role of MYDGF in the liver.

In general, a better understanding of the signaling pathways involved in liver regeneration might also be transferrable to other organ systems. Since all organs are vascularized and may experience vasodilation due to different stimuli such as organ growth or disease, it need to be investigated whether vasodilation and mechanically induced angiocrine signals play a role in organs other than the liver.

7. Publications

Lorenz L, Axnick J, Buschmann T, Henning C, Urner S, Fang S, Nurmi H, Eichhorst N, Holtmeier R, Bódis K, Hwang J-H, Müssig K, Eberhard D, Stypmann J, Kuss O, Roden M, Alitalo K, Häussinger D, Lammert E. **Mechanosensing by β1 integrin induces angiocrine signals for liver growth and survival**. Nature, 2018.

8. References

Abdel-Misih, S. R. & Bloomston, M. 2010. Liver anatomy. *Surg Clin North Am,* 90**,** 643-53.

Aizarani, N., Saviano, A., Sagar, Mailly, L., Durand, S., Herman, J. S., Pessaux, P., Baumert, T. F. & Grun, D. 2019. A human liver cell atlas reveals heterogeneity and epithelial progenitors. *Nature,* 572**,** 199-204.

Akerman, P., Cote, P., Yang, S. Q., McClain, C., Nelson, S., Bagby, G. J. & Diehl, A. M. 1992. Antibodies to tumor necrosis factor-alpha inhibit liver regeneration after partial hepatectomy. *Am J Physiol,* 263**,** G579-85.

Alam, A., Herault, J. P., Barron, P., Favier, B., Fons, P., Delesque-Touchard, N., Senegas, I., Laboudie, P., Bonnin, J., Cassan, C., Savi, P., Ruggeri, B., Carmeliet, P., Bono, F. & Herbert, J. M. 2004. Heterodimerization with vascular endothelial growth factor receptor-2 (VEGFR-2) is necessary for VEGFR-3 activity. *Biochem Biophys Res Commun,* 324**,** 909-15.

Alamri, Z. Z. 2018. The role of liver in metabolism: An updated review with physiological emphasis. *Int. J. Basic Clin. Pharmacol,* 7**,** 2271-2276.

Andrique, L., Recher, G., Alessandri, K., Pujol, N., Feyeux, M., Bon, P., Cognet, L., Nassoy, P. & Bikfalvi, A. 2019. A model of guided cell self-organization for rapid and spontaneous formation of functional vessels. *Sci Adv,* 5**,** eaau6562.

Asrani, S. K., Devarbhavi, H., Eaton, J. & Kamath, P. S. 2019. Burden of liver diseases in the world. *J Hepatol,* 70**,** 151-171.

Augustin, H. G. & Koh, G. Y. 2017. Organotypic vasculature: From descriptive heterogeneity to functional pathophysiology. *Science,* 357.

Aurrand-Lions, M., Galland, F., Bazin, H., Zakharyev, V. M., Imhof, B. A. & Naquet, P. 1996. Vanin-1, a novel GPI-linked perivascular molecule involved in thymus homing. *Immunity,* 5**,** 391-405.

Bizzaro, D., Russo, F. P. & Burra, P. 2019. New Perspectives in Liver Transplantation: From Regeneration to Bioengineering. *Bioengineering (Basel),* 6.

Blouin, A., Bolender, R. P. & Weibel, E. R. 1977. Distribution of organelles and membranes between hepatocytes and nonhepatocytes in the rat liver parenchyma. A stereological study. *J Cell Biol,* 72**,** 441-55.

Bohm, F., Kohler, U. A., Speicher, T. & Werner, S. 2010. Regulation of liver regeneration by growth factors and cytokines. *EMBO Mol Med,* 2**,** 294-305.

Bortnov, V., Annis, D. S., Fogerty, F. J., Barretto, K. T., Turton, K. B. & Mosher, D. F. 2018. Myeloid-derived growth factor is a resident endoplasmic reticulum protein. *J Biol Chem,* 293**,** 13166-13175.

Bortnov, V., Tonelli, M., Lee, W., Lin, Z., Annis, D. S., Demerdash, O. N., Bateman, A., Mitchell, J. C., Ge, Y., Markley, J. L. & Mosher, D. F. 2019. Solution structure of human myeloid-derived growth factor suggests a conserved function in the endoplasmic reticulum. *Nat Commun,* 10**,** 5612.

Boyer, J. L. 2013. Bile formation and secretion. *Compr Physiol,* 3**,** 1035-78.

Braet, F. & Wisse, E. 2002. Structural and functional aspects of liver sinusoidal endothelial cell fenestrae: a review. *Comp Hepatol,* 1**,** 1.

Brockmann, J., Reddy, S., Coussios, C., Pigott, D., Guirriero, D., Hughes, D., Morovat, A., Roy, D., Winter, L. & Friend, P. J. 2009. Normothermic perfusion: a new paradigm for organ preservation. *Ann Surg,* 250**,** 1-6.

Carlson, T. R., Hu, H., Braren, R., Kim, Y. H. & Wang, R. A. 2008. Cell-autonomous requirement for beta1 integrin in endothelial cell adhesion, migration and survival during angiogenesis in mice. *Development,* 135**,** 2193-202.

Celton-Morizur, S. & Desdouets, C. 2010. Polyploidization of liver cells. *Adv Exp Med Biol,* 676**,** 123-35.

Cleaver, O. & Melton, D. A. 2003. Endothelial signaling during development. *Nat Med,* 9**,** 661-8.

Collaborators, G. B. D. C. o. D. 2018. Global, regional, and national age-sex-specific mortality for 282 causes of death in 195 countries and territories, 1980-2017: a systematic analysis for the Global Burden of Disease Study 2017. *Lancet,* 392**,** 1736-1788.

Coste, B., Mathur, J., Schmidt, M., Earley, T. J., Ranade, S., Petrus, M. J., Dubin, A. E. & Patapoutian, A. 2010. Piezo1 and Piezo2 are essential components of distinct mechanically activated cation channels. *Science,* 330**,** 55-60.

Couinaud, C. 1954. [Liver lobes and segments: notes on the anatomical architecture and surgery of the liver]. *Presse Med,* 62**,** 709-12.

Cressman, D. E., Greenbaum, L. E., DeAngelis, R. A., Ciliberto, G., Furth, E. E., Poli, V. & Taub, R. 1996. Liver failure and defective hepatocyte regeneration in interleukin-6-deficient mice. *Science,* 274**,** 1379-83.

DeLeve, L. D. 2013. Liver sinusoidal endothelial cells and liver regeneration. *J Clin Invest,* 123**,** 1861-6.

DeLeve, L. D. & Maretti-Mira, A. C. 2017. Liver Sinusoidal Endothelial Cell: An Update. *Semin Liver Dis,* 37**,** 377-387.

DeLeve, L. D., Wang, X. & Guo, Y. 2008. Sinusoidal endothelial cells prevent rat stellate cell activation and promote reversion to quiescence. *Hepatology,* 48**,** 920-30.

Ding, B. S., Cao, Z., Lis, R., Nolan, D. J., Guo, P., Simons, M., Penfold, M. E., Shido, K., Rabbany, S. Y. & Rafii, S. 2014. Divergent angiocrine signals from vascular niche balance liver regeneration and fibrosis. *Nature,* 505**,** 97-102.

Ding, B. S., Nolan, D. J., Butler, J. M., James, D., Babazadeh, A. O., Rosenwaks, Z., Mittal, V., Kobayashi, H., Shido, K., Lyden, D., Sato, T. N., Rabbany, S. Y. & Rafii, S. 2010. Inductive angiocrine signals from sinusoidal endothelium are required for liver regeneration. *Nature,* 468**,** 310-5.

Dixelius, J., Makinen, T., Wirzenius, M., Karkkainen, M. J., Wernstedt, C., Alitalo, K. & Claesson-Welsh, L. 2003. Ligand-induced vascular endothelial growth factor receptor-3 (VEGFR-3) heterodimerization with VEGFR-2 in primary lymphatic endothelial cells regulates tyrosine phosphorylation sites. *J Biol Chem,* 278**,** 40973-9.

Dixon, L. J., Barnes, M., Tang, H., Pritchard, M. T. & Nagy, L. E. 2013. Kupffer cells in the liver. *Compr Physiol,* 3**,** 785-97.

Duan, J. L., Ruan, B., Yan, X. C., Liang, L., Song, P., Yang, Z. Y., Liu, Y., Dou, K. F., Han, H. & Wang, L. 2018. Endothelial Notch activation reshapes the angiocrine of sinusoidal endothelia to aggravate liver fibrosis and blunt regeneration in mice. *Hepatology,* 68**,** 677-690.

Duncan, A. W., Taylor, M. H., Hickey, R. D., Hanlon Newell, A. E., Lenzi, M. L., Olson, S. B., Finegold, M. J. & Grompe, M. 2010. The ploidy conveyor of mature hepatocytes as a source of genetic variation. *Nature,* 467**,** 707-10.

Duval, K., Grover, H., Han, L. H., Mou, Y., Pegoraro, A. F., Fredberg, J. & Chen, Z. 2017. Modeling Physiological Events in 2D vs. 3D Cell Culture. *Physiology (Bethesda),* 32**,** 266-277.

Ebenhoch, R., Akhdar, A., Reboll, M. R., Korf-Klingebiel, M., Gupta, P., Armstrong, J., Huang, Y., Frego, L., Rybina, I., Miglietta, J., Pekcec, A., Wollert, K. C. & Nar, H. 2019. Crystal structure and receptor-interacting residues of MYDGF - a protein mediating ischemic tissue repair. *Nat Commun,* 10**,** 5379.

Eshmuminov, D., Becker, D., Bautista Borrego, L., Hefti, M., Schuler, M. J., Hagedorn, C., Muller, X., Mueller, M., Onder, C., Graf, R., Weber, A., Dutkowski, P., Rudolf von Rohr, P. & Clavien, P. A. 2020. An integrated perfusion machine preserves injured human livers for 1 week. *Nat Biotechnol,* 38**,** 189-198.

Fassler, R. & Meyer, M. 1995. Consequences of lack of beta 1 integrin gene expression in mice. *Genes Dev,* 9**,** 1896-908.

Fausto, N., Campbell, J. S. & Riehle, K. J. 2012. Liver regeneration. *J Hepatol,* 57**,** 692-4.

Fausto, N., Mead, J. E., Gruppuso, P. A., Castilla, A. & Jakowlew, S. B. 1991. Effects of TGF-beta s in the liver: cell proliferation and fibrogenesis. *Ciba Found Symp,* 157**,** 165-74; discussion 174-7.

Fazel Modares, N., Polz, R., Haghighi, F., Lamertz, L., Behnke, K., Zhuang, Y., Kordes, C., Haussinger, D., Sorg, U. R., Pfeffer, K., Floss, D. M., Moll, J. M., Piekorz, R. P., Ahmadian, M. R., Lang, P. A. & Scheller, J. 2019. IL-6 Trans-signaling Controls Liver Regeneration After Partial Hepatectomy. *Hepatology,* 70**,** 2075-2091.

Fraczek, J., Bolleyn, J., Vanhaecke, T., Rogiers, V. & Vinken, M. 2013. Primary hepatocyte cultures for pharmaco-toxicological studies: at the busy crossroad of various anti-dedifferentiation strategies. *Arch Toxicol,* 87**,** 577-610.

Friedman, S. L. 2008. Hepatic stellate cells: protean, multifunctional, and enigmatic cells of the liver. *Physiological reviews,* 88**,** 125-172.

Gajdusek, C., DiCorleto, P., Ross, R. & Schwartz, S. M. 1980. An endothelial cell-derived growth factor. *The Journal of cell biology,* 85**,** 467-472.

Garnier, D., Li, R., Delbos, F., Fourrier, A., Collet, C., Guguen-Guillouzo, C., Chesne, C. & Nguyen, T. H. 2018. Expansion of human primary hepatocytes in vitro through their amplification as liver progenitors in a 3D organoid system. *Sci Rep,* 8**,** 8222.

Geraud, C., Evdokimov, K., Straub, B. K., Peitsch, W. K., Demory, A., Dorflinger, Y., Schledzewski, K., Schmieder, A., Schemmer, P., Augustin, H. G., Schirmacher, P. & Goerdt, S. 2012. Unique cell type-specific junctional complexes in vascular endothelium of human and rat liver sinusoids. *PLoS One,* 7**,** e34206.

Gilgenkrantz, H. & Collin de l'Hortet, A. 2018. Understanding Liver Regeneration: From Mechanisms to Regenerative Medicine. *Am J Pathol,* 188**,** 1316-1327.

Godoy, P., Hewitt, N. J., Albrecht, U., Andersen, M. E., Ansari, N., Bhattacharya, S., Bode, J. G., Bolleyn, J., Borner, C., Bottger, J., Braeuning, A., Budinsky, R. A., Burkhardt, B., Cameron, N. R., Camussi, G., Cho, C. S., Choi, Y. J., Craig Rowlands, J., Dahmen, U., Damm, G., Dirsch, O., Donato, M. T., Dong, J., Dooley, S., Drasdo, D., Eakins, R., Ferreira, K. S., Fonsato, V., Fraczek, J., Gebhardt, R., Gibson, A., Glanemann, M., Goldring, C. E., Gomez-Lechon, M. J., Groothuis, G. M., Gustavsson, L., Guyot, C., Hallifax, D., Hammad, S., Hayward, A., Haussinger, D., Hellerbrand, C., Hewitt, P., Hoehme, S., Holzhutter, H. G., Houston, J. B., Hrach, J., Ito, K., Jaeschke, H., Keitel, V., Kelm, J. M., Kevin Park, B., Kordes, C., Kullak-Ublick, G. A., LeCluyse, E. L., Lu, P., Luebke-Wheeler, J., Lutz, A., Maltman, D. J., Matz-Soja, M., McMullen, P., Merfort, I., Messner, S., Meyer, C., Mwinyi, J., Naisbitt,

D. J., Nussler, A. K., Olinga, P., Pampaloni, F., Pi, J., Pluta, L., Przyborski, S. A., Ramachandran, A., Rogiers, V., Rowe, C., Schelcher, C., Schmich, K., Schwarz, M., Singh, B., Stelzer, E. H., Stieger, B., Stober, R., Sugiyama, Y., Tetta, C., Thasler, W. E., Vanhaecke, T., Vinken, M., Weiss, T. S., Widera, A., Woods, C. G., Xu, J. J., Yarborough, K. M. & Hengstler, J. G. 2013. Recent advances in 2D and 3D in vitro systems using primary hepatocytes, alternative hepatocyte sources and non-parenchymal liver cells and their use in investigating mechanisms of hepatotoxicity, cell signaling and ADME. *Arch Toxicol,* 87**,** 1315-530.

Gomez-Lechon, M. J., Castelli, J., Guillen, I., O'Connor, E., Nakamura, T., Fabra, R. & Trullenque, R. 1995. Effects of hepatocyte growth factor on the growth and metabolism of human hepatocytes in primary culture. *Hepatology,* 21**,** 1248-54.

Goulart, E., de Caires-Junior, L. C., Telles-Silva, K. A., Araujo, B. H. S., Rocco, S. A., Sforca, M., de Sousa, I. L., Kobayashi, G. S., Musso, C. M., Assoni, A. F., Oliveira, D., Caldini, E., Raia, S., Lelkes, P. I. & Zatz, M. 2019. 3D bioprinting of liver spheroids derived from human induced pluripotent stem cells sustain liver function and viability in vitro. *Biofabrication,* 12**,** 015010.

Greenhalgh, S. N., Matchett, K. P., Taylor, R. S., Huang, K., Li, J. T., Saeteurn, K., Donnelly, M. C., Simpson, E. E. M., Pollack, J. L., Atakilit, A., Simpson, K. J., Maher, J. J., Iredale, J. P., Sheppard, D. & Henderson, N. C. 2019. Loss of Integrin alphavbeta8 in Murine Hepatocytes Accelerates Liver Regeneration. *Am J Pathol,* 189**,** 258-271.

Guguen-Guillouzo, C. & Guillouzo, A. 2010. General review on in vitro hepatocyte models and their applications. *Methods Mol Biol,* 640**,** 1-40.

Hackl, C., Schmidt, K. M., Susal, C., Dohler, B., Zidek, M. & Schlitt, H. J. 2018. Split liver transplantation: Current developments. *World J Gastroenterol,* 24**,** 5312-5321.

Harb, R., Xie, G., Lutzko, C., Guo, Y., Wang, X., Hill, C. K., Kanel, G. C. & DeLeve, L. D. 2009. Bone marrow progenitor cells repair rat hepatic sinusoidal endothelial cells after liver injury. *Gastroenterology,* 137**,** 704-12.

Hartwig, S., De Filippo, E., Goddeke, S., Knebel, B., Kotzka, J., Al-Hasani, H., Roden, M., Lehr, S. & Sell, H. 2019. Exosomal proteins constitute an essential part of the human adipose tissue secretome. *Biochim Biophys Acta Proteins Proteom,* 1867**,** 140172.

Häussinger, D. 2014. Liver - Overview. *In:* Lammert, E. & Zeeb, M. (eds.) *Metabolism of Human Diseases.* Wien Heidelberg New York Dordrcht London: Springer.

Häussinger, D., Keitel, V. & Kubitz, R. 2012. *Hepatobiliary transport in health and disease*, Walter de Gruyter.

Haussinger, D. & Kordes, C. 2019. Space of Disse: a stem cell niche in the liver. *Biol Chem,* 401**,** 81-95.

Higgins, G. M. 1931. Experimental pathology of the liver; I. Restoration of the liver of the white rat following partial surgical removal. *Arch pathol,* 12**,** 186-202.

Hilscher, M. B., Sehrawat, T., Arab, J. P., Zeng, Z., Gao, J., Liu, M., Kostallari, E., Gao, Y., Simonetto, D. A., Yaqoob, U., Cao, S., Revzin, A., Beyder, A., Wang, R. A., Kamath, P. S., Kubes, P. & Shah, V. H. 2019. Mechanical Stretch Increases Expression of CXCL1 in Liver Sinusoidal Endothelial Cells to Recruit Neutrophils, Generate Sinusoidal Microthombi, and Promote Portal Hypertension. *Gastroenterology,* 157**,** 193-209 e9.

Hu, C. & Li, L. 2015. In vitro culture of isolated primary hepatocytes and stem cell-derived hepatocyte-like cells for liver regeneration. *Protein Cell,* 6**,** 562-74.

Hu, H., Gehart, H., Artegiani, B., C, L. O.-I., Dekkers, F., Basak, O., van Es, J., Chuva de Sousa Lopes, S. M., Begthel, H., Korving, J., van den Born, M., Zou, C., Quirk, C., Chiriboga, L., Rice, C. M., Ma, S., Rios, A., Peters, P. J., de Jong, Y. P. & Clevers, H. 2018. Long-Term Expansion of Functional Mouse and Human Hepatocytes as 3D Organoids. *Cell,* 175**,** 1591-1606 e19.

Hu, J., Srivastava, K., Wieland, M., Runge, A., Mogler, C., Besemfelder, E., Terhardt, D., Vogel, M. J., Cao, L., Korn, C., Bartels, S., Thomas, M. & Augustin, H. G. 2014. Endothelial cell-derived angiopoietin-2 controls liver regeneration as a spatiotemporal rheostat. *Science,* 343**,** 416-9.

Huang, W., Ma, K., Zhang, J., Qatanani, M., Cuvillier, J., Liu, J., Dong, B., Huang, X. & Moore, D. D. 2006. Nuclear receptor-dependent bile acid signaling is required for normal liver regeneration. *Science,* 312**,** 233-6.

Huh, C. G., Factor, V. M., Sanchez, A., Uchida, K., Conner, E. A. & Thorgeirsson, S. S. 2004. Hepatocyte growth factor/c-met signaling pathway is required for efficient liver regeneration and repair. *Proc Natl Acad Sci U S A,* 101**,** 4477-82.

Hynes, R. O. 2002. Integrins: bidirectional, allosteric signaling machines. *Cell,* 110**,** 673-87.

Ingber, D. 1991. Integrins as mechanochemical transducers. *Curr Opin Cell Biol,* 3**,** 841-8.

Ingber, D. E. 2003. Mechanobiology and diseases of mechanotransduction. *Ann Med,* 35**,** 564-77.

Ishibashi, H., Nakamura, M., Komori, A., Migita, K. & Shimoda, S. 2009. Liver architecture, cell function, and disease. *Semin Immunopathol,* 31**,** 399-409.

Iwakiri, Y. & Groszmann, R. J. 2006. The hyperdynamic circulation of chronic liver diseases: from the patient to the molecule. *Hepatology,* 43**,** S121-31.

Jamieson, R. W., Zilvetti, M., Roy, D., Hughes, D., Morovat, A., Coussios, C. C. & Friend, P. J. 2011. Hepatic steatosis and normothermic perfusion-preliminary experiments in a porcine model. *Transplantation,* 92**,** 289-95.

Jenne, C. N. & Kubes, P. 2013. Immune surveillance by the liver. *Nat Immunol,* 14**,** 996-1006.

Jia, J. J., Li, J. H., Yu, H., Nie, Y., Jiang, L., Li, H. Y., Zhou, L. & Zheng, S. S. 2018. Machine perfusion for liver transplantation: A concise review of clinical trials. *Hepatobiliary Pancreat Dis Int,* 17**,** 387-391.

Jungermann, K. & Kietzmann, T. 1996. Zonation of parenchymal and nonparenchymal metabolism in liver. *Annu Rev Nutr,* 16**,** 179-203.

Katsumi, A., Orr, A. W., Tzima, E. & Schwartz, M. A. 2004. Integrins in mechanotransduction. *J Biol Chem,* 279**,** 12001-4.

Keitel, V., Kubitz, R. & Haussinger, D. 2008. Endocrine and paracrine role of bile acids. *World J Gastroenterol,* 14**,** 5620-9.

Kiernan, F. 1833. XXIX. The anatomy and physiology of the liver.

Kietzmann, T. 2017. Metabolic zonation of the liver: The oxygen gradient revisited. *Redox Biol,* 11**,** 622-630.

Kim, M. Y., Baik, S. K. & Lee, S. S. 2010. Hemodynamic alterations in cirrhosis and portal hypertension. *Korean J Hepatol,* 16**,** 347-52.

Kim, T. H., Mars, W. M., Stolz, D. B. & Michalopoulos, G. K. 2000. Expression and activation of pro-MMP-2 and pro-MMP-9 during rat liver regeneration. *Hepatology,* 31**,** 75-82.

Kim, T. H., Mars, W. M., Stolz, D. B., Petersen, B. E. & Michalopoulos, G. K. 1997. Extracellular matrix remodeling at the early stages of liver regeneration in the rat. *Hepatology,* 26**,** 896-904.

Knolle, P. A. & Wohlleber, D. 2016. Immunological functions of liver sinusoidal endothelial cells. *Cell Mol Immunol,* 13**,** 347-53.

Koch, P. S., Olsavszky, V., Ulbrich, F., Sticht, C., Demory, A., Leibing, T., Henzler, T., Meyer, M., Zierow, J., Schneider, S., Breitkopf-Heinlein, K., Gaitantzi, H., Spencer-Dene, B., Arnold, B., Klapproth, K., Schledzewski, K., Goerdt, S. & Geraud, C. 2017. Angiocrine Bmp2 signaling in murine liver controls normal iron homeostasis. *Blood,* 129**,** 415-419.

Korf-Klingebiel, M., Reboll, M. R., Klede, S., Brod, T., Pich, A., Polten, F., Napp, L. C., Bauersachs, J., Ganser, A., Brinkmann, E., Reimann, I., Kempf, T., Niessen, H. W., Mizrahi, J., Schonfeld, H. J., Iglesias, A., Bobadilla, M., Wang, Y. & Wollert, K. C. 2015. Myeloid-derived growth factor (C19orf10) mediates cardiac repair following myocardial infarction. *Nat Med,* 21**,** 140-9.

Kostallari, E. & Shah, V. H. 2016. Angiocrine signaling in the hepatic sinusoids in health and disease. *Am J Physiol Gastrointest Liver Physiol,* 311**,** G246-51.

Kowalski, H. J. & Abelmann, W. H. 1953. The cardiac output at rest in Laennec's cirrhosis. *J Clin Invest,* 32**,** 1025-33.

Kwak, B. R., Back, M., Bochaton-Piallat, M. L., Caligiuri, G., Daemen, M. J., Davies, P. F., Hoefer, I. E., Holvoet, P., Jo, H., Krams, R., Lehoux, S., Monaco, C., Steffens, S., Virmani, R., Weber, C., Wentzel, J. J. & Evans, P. C. 2014. Biomechanical factors in atherosclerosis: mechanisms and clinical implications. *Eur Heart J,* 35**,** 3013-20, 3020a-3020d.

Laflamme, M. A., Sebastian, M. M. & Buetow, B. S. 2012. Cardiovascular. *Comparative Anatomy and Histology.*

Lambert, C., Preijers, F., Yanikkaya Demirel, G. & Sack, U. 2017. Monocytes and macrophages in flow: an ESCCA initiative on advanced analyses of monocyte lineage using flow cytometry. *Cytometry B Clin Cytom,* 92**,** 180-188.

Lammert, E., Cleaver, O. & Melton, D. 2001. Induction of pancreatic differentiation by signals from blood vessels. *Science,* 294**,** 564-7.

LeCluyse, E. L., Audus, K. L. & Hochman, J. H. 1994. Formation of extensive canalicular networks by rat hepatocytes cultured in collagen-sandwich configuration. *Am J Physiol,* 266**,** C1764-74.

Lei, L., Liu, D., Huang, Y., Jovin, I., Shai, S. Y., Kyriakides, T., Ross, R. S. & Giordano, F. J. 2008. Endothelial expression of beta1 integrin is required for embryonic vascular patterning and postnatal vascular remodeling. *Mol Cell Biol,* 28**,** 794-802.

Leibing, T., Geraud, C., Augustin, I., Boutros, M., Augustin, H. G., Okun, J. G., Langhans, C. D., Zierow, J., Wohlfeil, S. A., Olsavszky, V., Schledzewski, K., Goerdt, S. & Koch, P. S. 2018. Angiocrine Wnt signaling controls liver growth and metabolic maturation in mice. *Hepatology,* 68**,** 707-722.

Lenter, M., Uhlig, H., Hamann, A., Jeno, P., Imhof, B. & Vestweber, D. 1993. A monoclonal antibody against an activation epitope on mouse integrin chain beta 1 blocks adhesion of lymphocytes to the endothelial integrin alpha 6 beta 1. *Proc Natl Acad Sci U S A,* 90**,** 9051-5.

Li, R., Oteiza, A., Sorensen, K. K., McCourt, P., Olsen, R., Smedsrod, B. & Svistounov, D. 2011. Role of liver sinusoidal endothelial cells and stabilins in elimination of oxidized low-density lipoproteins. *Am J Physiol Gastrointest Liver Physiol,* 300**,** G71-81.

Lorenz, L., Axnick, J., Buschmann, T., Henning, C., Urner, S., Fang, S., Nurmi, H., Eichhorst, N., Holtmeier, R., Bodis, K., Hwang, J. H., Mussig, K., Eberhard, D., Stypmann, J., Kuss, O., Roden, M., Alitalo, K., Haussinger, D. & Lammert, E. 2018. Mechanosensing by beta1 integrin induces angiocrine signals for liver growth and survival. *Nature,* 562**,** 128-132.

Luo, D. Z., Vermijlen, D., Ahishali, B., Triantis, V., Plakoutsi, G., Braet, F., Vanderkerken, K. & Wisse, E. 2000. On the cell biology of pit cells, the liver-specific NK cells. *World J Gastroenterol,* 6**,** 1-11.

Mammoto, A., Connor, K. M., Mammoto, T., Yung, C. W., Huh, D., Aderman, C. M., Mostoslavsky, G., Smith, L. E. & Ingber, D. E. 2009. A mechanosensitive transcriptional mechanism that controls angiogenesis. *Nature,* 457**,** 1103-8.

Manavski, Y., Abel, T., Hu, J., Kleinlutzum, D., Buchholz, C. J., Belz, C., Augustin, H. G., Boon, R. A. & Dimmeler, S. 2017. Endothelial transcription factor KLF2 negatively regulates liver regeneration via induction of activin A. *Proc Natl Acad Sci U S A,* 114**,** 3993-3998.

Mangnall, D., Smith, K., Bird, N. C. & Majeed, A. W. 2004. Early increases in plasminogen activator activity following partial hepatectomy in humans. *Comp Hepatol,* 3**,** 11.

Maras, B., Barra, D., Dupre, S. & Pitari, G. 1999. Is pantetheinase the actual identity of mouse and human vanin-1 proteins? *FEBS Lett,* 461**,** 149-52.

Marcos, A. 2000. Right-lobe living donor liver transplantation. *Liver Transpl,* 6**,** S59-63.

Mars, W. M., Liu, M. L., Kitson, R. P., Goldfarb, R. H., Gabauer, M. K. & Michalopoulos, G. K. 1995. Immediate early detection of urokinase receptor after partial hepatectomy and its implications for initiation of liver regeneration. *Hepatology,* 21**,** 1695-701.

Marubashi, S., Sakon, M., Nagano, H., Gotoh, K., Hashimoto, K., Kubota, M., Kobayashi, S., Yamamoto, S., Miyamoto, A., Dono, K., Nakamori, S., Umeshita, K. & Monden, M. 2004. Effect of portal hemodynamics on liver regeneration studied in a novel portohepatic shunt rat model. *Surgery,* 136**,** 1028-37.

Matsumoto, K., Yoshitomi, H., Rossant, J. & Zaret, K. S. 2001. Liver organogenesis promoted by endothelial cells prior to vascular function. *Science,* 294**,** 559-63.

Michalopoulos, G. K. 2007. Liver regeneration. *J Cell Physiol,* 213**,** 286-300.

Michalopoulos, G. K. 2010. Liver regeneration after partial hepatectomy: critical analysis of mechanistic dilemmas. *Am J Pathol,* 176**,** 2-13.

Michalopoulos, G. K. 2017. Hepatostat: Liver regeneration and normal liver tissue maintenance. *Hepatology,* 65**,** 1384-1392.

Michalopoulos, G. K. & DeFrances, M. C. 1997. Liver regeneration. *Science,* 276**,** 60-6.

Miller, C. & Diago Uso, T. 2013. The liver transplant operation. *Clin Liver Dis (Hoboken),* 2**,** 192-196.

Mohn, K. L., Laz, T. M., Hsu, J. C., Melby, A. E., Bravo, R. & Taub, R. 1991. The immediate-early growth response in regenerating liver and insulin-stimulated H-35 cells: comparison with serum-stimulated 3T3 cells and identification of 41 novel immediate-early genes. *Mol Cell Biol,* 11**,** 381-90.

Morell, C. M. & Strazzabosco, M. 2014. Notch signaling and new therapeutic options in liver disease. *J Hepatol,* 60**,** 885-90.

Morello, D., Fitzgerald, M. J., Babinet, C. & Fausto, N. 1990. c-myc, c-fos, and c-jun regulation in the regenerating livers of normal and H-2K/c-myc transgenic mice. *Mol Cell Biol,* 10**,** 3185-93.

Mori, N., Akagi, Y., Imai, Y., Takayama, Y. & Kida, Y. S. 2020. Fabrication of Perfusable Vascular Channels and Capillaries in 3D Liver-like Tissue. *Sci Rep,* 10**,** 5646.

Morsiani, E., Aleotti, A. & Ricci, D. 1998. Haemodynamic and ultrastructural observations on the rat liver after two-thirds partial hepatectomy. *J Anat,* 192 (Pt 4)**,** 507-15.

Mousavi, S. A., Sporstol, M., Fladeby, C., Kjeken, R., Barois, N. & Berg, T. 2007. Receptor-mediated endocytosis of immune complexes in rat liver sinusoidal endothelial cells is mediated by FcgammaRIIb2. *Hepatology,* 46**,** 871-84.

Mouta Carreira, C., Nasser, S. M., di Tomaso, E., Padera, T. P., Boucher, Y., Tomarev, S. I. & Jain, R. K. 2001. LYVE-1 is not restricted to the lymph vessels: expression in normal liver blood sinusoids and down-regulation in human liver cancer and cirrhosis. *Cancer Res,* 61**,** 8079-84.

Murray, J. F., Dawson, A. M. & Sherlock, S. 1958. Circulatory changes in chronic liver disease. *Am J Med,* 24**,** 358-67.

Nasralla, D., Coussios, C. C., Mergental, H., Akhtar, M. Z., Butler, A. J., Ceresa, C. D. L., Chiocchia, V., Dutton, S. J., Garcia-Valdecasas, J. C., Heaton, N., Imber, C., Jassem, W., Jochmans, I., Karani, J., Knight, S. R., Kocabayoglu, P., Malago, M., Mirza, D., Morris, P. J., Pallan, A., Paul, A., Pavel, M., Perera, M., Pirenne, J., Ravikumar, R., Russell, L., Upponi, S., Watson, C. J. E., Weissenbacher, A., Ploeg, R. J., Friend, P. J. & Consortium for Organ Preservation in, E. 2018. A randomized trial of normothermic preservation in liver transplantation. *Nature,* 557**,** 50-56.

Neubauer, K., Wilfling, T., Ritzel, A. & Ramadori, G. 2000. Platelet-endothelial cell adhesion molecule-1 gene expression in liver sinusoidal endothelial cells during liver injury and repair. *J Hepatol,* 32**,** 921-32.

Nikolova, G. & Lammert, E. 2003. Interdependent development of blood vessels and organs. *Cell Tissue Res,* 314**,** 33-42.

Nilsson, I., Bahram, F., Li, X., Gualandi, L., Koch, S., Jarvius, M., Soderberg, O., Anisimov, A., Kholova, I., Pytowski, B., Baldwin, M., Yla-Herttuala, S., Alitalo, K., Kreuger, J. & Claesson-Welsh, L. 2010. VEGF receptor 2/-3 heterodimers detected in situ by proximity ligation on angiogenic sprouts. *EMBO J,* 29**,** 1377-88.

Olle, E. W., Ren, X., McClintock, S. D., Warner, R. L., Deogracias, M. P., Johnson, K. J. & Colletti, L. M. 2006. Matrix metalloproteinase-9 is an important factor in hepatic regeneration after partial hepatectomy in mice. *Hepatology,* 44**,** 540-9.

Pastor, C. M. & Hadengue, A. 2000. Shear stress modulates the vascular tone in perfused livers isolated from normal rats. *Hepatology,* 32**,** 786-91.

Patijn, G. A., Lieber, A., Schowalter, D. B., Schwall, R. & Kay, M. A. 1998. Hepatocyte growth factor induces hepatocyte proliferation in vivo and allows for efficient retroviral-mediated gene transfer in mice. *Hepatology,* 28**,** 707-16.

Pean, N., Doignon, I., Garcin, I., Besnard, A., Julien, B., Liu, B., Branchereau, S., Spraul, A., Guettier, C., Humbert, L., Schoonjans, K., Rainteau, D. & Tordjmann, T. 2013. The receptor TGR5 protects the liver from bile acid overload during liver regeneration in mice. *Hepatology,* 58**,** 1451-60.

Peng, W. C., Logan, C. Y., Fish, M., Anbarchian, T., Aguisanda, F., Alvarez-Varela, A., Wu, P., Jin, Y., Zhu, J., Li, B., Grompe, M., Wang, B. & Nusse, R. 2018. Inflammatory Cytokine TNFalpha Promotes the Long-Term Expansion of Primary Hepatocytes in 3D Culture. *Cell,* 175**,** 1607-1619 e15.

Petit, I., Jin, D. & Rafii, S. 2007. The SDF-1-CXCR4 signaling pathway: a molecular hub modulating neo-angiogenesis. *Trends Immunol,* 28**,** 299-307.

Planas-Paz, L., Orsini, V., Boulter, L., Calabrese, D., Pikiolek, M., Nigsch, F., Xie, Y., Roma, G., Donovan, A., Marti, P., Beckmann, N., Dill, M. T., Carbone, W., Bergling, S., Isken, A., Mueller, M., Kinzel, B., Yang, Y., Mao, X., Nicholson, T. B., Zamponi, R., Capodieci, P., Valdez, R., Rivera, D., Loew, A., Ukomadu, C., Terracciano, L. M., Bouwmeester, T., Cong, F., Heim, M. H., Forbes, S. J., Ruffner, H. & Tchorz, J. S. 2016. The RSPO-LGR4/5-ZNRF3/RNF43 module controls liver zonation and size. *Nat Cell Biol,* 18**,** 467-79.

Planas-Paz, L., Strilic, B., Goedecke, A., Breier, G., Fassler, R. & Lammert, E. 2012. Mechanoinduction of lymph vessel expansion. *EMBO J,* 31**,** 788-804.

Poisson, J., Lemoinne, S., Boulanger, C., Durand, F., Moreau, R., Valla, D. & Rautou, P. E. 2017. Liver sinusoidal endothelial cells: Physiology and role in liver diseases. *J Hepatol,* 66**,** 212-227.

Polten, F., Reboll, M. R., Widera, C., Kempf, T., Bethmann, K., Gupta, P., Miglietta, J., Pekcec, A., Tillmanns, J., Bauersachs, J., Giannitsis, E., Pich, A. & Wollert, K. C. 2019. Plasma Concentrations of Myeloid-Derived Growth Factor in Healthy Individuals and Patients with Acute Myocardial Infarction as Assessed by Multiple Reaction Monitoring-Mass Spectrometry. *Anal Chem,* 91**,** 1302-1308.

Qian, H., Johansson, S., McCourt, P., Smedsrod, B., Ekblom, M. & Johansson, S. 2009. Stabilins are expressed in bone marrow sinusoidal endothelial cells and mediate scavenging and cell adhesive functions. *Biochem Biophys Res Commun,* 390**,** 883-6.

Quesenberry, P. J. & Gimbrone, M. J. 1980. Vascular endothelium as a regulator of granulopoiesis: production of colony-stimulating activity by cultured human endothelial cells.

Rafii, S., Butler, J. M. & Ding, B. S. 2016. Angiocrine functions of organ-specific endothelial cells. *Nature,* 529**,** 316-25.

Rafii, S. & Lyden, D. 2003. Therapeutic stem and progenitor cell transplantation for organ vascularization and regeneration. *Nat Med,* 9**,** 702-12.

Rai, R. 2013. Liver transplantatation- an overview. *Indian J Surg,* 75**,** 185-91.

Rappaport, A. M., Borowy, Z. J., Lougheed, W. M. & Lotto, W. N. 1954. Subdivision of hexagonal liver lobules into a structural and functional unit; role in hepatic physiology and pathology. *Anat Rec,* 119**,** 11-33.

Richman, R. A., Claus, T. H., Pilkis, S. J. & Friedman, D. L. 1976. Hormonal stimulation of DNA synthesis in primary cultures of adult rat hepatocytes. *Proc Natl Acad Sci U S A,* 73**,** 3589-93.

Rocha, A. S., Vidal, V., Mertz, M., Kendall, T. J., Charlet, A., Okamoto, H. & Schedl, A. 2015. The Angiocrine Factor Rspondin3 Is a Key Determinant of Liver Zonation. *Cell Rep,* 13**,** 1757-64.

Romar, G. A., Kupper, T. S. & Divito, S. J. 2016. Research Techniques Made Simple: Techniques to Assess Cell Proliferation. *J Invest Dermatol,* 136**,** e1-e7.

Runge, D., Michalopoulos, G. K., Strom, S. C. & Runge, D. M. 2000a. Recent advances in human hepatocyte culture systems. *Biochem Biophys Res Commun,* 274**,** 1-3.

Runge, D., Runge, D. M., Jager, D., Lubecki, K. A., Beer Stolz, D., Karathanasis, S., Kietzmann, T., Strom, S. C., Jungermann, K., Fleig, W. E. & Michalopoulos, G. K. 2000b. Serum-free, long-term cultures of human hepatocytes: maintenance of cell morphology, transcription factors, and liver-specific functions. *Biochem Biophys Res Commun,* 269**,** 46-53.

Schmidt, C., Bladt, F., Goedecke, S., Brinkmann, V., Zschiesche, W., Sharpe, M., Gherardi, E. & Birchmeler, C. 1995. Scatter factor/hepatocyte growth factor is essential for liver development. *Nature,* 373**,** 699-702.

Schmittgen, T. D. & Livak, K. J. 2008. Analyzing real-time PCR data by the comparative C(T) method. *Nat Protoc,* 3**,** 1101-8.

Schoen, J. M., Wang, H. H., Minuk, G. Y. & Lautt, W. W. 2001. Shear stress-induced nitric oxide release triggers the liver regeneration cascade. *Nitric Oxide,* 5**,** 453-64.

Seeger, F. H., Rasper, T., Koyanagi, M., Fox, H., Zeiher, A. M. & Dimmeler, S. 2009. CXCR4 expression determines functional activity of bone marrow-derived mononuclear cells for therapeutic neovascularization in acute ischemia. *Arterioscler Thromb Vasc Biol,* 29**,** 1802-9.

Shay-Salit, A., Shushy, M., Wolfovitz, E., Yahav, H., Breviario, F., Dejana, E. & Resnick, N. 2002. VEGF receptor 2 and the adherens junction as a mechanical transducer in vascular endothelial cells. *Proc Natl Acad Sci U S A,* 99**,** 9462-7.

Shetty, S., Lalor, P. F. & Adams, D. H. 2018. Liver sinusoidal endothelial cells - gatekeepers of hepatic immunity. *Nat Rev Gastroenterol Hepatol,* 15**,** 555-567.

Sies, H. 1978. The use of perfusion of liver and other organs for the study of microsomal electron-transport and cytochrome P-450 systems. *Methods Enzymol,* 52**,** 48-59.

Sorensen, K. K., McCourt, P., Berg, T., Crossley, C., Le Couteur, D., Wake, K. & Smedsrod, B. 2012. The scavenger endothelial cell: a new player in homeostasis and immunity. *Am J Physiol Regul Integr Comp Physiol,* 303**,** R1217-30.

Sorensen, K. K., Simon-Santamaria, J., McCuskey, R. S. & Smedsrod, B. 2015. Liver Sinusoidal Endothelial Cells. *Compr Physiol,* 5**,** 1751-74.

Speicher, T., Siegenthaler, B., Bogorad, R. L., Ruppert, R., Petzold, T., Padrissa-Altes, S., Bachofner, M., Anderson, D. G., Koteliansky, V., Fassler, R. & Werner, S. 2014. Knockdown and knockout of beta1-integrin in hepatocytes impairs liver regeneration through inhibition of growth factor signalling. *Nat Commun,* 5**,** 3862.

Stephens, L. E., Sutherland, A. E., Klimanskaya, I. V., Andrieux, A., Meneses, J., Pedersen, R. A. & Damsky, C. H. 1995. Deletion of beta 1 integrins in mice results in inner cell mass failure and peri-implantation lethality. *Genes Dev,* 9**,** 1883-95.

Sun, Z., Costell, M. & Fassler, R. 2019. Integrin activation by talin, kindlin and mechanical forces. *Nat Cell Biol,* 21**,** 25-31.

Sunagozaka, H., Honda, M., Yamashita, T., Nishino, R., Takatori, H., Arai, K., Yamashita, T., Sakai, Y. & Kaneko, S. 2011. Identification of a secretory protein c19orf10 activated in hepatocellular carcinoma. *Int J Cancer,* 129**,** 1576-85.

Tabibian, J. H., Masyuk, A. I., Masyuk, T. V., O'Hara, S. P. & LaRusso, N. F. 2013. Physiology of cholangiocytes. *Compr Physiol,* 3**,** 541-65.

Tammela, T., Enholm, B., Alitalo, K. & Paavonen, K. 2005. The biology of vascular endothelial growth factors. *Cardiovasc Res,* 65**,** 550-63.

Tanjore, H., Zeisberg, E. M., Gerami-Naini, B. & Kalluri, R. 2008. Beta1 integrin expression on endothelial cells is required for angiogenesis but not for vasculogenesis. *Dev Dyn,* 237**,** 75-82.

Tanriverdi, G., Kaya-Dagistanli, F., Ayla, S., Demirci, S., Eser, M., Unal, Z. S., Cengiz, M. & Oktar, H. 2016. Resveratrol can prevent CCl(4)-induced liver injury by inhibiting Notch signaling pathway. *Histol Histopathol,* 31**,** 769-84.

Taub, R. 2004. Liver regeneration: from myth to mechanism. *Nat Rev Mol Cell Biol,* 5**,** 836-47.

Torre, C., Perret, C. & Colnot, S. 2010. Molecular determinants of liver zonation. *Prog Mol Biol Transl Sci,* 97**,** 127-50.

Trefts, E., Gannon, M. & Wasserman, D. H. 2017. The liver. *Curr Biol,* 27**,** R1147-R1151.

Treuting, P. M., Dintzis, S. M., Liggitt, D. & Frevert, C. W. 2011. *Comparative anatomy and histology: a mouse and human atlas (expert consult)*, Academic Press.

Tsai, M. T., Katagiri, N., Ohbayashi, N., Iwasaki, K., Ohkohchi, N., Ding, S. T., Kanaho, Y. & Funakoshi, Y. 2017. Regulation of HGF-induced hepatocyte proliferation by the small GTPase Arf6 through the PIP2-producing enzyme PIP5K1A. *Sci Rep,* 7**,** 9438.

Tulin, E. E., Onoda, N., Nakata, Y., Maeda, M., Hasegawa, M., Nomura, H. & Kitamura, T. 2001. SF20/IL-25, a novel bone marrow stroma-derived growth factor that binds to mouse thymic shared antigen-1 and supports lymphoid cell proliferation. *J Immunol,* 167**,** 6338-47.

Tulin, E. E., Onoda, N., Nakata, Y., Maeda, M., Hasegawa, M., Nomura, H. & Kitamura, T. 2003. SF20/IL-25, a novel bone marrow stroma-derived growth factor that binds to mouse thymic shared antigen-1 and supports lymphoid cell proliferation. *J Immunol,* 170**,** 1593.

Tzima, E., Irani-Tehrani, M., Kiosses, W. B., Dejana, E., Schultz, D. A., Engelhardt, B., Cao, G., DeLisser, H. & Schwartz, M. A. 2005. A mechanosensory complex that mediates the endothelial cell response to fluid shear stress. *Nature,* 437**,** 426-31.

Urner, S., Kelly-Goss, M., Peirce, S. M. & Lammert, E. 2018. Mechanotransduction in Blood and Lymphatic Vascular Development and Disease. *Adv Pharmacol,* 81**,** 155-208.

Vinken, M. & Hengstler, J. G. 2018. Characterization of hepatocyte-based in vitro systems for reliable toxicity testing. *Arch Toxicol,* 92**,** 2981-2986.

Wang, B., Zhao, L., Fish, M., Logan, C. Y. & Nusse, R. 2015. Self-renewing diploid Axin2(+) cells fuel homeostatic renewal of the liver. *Nature,* 524**,** 180-5.

Wang, J. F., Zhang, X. F. & Groopman, J. E. 2001. Stimulation of beta 1 integrin induces tyrosine phosphorylation of vascular endothelial growth factor receptor-3 and modulates cell migration. *J Biol Chem,* 276**,** 41950-7.

Wang, L., Li, Y., Guo, B., Zhang, J., Zhu, B., Li, H., Ding, Y., Meng, B., Zhao, H., Xiang, L., Dong, J., Liu, M., Zhang, J., Xiang, L. & Xiang, G. 2020. Myeloid-Derived Growth Factor Promotes Intestinal Glucagon-Like Peptide-1 Production in Male Mice With Type 2 Diabetes. *Endocrinology,* 161.

Wang, L., Wang, X., Wang, L., Chiu, J. D., van de Ven, G., Gaarde, W. A. & Deleve, L. D. 2012a. Hepatic vascular endothelial growth factor regulates recruitment of rat liver sinusoidal endothelial cell progenitor cells. *Gastroenterology,* 143**,** 1555-1563 e2.

Wang, L., Wang, X., Xie, G., Wang, L., Hill, C. K. & DeLeve, L. D. 2012b. Liver sinusoidal endothelial cell progenitor cells promote liver regeneration in rats. *J Clin Invest,* 122**,** 1567-73.

Wang, P., Mariman, E., Keijer, J., Bouwman, F., Noben, J. P., Robben, J. & Renes, J. 2004. Profiling of the secreted proteins during 3T3-L1 adipocyte differentiation leads to the identification of novel adipokines. *Cell Mol Life Sci,* 61**,** 2405-17.

Wayner, E. A., Gil, S. G., Murphy, G. F., Wilke, M. S. & Carter, W. G. 1993. Epiligrin, a component of epithelial basement membranes, is an adhesive ligand for alpha 3 beta 1 positive T lymphocytes. *J Cell Biol,* 121**,** 1141-52.

Weiler, T., Du, Q., Krokhin, O., Ens, W., Standing, K., El-Gabalawy, H. & Wilkins, J. A. 2007. The identification and characterization of a novel protein, c19orf10, in the synovium. *Arthritis Res Ther,* 9**,** R30.

Xie, C., Wei, W., Zhang, T., Dirsch, O. & Dahmen, U. 2014. Monitoring of systemic and hepatic hemodynamic parameters in mice. *J Vis Exp*, e51955.

Xie, G., Wang, L., Wang, X., Wang, L. & DeLeve, L. D. 2010. Isolation of periportal, midlobular, and centrilobular rat liver sinusoidal endothelial cells enables study of zonated drug toxicity. *Am J Physiol Gastrointest Liver Physiol,* 299, G1204-10.

Xie, G., Wang, X., Wang, L., Wang, L., Atkinson, R. D., Kanel, G. C., Gaarde, W. A. & Deleve, L. D. 2012. Role of differentiation of liver sinusoidal endothelial cells in progression and regression of hepatic fibrosis in rats. *Gastroenterology,* 142, 918-927 e6.

Yamada, Y., Kirillova, I., Peschon, J. J. & Fausto, N. 1997. Initiation of liver growth by tumor necrosis factor: deficient liver regeneration in mice lacking type I tumor necrosis factor receptor. *Proc Natl Acad Sci U S A,* 94, 1441-6.

Zarkada, G., Heinolainen, K., Makinen, T., Kubota, Y. & Alitalo, K. 2015. VEGFR3 does not sustain retinal angiogenesis without VEGFR2. *Proc Natl Acad Sci U S A,* 112, 761-6.

Zhang, H., Pu, W., Tian, X., Huang, X., He, L., Liu, Q., Li, Y., Zhang, L., He, L., Liu, K., Gillich, A. & Zhou, B. 2016. Genetic lineage tracing identifies endocardial origin of liver vasculature. *Nat Genet,* 48, 537-43.

Zhang, J., Muri, J., Fitzgerald, G., Gorski, T., Gianni-Barrera, R., Masschelein, E., D'Hulst, G., Gilardoni, P., Turiel, G., Fan, Z., Wang, T., Planque, M., Carmeliet, P., Pellerin, L., Wolfrum, C., Fendt, S. M., Banfi, A., Stockmann, C., Soro-Arnaiz, I., Kopf, M. & De Bock, K. 2020a. Endothelial Lactate Controls Muscle Regeneration from Ischemia by Inducing M2-like Macrophage Polarization. *Cell Metab,* 31, 1136-1153 e7.

Zhang, X., Groopman, J. E. & Wang, J. F. 2005. Extracellular matrix regulates endothelial functions through interaction of VEGFR-3 and integrin alpha5beta1. *J Cell Physiol,* 202, 205-14.

Zhang, X. J., Olsavszky, V., Yin, Y., Wang, B., Engleitner, T., Ollinger, R., Schledzewski, K., Koch, P. S., Rad, R., Schmid, R. M., Friess, H., Goerdt, S., Huser, N., Geraud, C., von Figura, G. & Hartmann, D. 2020b. Angiocrine Hepatocyte Growth Factor Signaling Controls Physiological Organ and Body Size and Dynamic Hepatocyte Proliferation to Prevent Liver Damage during Regeneration. *Am J Pathol,* 190, 358-371.

Zhou, B., Fan, Y., Rao, J., Xu, Z., Liu, Y., Lu, L. & Li, G. 2015. Matrix metalloproteinases-9 deficiency impairs liver regeneration through epidermal growth factor receptor signaling in partial hepatectomy mice. *J Surg Res,* 197, 201-9.

9. Supplementary information

Western blot scans with size marker indications used in this thesis:

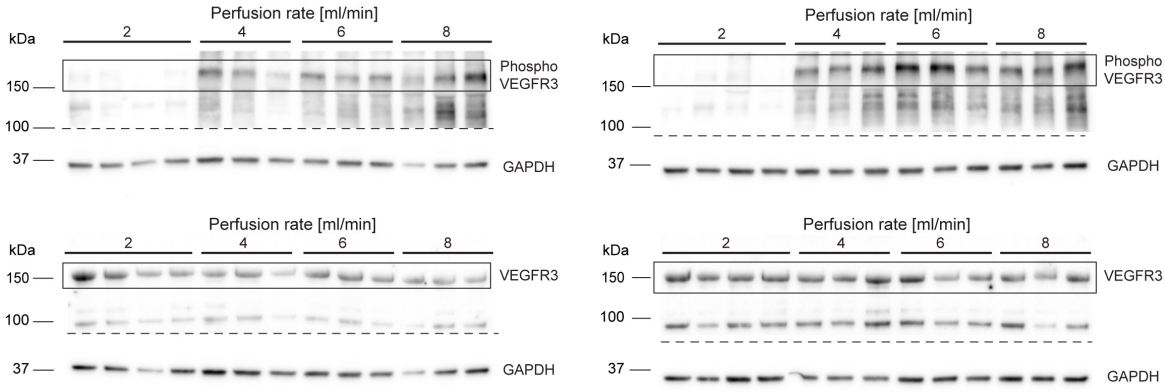

Supplementary Figure 1. Western blots used for Figure 5B.

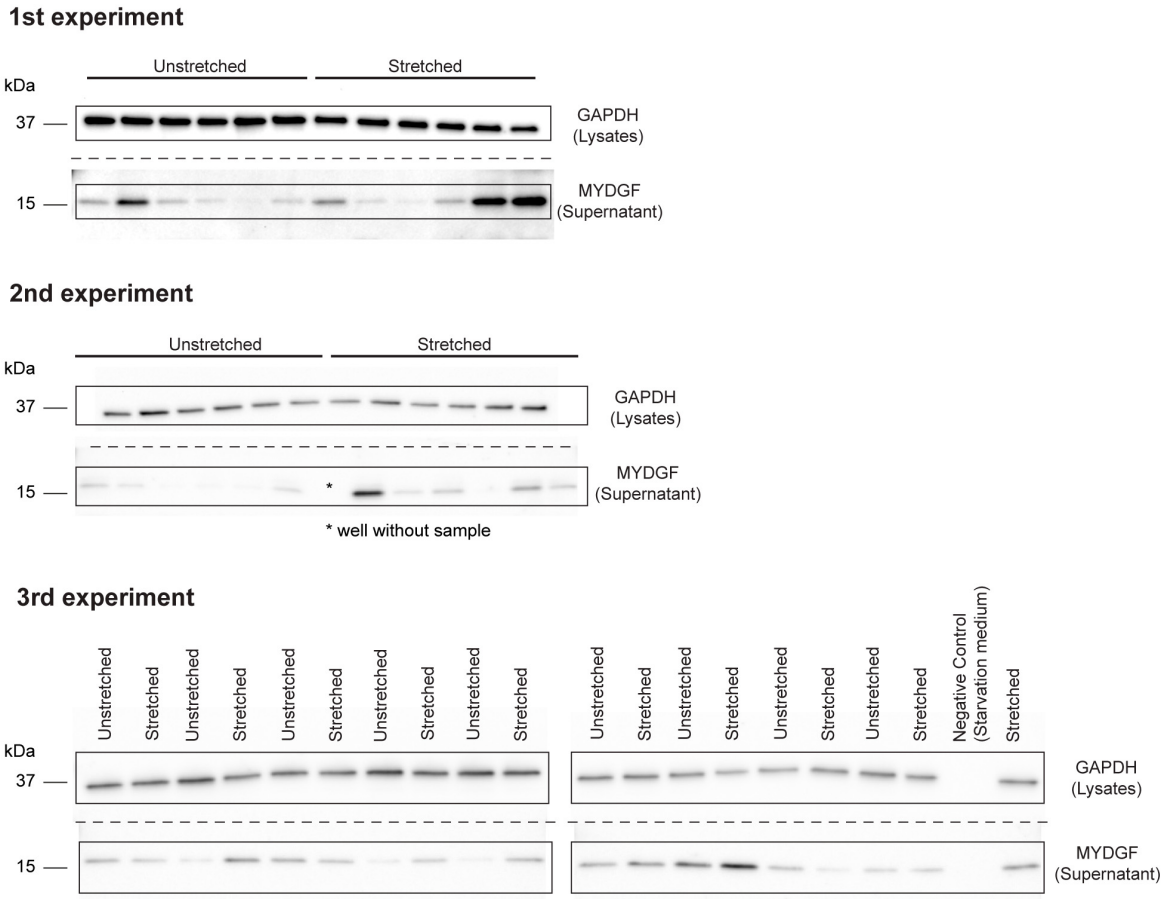

Supplementary Figure 2. Western blots used for Figure 19 D-F.

Supplementary Table 1. Protein list of LC-MS/MS data of supernatant from unstretched and stretched hepatic ECs, and of the medium used as negative control.

Protein Description	Found in sample group:		
	Unstretched	Stretched	Medium
Ubiquitin thioesterase otub1	Not Found	High	Not Found
chloride intracellular channel protein 1	Not Found	High	Not Found
phosphatidylethanolamine-binding protein 1	Not Found	High	Not Found
N-sulphoglucosamine sulphohydrolase	Not Found	High	Not Found
L-lactate dehydrogenase B chain	Not Found	High	Not Found
Myeloid-derived growth factor	**Not Found**	**High**	**Not Found**
Tropomyosin alpha-4 chain	Not Found	High	Not Found
Galectin-3	Not Found	High	Not Found
Beta-hexosaminidase subunit beta	Not Found	High	Not Found
beta-1,3-galactosyl-O-glycosyl-glycoprotein beta-1,6-N-acetylglucosaminyltransferase 4	Not Found	High	Not Found
serpin B6	Not Found	High	Not Found
nicotinamide phosphoribosyltransferase	Not Found	High	Not Found
coactosin-like protein	Not Found	High	Not Found
Epididymal secretory protein E1	Not Found	High	Not Found
Glycine--tRNA ligase	Not Found	High	Not Found
Reticulocalbin-1	Not Found	High	Not Found
Actin-related protein 2/3 complex subunit 2	Not Found	High	Not Found
aminopeptidase N	Not Found	High	Not Found
Protein-glutamine gamma-glutamyltransferase 2	Not Found	High	Not Found
Zinc finger protein 385C	Not Found	High	Not Found
Superoxide dismutase [Cu-Zn]	Not Found	High	Not Found
Gamma-glutamyl hydrolase	Not Found	High	Not Found
Collagen alpha-1(I) chain	High	Not Found	Not Found
Stanniocalcin-2	High	Not Found	Not Found
Collagen alpha-2(IV) chain	High	Not Found	Not Found
Cystatin-C [OS=Homo sapiens]	High	High	Not Found
purine nucleoside phosphorylase	High	High	Not Found
protein S100-A11	High	High	Not Found
Serpin B9	High	High	Not Found

Protein Description	Found in sample group:		
	Unstretched	Stretched	Medium
Glutathione S-transferase P	High	High	Not Found
Lysyl oxidase homolog 2	High	High	Not Found
Transaldolase	High	High	Not Found
3-ketoacyl-CoA thiolase, peroxisomal	High	High	Not Found
Dickkopf-related protein 3	High	High	Not Found
rho GDP-dissociation inhibitor 1	High	High	Not Found
Fatty acid synthase	High	High	Not Found
Serpin H1	High	High	Not Found
Fascin	High	High	Not Found
annexin A5	High	High	Not Found
Cadherin-5	High	High	Not Found
Protocadherin-12	High	High	Not Found
Macrophage Migration inhibitory factor	High	High	Not Found
Phosphoglycerate mutase 1	High	High	Not Found
thrombospondin-1	High	High	Not Found
Ras GTPase-activating-like protein IQGAP1	High	High	Not Found
peptidyl-prolyl cis-trans isomerase B	High	High	Not Found
Interstitial collagenase	High	High	Not Found
Isoform 4 of Acetyl-CoA carboxylase 1	High	High	Not Found
Lebercilin	High	High	Not Found
Beta-2-microglobulin	High	High	Not Found
Mesogenin-1	High	High	Not Found
Procollagen C-endopeptidase enhancer 1	High	High	Not Found
Malate dehydrogenase, mitochondrial	High	High	Not Found
Ribonuclease inhibitor	High	High	Not Found
Laminin subunit gamma-1	High	High	Not Found
Connective tissue growth factor	High	High	Not Found
Pentraxin-related protein PTX3	High	High	Not Found
Rho GDP-dissociation inhibitor 2	High	High	Not Found
Laminin subunit beta-1	High	High	Not Found
Multimerin-1	High	High	Not Found
Isoform 2 of Fanconi anemia group J protein	High	High	Not Found

Protein Description	Found in sample group:		
	Unstretched	Stretched	Medium
Ubiquitin carboxyl-terminal hydrolase isozyme L1	High	High	Not Found
Protein disulfide-isomerase A3	High	High	Not Found
Collagen alpha-2(I) chain	High	High	Not Found
Von Willebrand factor	High	High	Not Found
Myosin-9	High	High	Not Found
protein S100-A6	High	High	Not Found
Cathepsin B	High	High	Not Found
Transforming growth factor-beta-induced protein ig-h3	High	High	Not Found
Endothelial protein C receptor	High	High	Not Found

Statutory declaration

„Ich versichere an Eides Statt, dass die Dissertation von mir selbständig und ohne unzulässige fremde Hilfe unter Beachtung der „Grundsätze zur Sicherung guter wissenschaftlicher Praxis an der Heinrich-Heine-Universität Düsseldorf“ erstellt worden ist.“

Ich habe die Dissertation weder in der hier vorgelegten, noch in einer ähnlichen Form, bei einer anderen Fakultät eingereicht und habe bisher keine Promotionsversuche unternommen.

Mülheim an der Ruhr, den 30.07.2020

Linda Große-Segerath

Danksagung

Mein besonderer Dank gilt an erster Stelle meinem Doktorvater Prof. Dr. Eckhard Lammert, der es mir ermöglicht hat, meine Doktorarbeit in seinem Institut anzufertigen. Vielen Dank, Ecki, für deine Unterstützung und deine Motivation, für die fachlichen Ratschläge und für die intensive Betreuung mit viel Raum, mich wissenschaftlich weiterzuentwickeln. Danke, dass ich die letzten Jahre an dem für mich faszinierendsten Organ des menschlichen Körpers, der Leber, arbeiten durfte!

Ich möchte mich bei Prof. Dr. Verena Keitel-Anselmino für die Übernahme der Zweitgutachterin bedanken. Vielen Dank, Verena, für die wissenschaftlichen Diskussionen und die hilfreichen Ideen und Anregungen bezüglich meines Projektes. Danke, dass Du als Leiterin des integrierten Graduiertenkollegs 974 immer ein offenes Ohr für alle Doktorand*innen hattest.

Ich möchte mich bei Prof. Dr. Dieter Häussinger bedanken, dass ich ein Mitglied des SFB 974 sein durfte. Vielen Dank an alle Mitglieder des SFB 974 und des integrierten Graduiertenkollegs 974 für eine tolle Zeit.

Ich danke den aktuellen und ehemaligen Mitgliedern des Instituts für Stoffwechselphysiologie, insbesondere Laura W., Laura H., Okka, Jessi, Carina, Anna, Angela, Haiko, Paula, Lea, Tobi, Jenny, Silke O., Sofia und Daniel. Ich danke Euch allen für die schöne gemeinsame Zeit im Labor und für die vielen Erinnerungen. Daniel, Dir danke ich außerdem ganz besonders dafür, dass Du zu jeder Frage eine passende Antwort findest und mich mit deiner wissenschaftlichen Expertise jederzeit unterstützt hast. Ich danke Barbara, Andrea, Silke J. und Esther für die experimentelle sowie administrative Unterstützung und ein angenehmes Arbeitsklima. Mein Dank gilt auch den Mitgliedern des Instituts für Vaskular- und Inselzellbiologie am DDZ für die konstruktiven Diskussionen in den gemeinsamen Labmeetings.

*

Ich danke meiner gesamten Familie und meinen Freunden. Danke, dass Ihr mir immer mit Rat und Tat zur Seite steht und mich in jeder Lebenslage unterstützt.

Ich danke meinem Ehemann Julian aus tiefstem Herzen. Du bist mein Halt, meine Motivation und „mein Zuhause ist kein Ort, das bist Du“.

Zuletzt möchte ich mich bei meinen Eltern Elfriede und Raimund bedanken. Ihr habt immer an mich geglaubt und mich bedingungslos geliebt und unterstützt. Ich könnte mir keine besseren Eltern als Euch wünschen!